IMPACT OF DIFFERENT CURING METHODS AND DRYING CONDITIONS ON DRYING SHRINKAGE INDUCED CURLING

By

AMIR HAJIBABAEE

Bachelor of Science in Civil Engineering
University of Tehran
Tehran, Iran
2008

Master of Science in Structural Engineering
Oklahoma State University
Stillwater, Oklahoma
2011

Submitted to the Faculty of the
Graduate College of the
Oklahoma State University
in partial fulfillment of
the requirements for
the Degree of
DOCTOR OF PHILOSOPHY
December, 2016

IMPACT OF DIFFERENT CURING METHODS AND DRYING CONDITIONS ON DRYING SHRINKAGE INDUCED CURLING

Dissertation Approved:

Dr. Tyler Ley

Dissertation Adviser

Dr. Bruce Russell

Dr. Julie Ann Hartell

Dr. Peter Clark

ACKNOWLEDGEMENTS

I wish to express my deep gratitude to Dr. Tyler Ley (my MS and PhD adviser) for his continuous support, thoughtful advice and warm encouragement throughout my doctoral program. I sincerely enjoyed the experience of working with him which trained me for my future career and life. I am also highly thankful to Dr. Zachary Grasley (at Texas A&M University) for his insightful helps with the modeling work used in this study. I acquired an invaluable wealth of knowledge as he always inspired me as a true scientist. Thanks also to the members of my examination committee Drs. Bruce Russell, Julie Hartell, and Peter Clark for their suggestions and comments on the current work.

I would like to thank the Oklahoma Department of Transportation and the Oklahoma Transportation Center for funding the work. The following individuals also deserved acknowledgement for their kind help in completing the experiments: Basil Abdulkareem, David Porter, Paul Field, Mehdi Khanzadeh Moradllo, Gaurang Malviya, Morteza Khatib, Travis Ebisch, Katelyn Oquin, Bijaya Rai, Jake Hunter, Jake LeFlore, Nicholas Ley, and Shardul Kadam. I am truly grateful for the opportunity to work with so many considerate and talented people during the past few years.

I also want to thank my lovely family and friends. They have always supported me with love, patience, and dedication. I cannot imagine my life without them and their emotional support and encouragement during the preparation of this dissertation.

Name: AMIR HAJIBABAEE

Date of Degree: DECEMBER, 2016

Title of Study: IMPACT OF DIFFERENT CURING METHODS AND DRYING CONDITIONS ON DRYING SHRINKAGE INDUCED CURLING

Major Field: CIVIL ENGINEERING

Abstract: Prolonged wet curing is thought by many to provide only improvements in concrete performance. Also, because of the large surface to volume ratio of volume change sensitive structures such as slabs on grade, differential moisture loss can cause unwanted deflections, reduction in ride quality, and cracking. This work has shown that there is a potential increase in the amount of curling of these structures that are wet cured and then subject to 1-D drying in severe drying conditions. Experiments on paste beams with different water-to-cementitious ratios and cured for different durations with wet and sealed curing methods as well as alternative tests on concrete beams with different curing lengths suggested that the extended wet curing causes a pore structure refinement resulting in greater saturation and consequently greater shrinkage. A simplified 1-D, drying diffusion and shrinkage model was able to adequately predict experimentally measured peak curling deflections as well as the entire curling history after further adjustments to input parameters and confirmed the effect of saturation on curling. Also, the ability of this analytical model to capture the mechanistic sources of wet curing on peak deflections was evaluated by comparing its predictions to those acquired via a fully nonlinear diffusion model. It was shown the overall deflection predictions by the approximate linearized model were in greater agreement with the measured data than with the full, nonlinear solution.

Curing compounds are used to retain moisture which promotes hydration to develop a tight microstructure. This work provided a quantitative comparison between different curing compounds, wet, sealed, and no curing not made in previous studies and showed that adequate amounts of curing compounds are a useful curing method for members sensitive to differential drying such as concrete pavements in severe drying conditions. However, it was shown in less severe drying conditions that the curling strains caused by drying were minimal since the drying rate was less significant. So, if the concrete pavements are to be used in a moist environment, the type of curing that is used on pavements will have very little impact on their curling deformations.

TABLE OF CONTENTS

Chapter Page

LIST OF TABLES

LIST OF FIGURES

Figure Page

CHAPTER I

I. INTRODUCTION

The main concern of this research is to study the impacts of different curing methods on the deflection of volume change sensitive structures, such as slabs on grade, at different drying conditions. This deflection can happen due to the 1-D drying shrinkage differential and moisture gradient with or without curing. This dimensional instability causes the pavement to curl and consequently crack under traffic loads. Better understanding of drying shrinkage helps one to find cost effective curing methods for different drying conditions to reduce this moisture gradient induced curling and risk of subsequent cracking. In this project, funded by the Oklahoma Department of Transportation (ODOT), results from the effects of curing techniques at different drying conditions on curling of paste beams, shrinkage of concrete beams, field investigation, full scale pavement, and analytical modeling and numerical solutions will be discussed separately.

In this dissertation, chapters two to five were recently published in peer reviewed journals and chapters six and seven were written in a journal paper format to ease future publishing. Each chapter starts with a brief review of the recent works and continues with methods, results, discussions, and finally the chapter's conclusion:

- Chapter two aims to quantify the impact of wet curing on the curling and drying rate of cement paste which is useful to understand performance of concrete. This chapter has been published in ACI Materials Journal.

- Chapter three aims to quantitatively compare the moisture loss and volume change caused by differential drying of paste samples with different wet curing lengths as well as different types of curing compounds used at different coverage rates and with multiple layers in addition to a cost analysis. This has been published in International Journal of Pavement Engineering.
- Chapter four focuses specifically on how different durations of wet curing can impact the drying shrinkage gradient of concrete beams and the consequent curling of the element when it dries from only one surface, which has been published in Materials and Structures.
- Chapter five aims to verify the drying shrinkage mechanisms by using additional experiments on paste cylinders and a 1-D drying diffusion and shrinkage model implementing common simplifications from the literature to simulate max curling deflections of paste beams. This chapter has been published in Cement and Concrete Research.
- In chapter six, the previously presented approximate model will be further adjusted to investigate the ability of model to predict the shrinkage of concrete elements and to compare to experimental results presented in chapter four and to verify the accuracy or limitations of the model.
- Chapter seven examines the curling of cement and concrete samples in laboratory conditions that are close to the average relative humidity in Oklahoma and compares the results to those from simulations. Also, the performances of different curing methods on concrete beams in the field and on a continuous reinforced concrete pavement are investigated.
- Chapter eight concludes the dissertation and will provide important insight into the volume stability of slabs and the potential negative impact of wet curing on slab curling, suggest some key points to have a better selection of appropriate curing methods, and highlight required improvements to future modeling work.

CHAPTER II

II. THE IMPACT OF WET AND SEALED CURING ON CURLING IN CEMENT PASTE BEAMS FROM DRYING SHRINKAGE

2.1 ABSTRACT

Paste beams with different water-to-cementitious ratios were cured for different durations with wet and sealed curing methods and then the impact on curling was observed. The results show that samples that were cured showed greater curling deflection and these effects increased with the length of curing for the drying conditions investigated. These findings could impact construction techniques for volume change sensitive structures such as slabs on grade in drying environments.

Keywords: concrete pavement, curling, drying shrinkage, slabs on grade, wet curing

2.2 INTRODUCTION

The purpose of curing is to maintain adequate moisture and temperature in concrete to promote the development of microstructure and strength (Kosmatka, Kerkhoff, & Panarese, 2011). Curing can increase durability, strength, water-tightness, and abrasion resistance (ACI-308R, 2001; Dhir, Hewlett, & Chan, 1991; Gowriplan, Cabrera, Cusens, & Wainwright, 1990; Montgomery, Basheer, & Long, 1992). Wet curing methods include ponding, fogging, and saturated wet coverings.

The moisture distribution in a hardened slab is assumed to be uniform before drying begins and

becomes non-uniform as moisture is lost (Hedenblad, 1997). As concrete loses moisture it will shrink from drying. If there is more moisture loss at the top of the slab than at the bottom then the shrinkage will be greater at the surface and this will cause the element to curl upwards at the edge of the slab (Ytterberg, 1987a, 1987b, 1987c). This upwards curl can cause the slab to lose contact with the base at the edges or to crack if it is restrained (ACI-302.1R, 2004). To minimize curling from drying shrinkage a uniform moisture gradient is required.

2.2.1 Mechanisms of Drying Shrinkage

The drying shrinkage in cement paste is thought to be caused by a negative pore fluid pressure caused by menisci forming within pores upon drying (Bentz, Garboczi, & Quenard, 1998; Coussy, Dangla, Lassabatere, & Baroghel-Bouny, 2004; Mackenzie, 1950). The drying that occurs may be external (i.e., vapor diffusion) or caused by self-desiccation due to the hydration reaction; shrinkage due to this latter component – autogenous shrinkage – may be more important for concrete mixtures with w/cm less than 0.40 (Tazawa, 1999). The autogenous shrinkage increases when the water to cementitious ratio (w/cm) is decreased or the cement fineness is increased. For autogenous shrinkage, this increase is because the capillary pressure will cause higher tension in the pore water of the finer microstructure (Bentz et al., 2001; Jensen & Hansen, 1996). Also, due to the low permeability of the mixture at low w/cm, the curing water infiltrates at a slower rate and cannot penetrate deep within the sample replacing moisture lost due to hydration (Cather, 1994; Meeks & Carino, 1999; Pihlajavaara, 1964).

Regardless of the source of drying, the formation of the menisci and generation of the capillary pressure (P_{cap}) can be related, according to the Laplace-Young Eq. (2.1). If γ is the surface tension of the pore fluid, θ is the liquid-solid contact angle, and r is the average radius of the curvature of the meniscus (Adamson & Gast, 1967; Radlinska et al., 2008):

$$P_{cap} = -\frac{2\gamma\cos(\theta)}{r}. \qquad \text{Eq. (2.1)}$$

As drying occurs pores of decreasing size will begin to empty leading to increased capillary pressures as described by the Kelvin-Laplace equation (Eq. (2.2)) (Coussy et al., 2004). If ρ_w is the density of water, R the ideal gas constant, T the temperature, M_v the water molar mass, and RH is the relative humidity:

$$P_{cap} = -\frac{\rho_w RT}{M_v}\ln(RH). \qquad \text{Eq. (2.2)}$$

2.2.2 Impact of Curing on Drying Shrinkage

While it is widely understood that wet curing can have positive impacts on concrete it has also been reported that wet curing may have a negative impact on drying shrinkage. For example Perenchio (1997) observed that drying shrinkage was increased by wet curing up to seven days. Others have observed that a shorter curing time will result in a faster drying rate (Hedenblad, 1997; Jackson & Kellermann, 1939). This faster drying rate may minimize internal moisture gradients and therefore reduce curling caused by drying shrinkage. However, others have suggested that longer moist-curing periods will have little effect on drying shrinkage and therefore curling, other than delaying the onset of shrinkage (Suprenant, 2002). Based on this previous work it appears that conflicting results have been reported in the literature.

2.2.3 Impact of Aggregates on Drying Shrinkage

The aggregates in a concrete mixture do not significantly shrink upon drying and therefore dilutes and restrains the shrinkage of the paste. Others have noticed this as the drying shrinkage of the cement paste is six to eight times greater than values observed in concrete (Bisschop, 2002) and paste shrinks about 1.7 times more than mortar (Holt, 2002). This suggests that one should be able to study the performance of the paste and gain an indication of the subsequent performance

in mortar or concrete. Because of the correlation between paste and concrete shrinkage, paste samples have been used in this study as a means to gain insight into concrete behavior. Pastes have the advantage of yielding greater strains, resulting in greater measured displacements and higher measurement accuracy and resolution. Furthermore, quality control of pastes is simpler than for concrete, resulting in greater measurement repeatability and a higher confidence level in mechanisms evoked from the results.

2.2.4 Impact of Member Geometry on Drying Shrinkage

Many researchers have shown that the magnitude and rate of shrinkage for concrete is dependent on the specimen size (Browne, 1967; McDonald & Roper, 1993; Pickett, 1946). As the surface area to volume ratio of a specimen increases then this impacts the magnitude and the rate of shrinkage (T. C. Hansen & Mattock, 1966). These observations were used to help guide the specimen size in order to obtain rapid results.

2.3 RESEARCH SIGNIFICANCE

While there are benefits in strength gain, decrease in permeability, and abrasion resistance from wet curing there is a discrepancy in previous research as to whether wet curing increases drying shrinkage and hence curling in concrete. This curling can be detrimental to the long-term behavior of pavements and slabs on grade. This work aims to quantify the impact of wet curing on the curling and drying rate of cement paste which is useful to understand performance of concrete.

2.4 EXPERIMENTAL METHODS

2.4.1 Materials

The Portland cement used in this study meets the requirements of both a type I and II cement, according to ASTM C150 (2011) and AASHTO M85 (2012). The oxide analysis and the

estimated phases are given in Table 2.1. The paste mixutures in this experiment had a w/cm of 0.34, and 0.42 and were compared in a constant batch size.

Table II.1 Oxide analysis of the cement used for paste beams and the phase concentrations

chemical test results (%)					
SiO2	Al_2O_3	MgO	Fe_2O_3	CaO	SO_3
20.23	4.77	1.90	3.23	64.15	2.52

phase concentrations (%)				blaine
C_3S	C_2S	C_3A	A_4AF	(cm^2/g)
63.56	10.05	7.18	9.83	3713

Note: (1 cm = 10 mm = 0.3037 in; 1 g = 0.0022 lb)

2.4.2 Sample Preperation and Curing Methods

The paste mixtures were prepared according to ASTM C305 (2011). Three paste beams with dimensions of 100 cm × 6.1 cm × 1.3 cm (39.4 in × 2.4 in × 0.5 in) were consolidated in plastic molds from each mixture. This specimen size was chosen so that the sample was thin but had a large surface area. Several others have found that the developed stresses and shrinkage strains due to the moisture gradients during drying is highly related to specimen size (Browne, 1967; McDonald & Roper, 1993; Pickett, 1946). After casting, all specimens were cured with wet burlap on the finished surface for 24 hours at 23 °C (73 °F) and then demolded. This was done to ensure that the sample had some initial strength for handling. After removing the specimens from the molds the samples were sealed with wax on all sides but the finished surface. A few samples were also sealed with aluminum tape for comparison and no difference was found in drying performance. The wax was used because it is economical and easy to apply.

After demolding, the specimens were weighed before and after sealing with wax. The finished surface of the beam was cured for different durations while the beams were stored in a 23 °C (73 °F) and 40% relative humidity environmental chamber. After the specified curing period the curing material was removed from the sample. The sample was then left in the chamber to lose moisture from the unsealed, finished surface.

Since only the top surface of the sample was exposed to the drying environment this created a moisture gradient in the sample. This gradient caused differential shrinkage strains to occur that caused the specimen to curl. This test is advantageous, as the moisture loss is quick and the resulting gradients can be large. This leads to a significant curling deformation of the specimens that is easy to measure. To ensure that the curling measurements were not impacted by gravity the beams were stored on their sides. This test was modeled after previous work by Berke and Li (2004) to investigate the effectiveness of shrinkage reducing admixtures to minimize curling.

Specimens with different durations of wet and sealed curing were compared. For wet curing, samples were kept in saturated burlap for 1, 3, 7, and 14 days of additional curing after demolding and waxing. The burlap was wetted every day to ensure that it remained saturated. After the curing was removed the specimens were subjected to a 40% relative humidity and 23 °C (73 °F) drying environment within an environmental chamber. In addition to wet curing, several specimens were cured in a sealed plastic bag for 1 and 3 days within this chamber. This curing was similar to the wet burlap, but no external moisture was added to the specimens during the curing process. Other samples received no curing after demolding. All specimens were stored at 23 °C throughout the testing.

2.4.3 Specimen Measurement

To measure the curling, rubber bands were used to hold the ends of the specimen to a flat aluminum plate with the uncoated surface of the specimen facing the plate. The distance between the aluminum plate and the specimen is measured at regular locations along the length with a caliper of 0.0127 mm (0.0005 in) accuracy. The curling of the beam was symmetric with a maximum at the middle of the beam. The loss of moisture of the sample was measured through the mass loss over time with 0.1 g (0.00022 lb) accuracy. After finishing the measurements, the specimen is returned to the chamber room until the next measurement.

2.5 RESULTS

A typical result for the deflection of a specimen with time is shown in Figure 2.1 for a 0.42 w/cm paste after demolding.

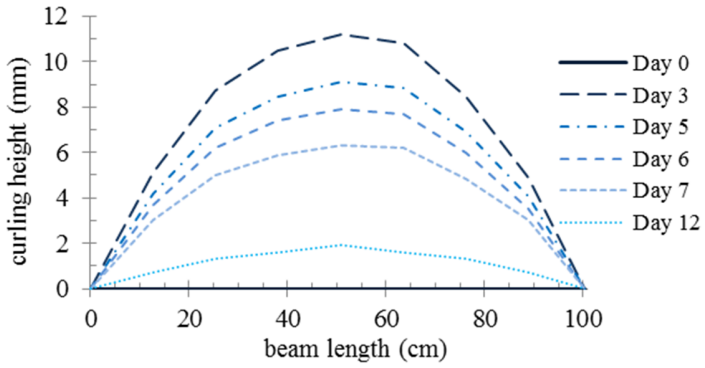

Figure II.1 Curling height over the beam length for different days of drying at 23 °C and 40% RH for a 0.42 w/cm sample with no additional curing. (1 cm = 10 mm = 0.3037 in)

Since the deflected shape was parabolic and symmetric in nature this means that uniform drying was occurring and that the maximum curling value can be used to describe the test results. The mass change for this sample is plotted compared to samples that were cured with wet and sealed curing for 1 and 3 days and samples of 0.34 w/cm cured with wet curing for 1 and 3 days as shown in Figure 2.2. The mass loss has been normalized by the initial mass of the sample to compare the data.

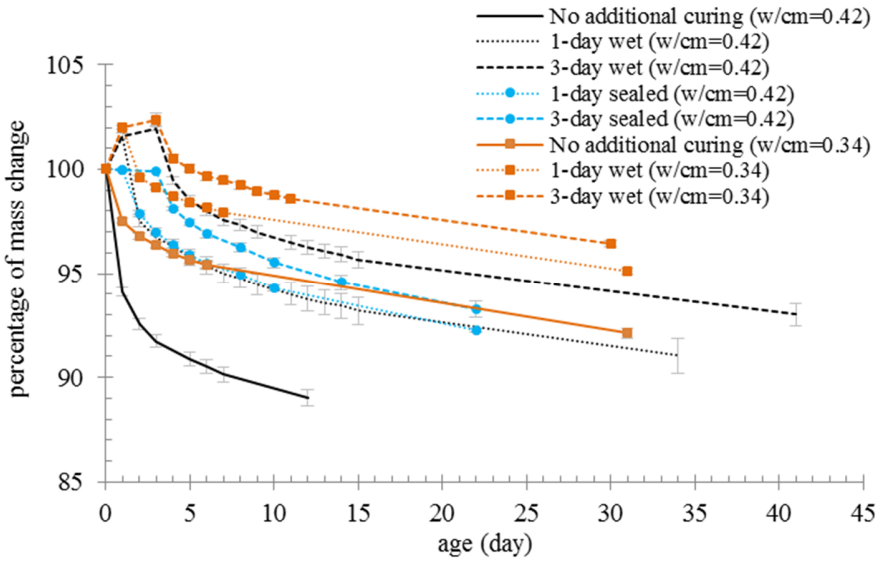

Figure II.2 The mass change versus drying time for specimens with 0.34 and 0.42 w/cm for wet and sealed curing of 0, 1, and 3 days when exposed to a 23 °C and 40% RH environment.

Figure 2.3 shows the idealized behavior of the specimens investigated.

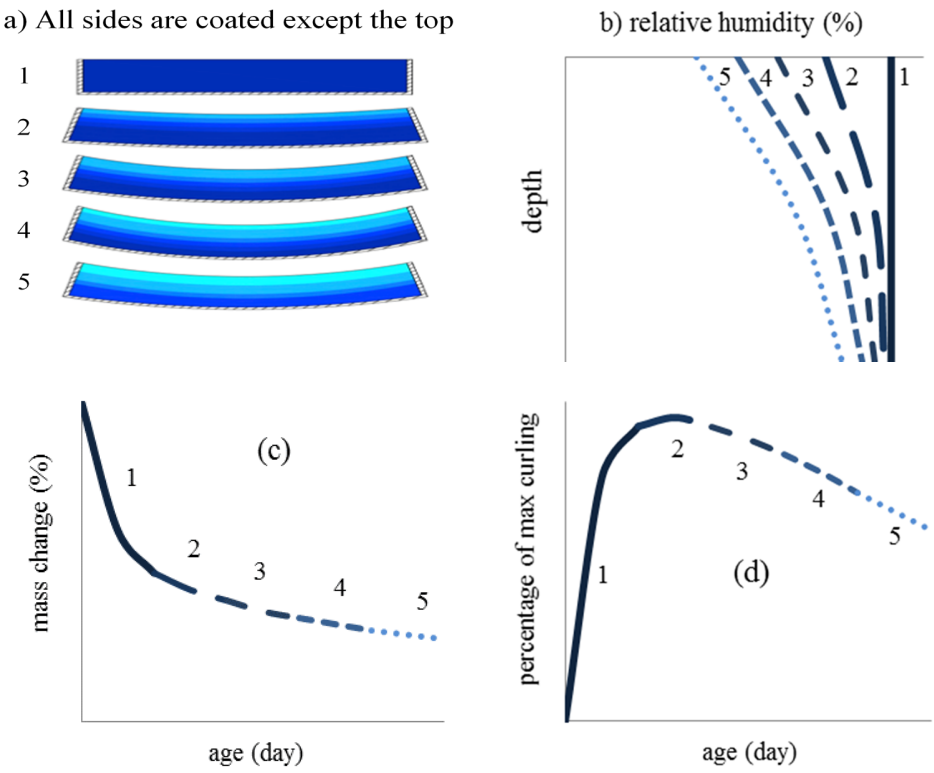

Figure II.3 The idealized behavior of the specimens investigated.

The mass loss and the maximum curling height of samples of 0.42 w/cm for 0, 1, 3, 7, and 14 days of additional wet curing is shown versus the days of drying in Figure 2.4. Markers have been added to both graphs to highlight the point of maximum curling.

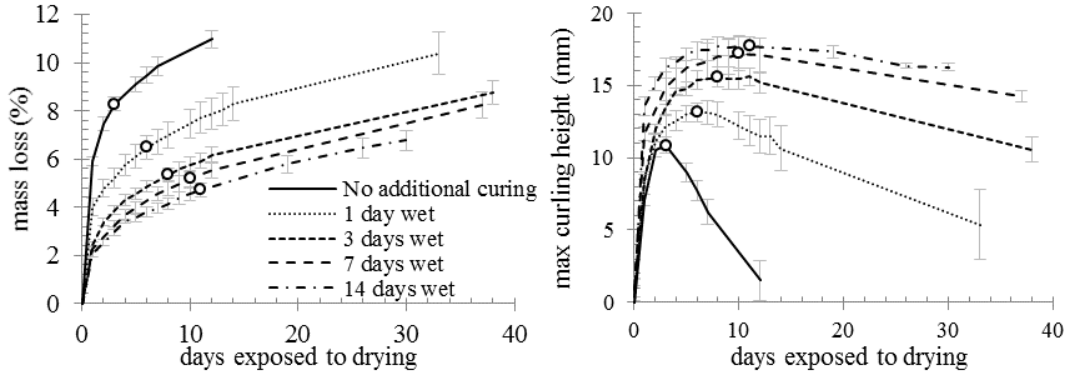

Figure II.4 The mass loss and maximum curling height during drying at 23 °C and 40% RH environment for a 0.42 w/cm specimen with different durations of wet curing; the circles show the maximum curling height. (1 cm = 10 mm = 0.3037 in)

The mass loss and the maximum curling height of samples of 0.42 w/cm that were sealed for 1 and 3 days is compared with samples with 0, 1, and 3 days of wet curing in Figure 2.5. Again markers have been added to highlight the points of maximum curling.

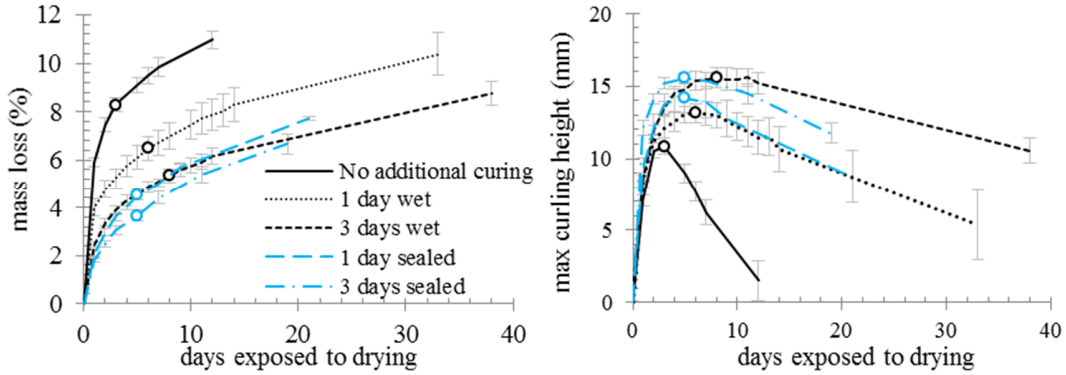

Figure II.5 The mass loss and maximum curling height during drying at 23 °C and 40% RH environment for a 0.42 w/cm specimen for wet and sealed curing; the circles show the maximum curling height. (1 cm = 10 mm = 0.3037 in)

A comparison between the 0.34 and 0.42 w/cm specimens for mass loss and the maximum curling height is compared in Figure 2.6. Again markers have been added to highlight the points of maximum curling.

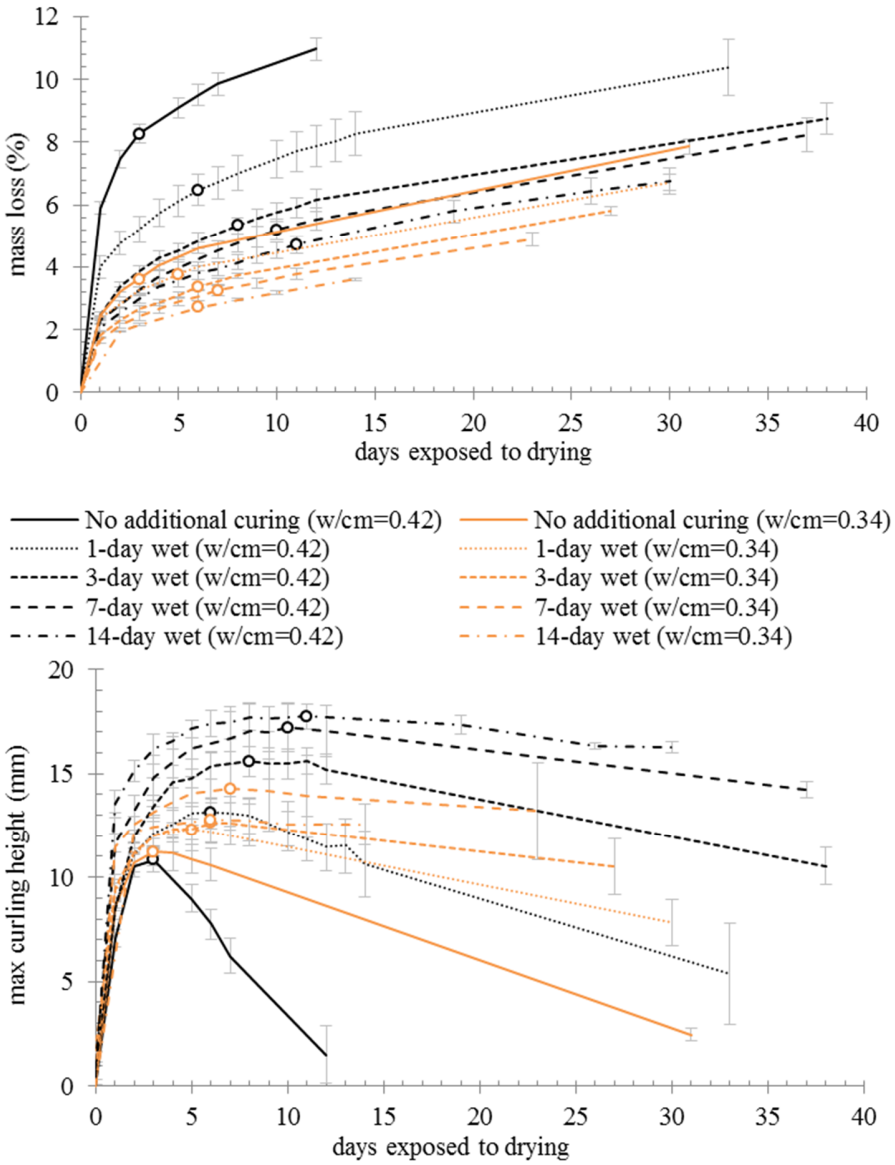

Figure II.6 The mass loss and maximum curling height for 0.34 w/cm compared to 0.42 w/cm specimen with different durations of wet curing; the circles show the maximum curling height. (1 cm = 10 mm = 0.3037 in)

2.6 DISCUSSION

2.6.1 General Behavior

The general performance of the curling and mass loss of the samples are summarized in Figure 2.1 and the solid black line in Figure 2.2. Since the curling shown in Figure 2.1 is symmetric this suggests that the moisture loss is uniform. As can be seen in Figure 2.1 the samples curl up over the first three days of drying and then this curling decreases as the mass continues to decrease.

In the top two panels of Figure 2.3 the idealized moisture gradients are shown along with the overall curling of the sample. The lower two panels of Figure 2.3 show the moisture loss and the deflection of the sample. Over the first few days of drying the sample loses moisture at a high rate and begins to curl upward. With subsequent drying the sample is observed to decrease in curling height. This mass loss will continue until the internal relative humidity reaches equilibrium with the environment. However, because the moisture loss at the top and bottom of the sample is different there is a differential in shrinkage and so the sample curls. With increased drying the curl decreases as the material in the bottom of the sample begins to shrink and the differential in shrinkage between the top and bottom is reduced. Figure 2.3 shows a generalized behavior of the specimens.

2.6.2 Impact of Wet Curing on Curling

Figure 2.4 shows that the rate of drying and the time needed to reach the maximum amount of curling increased as the length of wet curing increased. However this Figure also shows that as the curing duration increases then so does the maximum amount of curling. In contrast, the samples with no additional curing showed the least amount of curling while having the highest amount of moisture loss.

These findings are in conflict with previous work which suggests the length of curing only impacts when curling will start and not the magnitude (ACI-360R, 2006; Suprenant, 2002).

However, this supports work by Perenchio (1997) that showed that the drying shrinkage increased for wet cured samples in these drying conditions.

Additional curing will sustain hydration and decrease the porosity and permeability of cement paste. Because the pore sizes are smaller for materials with a greater degree of hydration, the degree of saturation will be higher at a given relative humidity. This increase in saturation may be explained by the Kelvin equation, which describes the minimum pore size emptied at a given relative humidity at equilibrium. This means that curing will cause a higher level of saturation and will increase the effective pressure in the pore network and therefore the shrinkage on drying (Coussy et al., 2004). Also, this decrease in permeability makes it more difficult for a specimen to lose moisture from drying. This is why specimens that are cured longer lost moisture at slower rates, required more time to reach their maximum amount of curling. Hedenblad (1997) has made direct measurement of the decrease in permeability with increased curing. However, according to Eq. (2.1) this decrease in pore size will cause an increase in pressures upon drying. This explains why there is an increase in curling deflection, but a decrease in mass loss from the samples with a longer period of wet curing. Moreover, the additional wet curing may increase the water content of the samples as shown in Figure 2.2, which will increase the length of drying time needed for the samples to reach their maximum curling height.

2.6.3 Comparing Sealed and Wet Curing

As shown in Figure 2.2, specimens that were wet cured increased in mass due to capillary and osmotic suction during the wet curing while the specimens that were sealed showed no increase in mass during curing. Once the curing was removed the wet cured samples showed a greater rate of water loss for the first day of drying and then similar rates of mass loss. With increased curing the wet cured samples lost mass at a lower rate while the sealed cured samples lost mass at a similar rate regardless of the curing length. Also, it can be observed that with increased curing time there was an increase in the maximum curling height.

The increased drying rate during the period before maximum curling is likely caused by the loss of the additional water added during the wet curing. However, despite this difference in rate of mass loss and time of maximum curling the magnitude of the maximum curling is similar between the wet and sealed cured samples cured for comparable durations. This suggests that the capillary pore size range and hence the shrinkage of the hydration products on drying were similar between the samples despite the additional water used in the wet curing for the durations investigated. Therefore, the extra water supplied by the wet curing does not seem to impact the magnitude of the curling, only the drying rate and the amount needed to reach the maximum amount of curling. It is likely that this additional water supplied during wet curing fills the larger pores in the paste that are able to lose water more easily and not impact the drying shrinkage and hence the curling.

2.6.4 Impact of w/cm on Curling

As shown in Figure 2.2 as the w/cm increased then so did the rate of water loss during the early drying. This is expected as the samples with the higher w/cm will have a higher permeability and so it is easier for the samples to dry. Figure 2.6 shows that samples with a w/cm of 0.42 showed more curling from drying than samples with a w/cm of 0.34 for similar curing durations. Other researchers have shown that as the w/cm increases then so does the drying shrinkage (Darwin, Browning, & Lindquist, 2004; Schmitt & Darwin, 1999).

For the 0.34 w/cm samples it appears that after one day of wet curing, that the curling heights were similar. This holds for all of the 0.34 w/cm samples except for the sample cured for 7 days. This sample is likely an outlier. Similarly for the 0.42 w/cm samples the maximum curling height did not significantly change for samples that were cured for 7 and 14 days. This suggests that once a critical duration of curing occurs then additional curing does not have a significant impact on the moisture loss or the curling of a sample. This critical duration appears to be shorter with

lower w/cm. This could be caused by the low rate at which the curing water is able to further penetrate the sample because of the low permeability of the microstructure.

Another interesting observation is that there was little difference in curling height or drying time to maximum curling when comparing uncured samples with 0.34 and 0.42 w/cm, despite the mass loss being different by a factor of two. At this time it is not clear why this occurs. One would expect the 0.34 w/cm sample to be stiffer and have an overall smaller pore size. However at this time the microstructure is not well formed and not well understood.

In general more work is needed to understand the coupling between pore size, water content, and physical properties of the paste. Analytical models are currently being used to provide insight to these problems for future publications.

2.6.5 Practical Implications

Although there are many benefits from wet and sealed curing, this work has shown that they can increase the potential for surface drying shrinkage and curling. However, there are things that can be done with the mixture design and slab construction that can minimize volume change from drying. These recommendations are useful for the construction of concrete flatwork that will only have drying from one side such as in slabs on grade or pavements. For these elements it is recommended that mixtures with a lower w/cm should be used and to avoid curing for extended periods. For members with high sensitivity to volume change long term wet curing is not suggested and in some cases it may be desirable to not cure the element. The curing duration should be decided based on the application of the slab and the need for durability, strength, and allowable curling deflection. However, this recommendation may change for different curing conditions, materials, mixture designs, and element sizes. Judgment should be used on the part of practitioners. Sometimes it is necessary to wait until concrete floors have dried before applying coverings in order to minimize mold or ensure adhesives will properly function. In these cases

this work supports using a low w/cm and a sealed curing method instead of a wet cure. This is suggested as wet curing was shown to prolong the time required for drying.

It should be noted that the drying environment in this work was severe but representative of what may happen to concrete slabs from prolonged exposure to low relative humidity. Rewetting was not investigated in this paper, and it is not clear what magnitude this will have on the performance because of the typically short duration of moisture exposure and the low permeability of the concrete. The impact of rewetting is currently being investigated and will be described in future publications.

2.7 CONCLUSIONS

In this paper effects of wet curing were compared to that of sealed and no-curing in a 40% RH and 23 °C drying environment for paste beams. A number of useful observations have been made:

- As the curing time increased there was a subsequent decrease in the rate of mass loss from drying but an increase in the ultimate differential shrinkage or curling. This was true for a range of w/cms and curing durations and methods.
- There was little difference in the maximum curling height of specimens that used a wet and sealed cure; however the wet cured samples were observed to curl at a faster rate than the sealed cure samples.
- Samples with a w/cm of 0.34 had a lower maximum curling height and a lower drying rate than samples with a w/cm of 0.42 for the same curing periods.
- There was little difference in the maximum curling height for samples with a 0.34 and 0.42 w/cm that did not receive additional curing, despite having a significant difference in the rate and amount of moisture loss.

Several recommendations have been made on possible modifications to concrete slab construction to minimize volume change from drying. Although these observations were made in paste samples, similar behavior would be expected in concrete as suggested by Pickett (1956).

2.8 ACKNOWLEDGMENTS

The authors would like to thank the Oklahoma Department of Transportation (ODOT 2208) and the Oklahoma Transportation Center (OTCREOS10.1-24) for funding the work. The following individuals also deserved acknowledgement for their help in completing the experiments: Basil Abdulkareem, Travis Ebisch, Jake LeFlore, Nicholas Ley, David Porter, Paul Field, and Shardul Kadam. The authors would also like to thank Dr. Zach Grasley for his thorough review and thoughtful comments on the manuscript.

CHAPTER III

III. COMPARISON OF CURING COMPOUNDS TO REDUCE VOLUME CHANGE FROM DIFFERENTIAL DRYING IN CONCRETE PAVEMENT

3.1 ABSTRACT

Curing compounds are used to retain moisture which promotes hydration to develop a tight microstructure. Because of the large surface to volume ratio of these structures, differential moisture loss can cause unwanted deflections, reduction in ride quality, and cracking. This paper quantitatively compares the effectiveness of different curing methods with an emphasis on curing compounds to resist moisture loss and subsequent volume change caused by differential shrinkage. This work provides a quantitative comparison between different curing compounds, wet, sealed, and no curing not made in previous publications. A performance based cost analysis over the different curing compounds is also included. The result shows that the poly-alphamethylstyrene curing compound causes the lowest mass loss and subsequent deflection compared to the water-resin and water-wax based curing compounds at equal coverage rates at equal costs. The work also shows that a double application of curing compound shows greater benefit than a single layer with the same volume for water-wax based curing compounds. The results show that if adequate amounts of curing compounds are used then they are a useful curing method for members sensitive to differential drying such as concrete pavements.

Keywords: Curing compound; Curling; Drying shrinkage; Poly-alphamethylstyrene; Resin; Wax

3.2 INTRODUCTION

When a concrete pavement dries, the moisture profile will change over time and shrinkage at the exposed surface will cause the element to deflect or curl and crack if it is restrained and the stress exceeds the strength of the concrete (ACI-302.1R, 2004; D'ambrosia, 2012; Hedenblad, 1997; Ytterberg, 1987a). These cracks can lead to early failures and costly repairs. Concrete is typically protected to retain moisture by different curing methods. Membrane-forming curing compounds are the most widely used method to cure the freshly placed concrete (Kosmatka et al., 2011). Curing compounds are used to increase the moisture content and subsequent degree of hydration of the concrete (K. Wang, Cable, & Ge, 2002, 2006). According to ACI-308R (2001) membrane-forming curing compounds can be applied immediately after the final finish of the concrete. This means that supplemental moisture does not have to be added to keep the concrete moist. This paper quantifies the performance of different curing compounds to retain moisture and reduce volume changes caused by differential drying shrinkage.

3.2.1 Level of Effectiveness and Application Rate of Curing Compounds

Depending on the different types, application volume, and ambient conditions, curing compounds show a range of potential water retention (Mather, 1990; Senbetta, 1988; Shariat & Pant, 1984; J. Wang, Dhir, & Levitt, 1994). ASTM C156 (2011) is the most commonly used test method to investigate the performance of different curing compounds. However, this test method has been suggested to be highly variable, and able to give false results for curing compounds that are highly viscous (Taylor, 2013).

Since the surface texture of concrete can be variable, the amount of curing material needed to provide sufficient water retention can also be variable. Once the desired coverage has been determined then there are many details about the application equipment and method that impact the actual amount of material that is applied (Vandenbossche, 1999; Ye, Mukhopadhyay, & Zollinger, 2009). Therefore, different curing compounds with different levels of effectiveness

may be applied with different application rates and obtain equivalent performance. It has been suggested that curing compounds should be applied in two layers to ensure uniform coverage (ACI-308R, 2001). Unfortunately, there is little quantitative data to suggest this recommendation and justify the possible increases in cost and so few practitioners adopt this practice.

3.2.2 Use of Paste to Study the Differential Drying Shrinkage of Concrete

In this study curing compounds and their impact on moisture loss and volume change of paste were evaluated. The drying shrinkage of the cement paste is six to eight times greater than values observed in concrete (Bisschop, 2002) and paste shrinks about 1.7 times more than mortar (Holt, 2002). This difference is because the aggregates in concrete do not significantly dry and shrink compared to the hydrated paste (Hobbs, 1974; Pickett, 1956). This means that the aggregates restrain the shrinkage and reduce the amount of shrinking material. This also means that the performance of the paste should be a magnified version of the mortar or the concrete. Pastes will show larger shrinkage that will result in greater measured displacements and therefore will be easier to measure accurately. Furthermore, the quality control of paste is simpler than that of concrete, resulting in greater measurement repeatability. Because of this, paste samples have been used in this study as a means to gain insight into the behavior of concrete.

3.2.3 Performance of Wet and Sealed Curing Methods on Curling from Differential Drying

While this paper focuses on the performance of curing compounds, some other curing methods have been included as a method of comparison. While wet and sealed curing methods have been shown to promote hydration and reduce the porosity and the ingress of external chemicals, this decrease in porosity can also cause increases in drying shrinkage (Hajibabaee, 2011; Perenchio, 1997). Moreover, Hajibabaee and Ley (2015, 2016) showed that an increase in the length of wet or sealed curing can increase the maximum curling of paste and concrete and the time to reach the peak deflection. This behavior has been discussed in more details by Hajibabaee et al. (2016) using a one-dimensional drying diffusion and shrinkage model as well as a nonlinear diffusion

model. To simplify this behavior one can use a one-dimensional drying shrinkage model ε_d (Adamson & Gast, 1967; Baroghel-Bouny, 1997; Baroghel-Bouny, Mainguy, Lassabatere, & Coussy, 1999; Bentz et al., 1998; Coussy, 1995; Coussy, Eymard, & Lassabatere, 1998; Mackenzie, 1950)

$$\varepsilon_d = \frac{S_l}{3K_0} p_c, \qquad p_c = -\frac{RT}{V_m} \ln h = \frac{2\gamma \cos(\theta)}{a}, \qquad \text{Eq. (3.1)}$$

where S_l is the desorption isotherm, K_0 is the bulk modulus, p_c is the capillary pressure, R is the universal gas constant, T is the absolute temperature, V_m is the molar volume of water ($\approx 1.82 \times 10^{-5} \frac{L}{mol}$), h is the internal relative humidity with values between 0 and 1, γ is the surface tension of pore fluid, θ is the liquid-solid contact angle, and a is the radius of cylindrical pore. The maximum curling deflection δ_{max} of the beam is estimated by Euler-Bernoulli equation

$$\delta_{\max}(t) = \frac{3l^2}{2L^3} \int_0^L \varepsilon(y,t) y dy, \qquad \text{Eq. (3.2)}$$

where $\varepsilon(y,t)$ is the strain function at certain time t and different heights, l is the length of the beam, and L is the thickness of the concrete beam. The higher capillary pressure in the samples with longer wet curing duration causes a larger drying shrinkage gradient and consequently higher curling deflection (Hajibabaee, Grasley, et al., 2016). This suggests that curing compounds may be the desired curing method for structures, such as concrete pavements, that are sensitive to differential drying and subsequent curling. However, little work has been done to quantitatively compare the performance and cost of different curing compounds.

3.2.4 Objectives

This work aims to quantitatively compare the moisture loss and volume change caused by differential drying of samples with different types of curing compounds used at different coverage rates and with multiple layers. Next, this quantitative performance information is combined with the cost of these materials so that an equal cost comparison can be made. In addition, results from curing compounds are compared to sealed, wet cured, and no cured samples. This analyses and quantitative comparisons are useful for practitioners and have not been evaluated in this way in previous publications.

3.3 EXPERIMENTAL METHODS

3.3.1 Materials

The Portland cement used in this study meets the requirements of both a type I and II, according to ASTM C150 (2011) and AASHTO M85 (2012). The oxide analysis and the estimated phases are given in Table 3.1. The paste mixtures in this experiment had a water-to-cement ratio (w/c) of 0.42 and were prepared in a constant batch size 3000 cm^3.

Table III.1 Oxide analysis of the cement, blaine fineness, and phase concentrations

Oxide mass fractions (%)					
SiO_2	Al_2O_3	MgO	Fe_2O_3	CaO	SO_3
20.23	4.77	1.90	3.23	64.15	2.52
Phase mass concentrations (%)				Blaine	
C_3S	C_2S	C_3A	C_4AF	3713	
63.56	10.05	7.18	9.83	cm^2/g	

Three different curing compounds were chosen to represent different chemical families that are the most commonly used in North America. The summary of these compounds is given in Table 3.2. This table also provides the cost and the volatile organic compound (VOC) level for the curing compounds investigated.

Table III.2 Specifications of the curing compounds used

Compounds	ASTM Type	Density (kg/m^3)	Solid content	Chemistry	VOC (g/L)	Cost†
C1	Type 2, Class B	1019.7	32.8 %	poly-alphamethylstyrene	349	3x
C2	Type 2, Class B	1017.3	21.7 %	water-resin	186.5	2x
C3	Type 2, Class A	969.4	23.9 %	water-wax	<100	1x

†Cost is relative to C3

3.3.2 Sample Preparation

The paste mixtures were prepared according to ASTM C305 (2011). Three paste beams with dimensions of 100 cm × 6.1 cm × 1.3 cm were prepared in plastic molds from each mixture. An overview of these specimens is shown in Figure 3.1. This test was developed by Berke and Li (2004) and subsequently used by Hajibabaee and Ley (2015) and Hajibabaee et al. (2016) to investigate wet and sealed curing of different durations on cement paste.

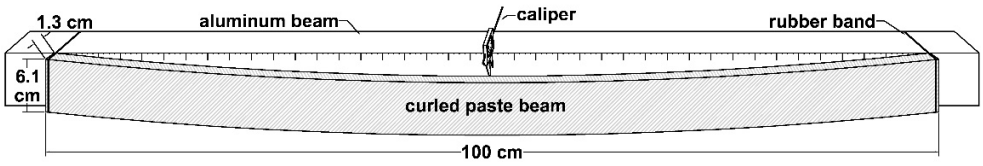

Figure III.1 Typical paste beam used in the testing and the measurement setup; all sides except the finished surface are coated with wax.

To evaluate the effectiveness of different curing compounds, specimens were kept moist by suspending wet burlap near their surface for five hours before being covered in curing compound. This was done to ensure that the sample had enough initial strength for handling and the bleed water disappeared from the surface of the specimen before applying the curing compound, as suggested by Mather (1990).

The samples were weighed before and after the application of the curing compound and then stored at 23 °C and 40% relative humidity until 24 hours after mixing. Next the samples were

demolded, weighed, sealed with wax on all sides but the finished surface. They were then reweighed and stored on their sides on a plastic sheet to minimize the friction and to ensure that the curling measurements were not impacted by gravity. The wax was used because it is economical and easy to apply. The test has been found to be highly consistent, repeatable, economic, quantitative, and provides insight into both moisture loss (average coefficient of variation (COV) = 5.5%) and also the subsequent deflection caused by volume change of the paste (COV = 8%).

3.3.3 Measurement

As shown in previous works by Hajibabaee and Ley (2015) and Berke and Li (2004), these samples provide rapid results to compare many different curing techniques in a short time. Since the top surface of the sample was exposed to the drying environment this created a moisture gradient in the sample. This gradient caused differential shrinkage strains to occur and caused the specimen to curl significantly. These large deformations made them easy to measure. The sample was also easy to weigh because it was not too large.

To measure the curling, rubber bands were used to hold the ends of the specimen tightly against a flat aluminium plate with the uncoated surface of the specimen facing the plate. The distance between the aluminium plate and the specimen was measured at regular locations along the length with a caliper of 0.0127 mm accuracy. An overview is shown in Figure 3.1. The curling of the beam was symmetric and the maximum was at the middle of the beam. The loss of moisture of the sample was measured as weight loss over time with 0.1 g accuracy. Additional details can be found in (Hajibabaee & Ley, 2015).

3.3.4 Curing Methods

A flat nozzle (Chapin 5797) was used, as per the manufacturer, to apply the curing compounds. For all of the products, a pump pressure of 276 kilopascals was used to produce a spray angle of

80° and a flow of 1.4 kg/min. The suggested application rate by the manufacturer is 5.0 m^2/L, or 0.2 kg/m^2 for the curing compounds used in this study. Values above and below this rate were investigated to understand and quantify the impact of coverage on the performance.

To modify the application of the compounds, three different nozzle heights were used with the same cart velocity. A cart was constructed that holds the nozzle at a controlled height. The cart was moved across the sample at a constant velocity by placing marks on the track at a known distance apart. A metronome was used to help the cart operator move at the desired velocity. An overview of the cart is shown in Figure3.2. For this testing the velocity of the cart was kept constant and the application rate was adjusted by changing the height of the spray nozzle. To check the uniformity of the coverage, tests were done using steel plates of known areas placed at the same height as the specimen. These plates were weighed before and after applying curing compounds. By using the area of the plate and the weight of the curing compound the coverage was calculated.

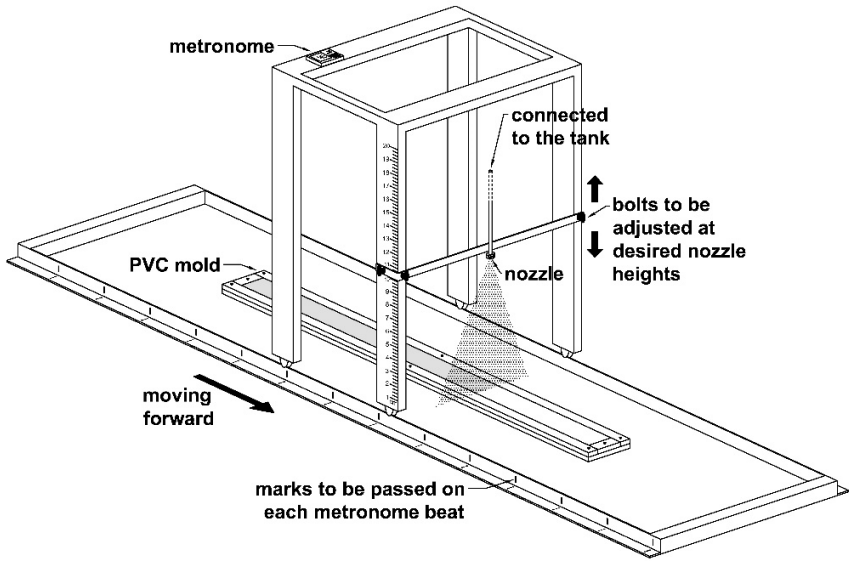

Figure III.2 The cart, nozzle, and tracks and holds to uniformly spray the curing compound

Curing compounds were applied in a single layer on the finished surface of the samples. Also a double layer of curing compound C3 was applied in two equal layers whose sum equaled the reported values. The second layer was applied right after the first one at the same rate and in the same direction. A combination of wet curing for one day followed by an average coverage 0.15 kg/m^2 of C3 was also investigated. Samples were also wet or sealed cured for one and three days. For wet curing, samples were kept in saturated burlap for one and three days of additional curing after demolding and waxing. The burlap was wetted every day to ensure that it remained saturated. After the curing was removed the specimens were subjected to a 40% relative humidity and 23 °C drying environment within an environmental chamber. Sealed cured samples were kept in sealed plastic bags for one and three days within this chamber. This curing was similar to the wet burlap, but no external moisture was added to the specimens during the curing process. Also, three samples were sealed continuously in the plastic bag to cease the external drying. These samples represent an ideal case with the curing compounds and so show a useful comparison.

3.3.5 Statistical Analysis Methods

The results were statistically analyzed with an analysis of variance (ANOVA) together with a Duncan's multiple range pairwise comparison. ANOVA is an appropriate procedure for testing the equality of several means. Duncan's multiple range pairwise comparison is useful for pairwise comparison of group means. This is useful to establish the population means of two groups are statistically different from one another (Duncan, 1955; W. G. Hunter, Hunter, & George, 1978). In the ANOVA, the dependent variable was the mean of the weight loss value or the maximum curling values, and the independent variable was the curing method or application rate. The statistical analysis was undertaken to evaluate the significance of difference between averages of weight losses or curling values for different curing methods. In addition, one-way ANOVA was used to determine the significance of difference between results of different application rates for

various curing types. A Duncan's grouping was also performed to determine statistically different and similar means.

Also, a regression analysis was used to find regression models for the maximum curling versus application rate and weight loss versus application rate for each of the curing compounds and to approximately interpolate the weight loss and maximum curling of a given application rate (manufacturer's recommended application rate). It should be noted that the regression with the highest F-statistic, lowest p-value, and highest adjusted R-squared was taken as the most reliable (Kutner, Nachtsheim, & Neter, 2004).

3.4 RESULTS

The weight loss after 72 hours of drying versus the coverage for different curing compounds is shown in Figure 3.3.

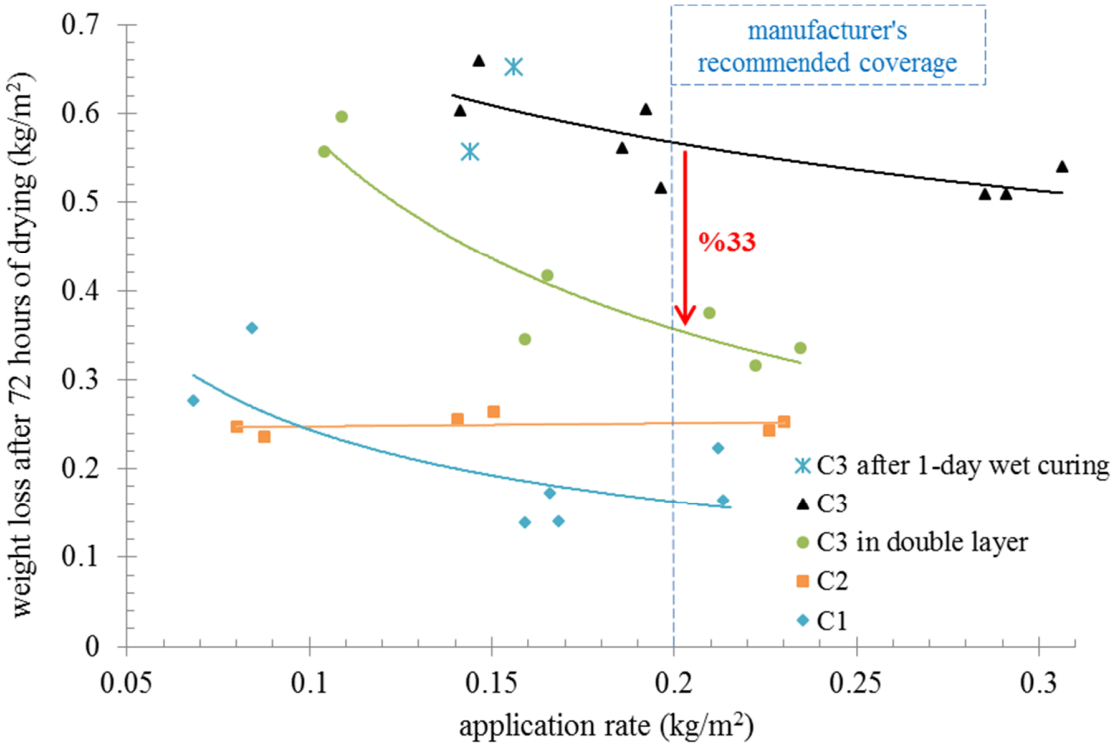

Figure III.3 Comparison between the weight loss of samples after 72 hours versus different coverage of curing compounds. The solid lines show the trendlines as described in Table A1.

While it is possible that these membranes may be removed or abraded over time, this work is focused on the effectiveness of curing over a three day period, because:

- ASTM C309 restricts the loss of water in 72 hours to not more than 0.55 kg/m^2 for mortar samples. Although this moisture loss limit was not used in this testing, the 72 hour time period still proved to be a useful point to compare the performance of the materials.
- Previous research found that over 75% of the weight loss happened within the first 72 hours of drying (Hajibabaee & Ley, 2015).

Figure 3.4 shows the maximum curling deflection versus the application rate of the different curing compounds. Samples were measured each day until the maximum amount of curling was

reached. This typically occurred within 10 days. Afterwards curling was measured every three days for a few months. Also included in the graph is a specimen that was wet cured for one day and covered with a single layer of curing compound C3, labeled as "C3 after 1-day wet". The manufacturer's recommended dosage is shown as a dashed line.

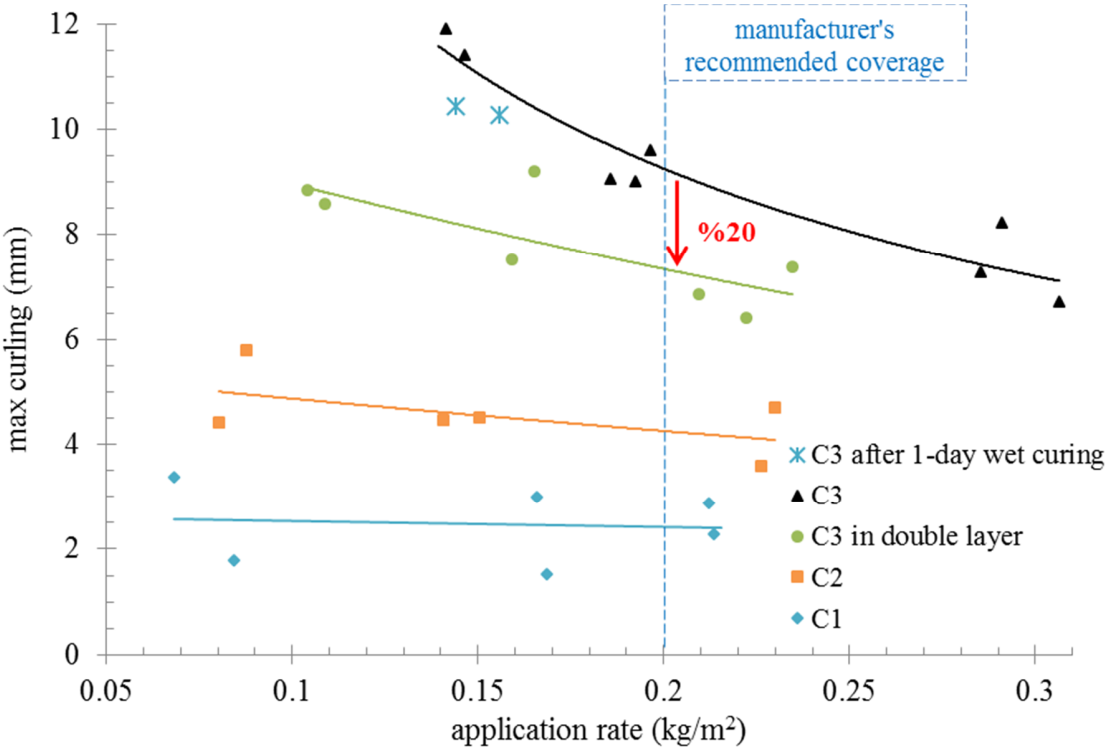

Figure III.4 Comparison between the maximum curling of samples cured with different coverage of curing compounds. The solid lines show the trendlines as described in Table A1.

Figures 3.5 and 3.6 use bar charts to show the calculated values from the regression analysis for the weight loss after 72 hours and the maximum curling deflection for a collection of samples. These calculated values are also normalized to weight loss and maximum curling of no cured samples, respectively. The regression analysis allowed all curing compounds to be compared at a known value. The maximum curling deflection occurred at different times for different samples.

Samples that are wet or sealed cured for one day, three days, and continuously sealed are also included for comparison using their average weight losses and maximum curling deflections measured from three samples for each curing method. Therefore, the standard deviation values for these average values are shown as well.

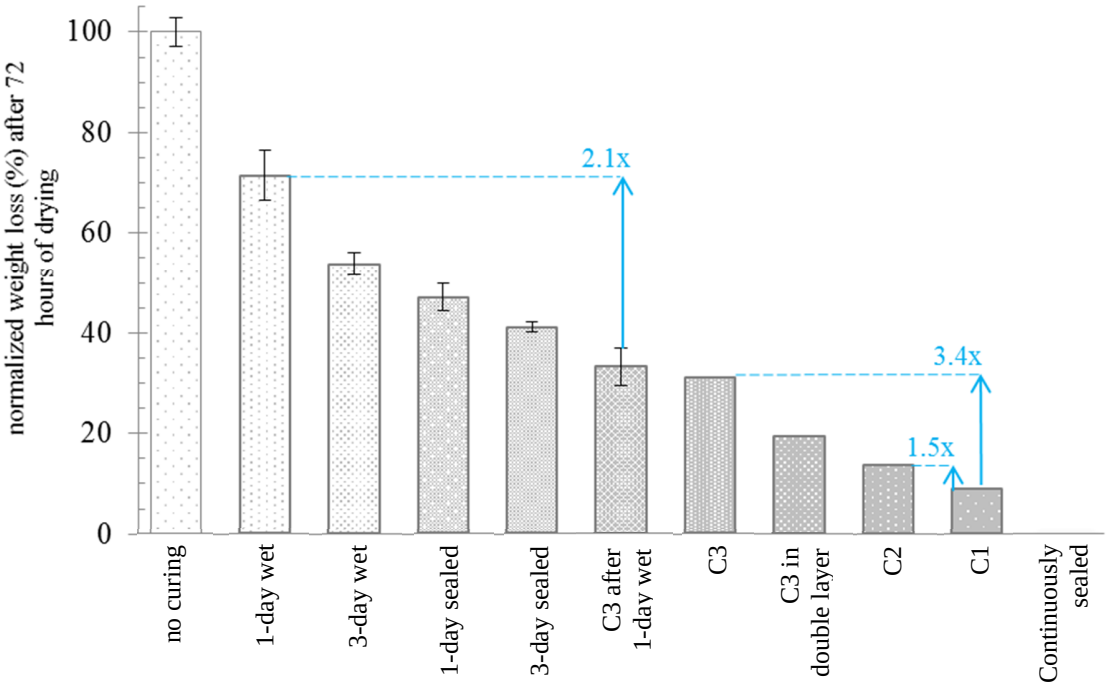

Figure III.5 The weight loss of samples after 72 hours; curing compound methods have a manufacturer's recommended application rate of 0.2 kg/m^2. The Y-axis is normalized to weight loss of no cured samples. The error bars represent one standard deviation from three different samples.

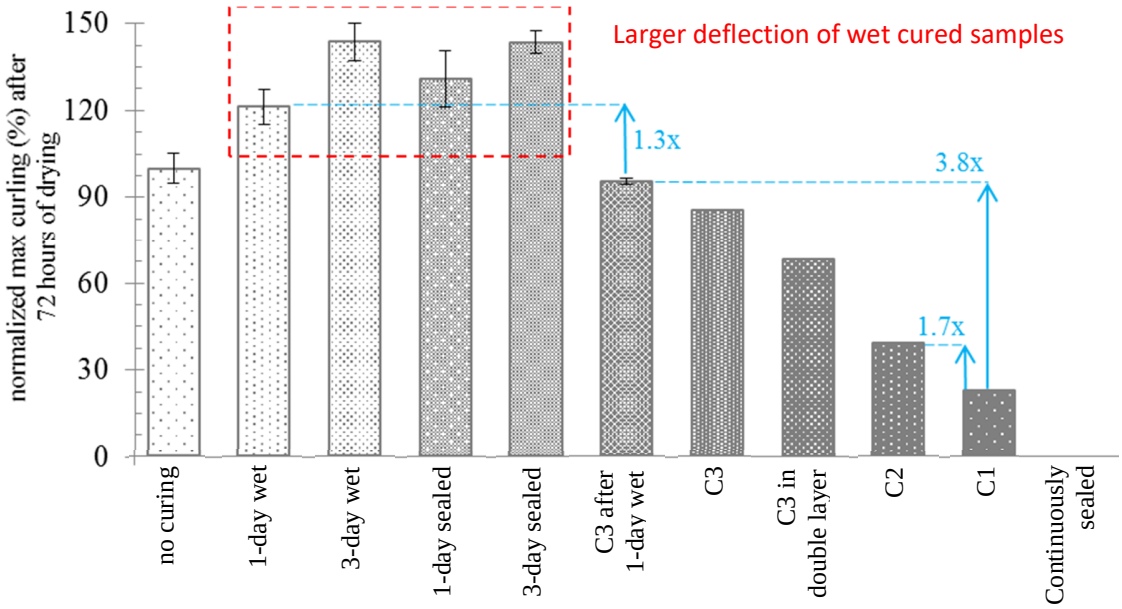

Figure III.6 The maximum curling of samples after 72 hours; curing compound methods have a manufacturer's recommended application rate of 0.2 kg/m^2. The Y-axis is normalized to maximum curling of no cured samples. The error bars represent one standard deviation from three different samples.

Next, the regression models were used in Figure 3.7 to show the performance of the different curing methods at equivalent costs. Three different equivalent costs were shown in the graph.

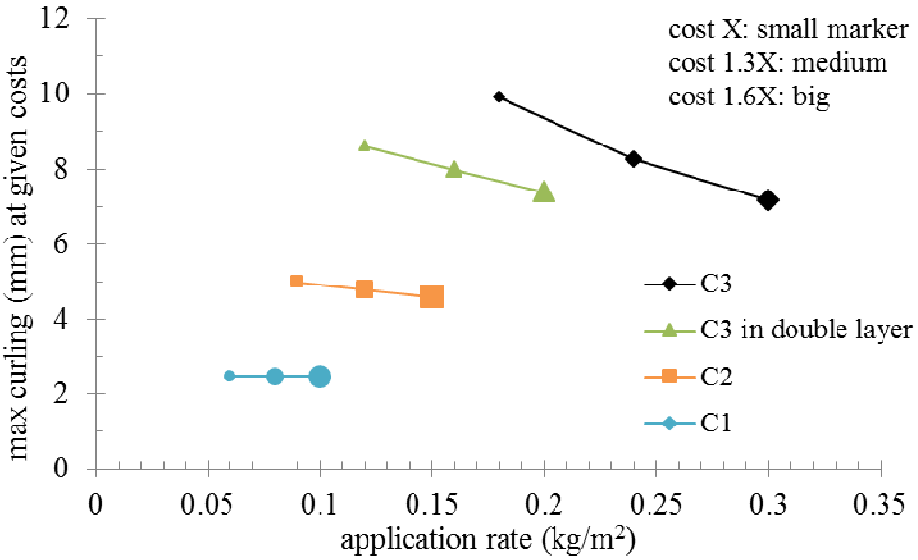

Figure III.7 The maximum curling of samples cured with different methods for costs X, 1.3X, 1.6X shown with markers small, medium, and big, respectively.

A summary of the regression analysis for the weight loss and maximum curling has been included in Table A1 in the appendix. These regression models are used in Figures 3.3 and 3.4. A summary of the statistical analysis are given in Tables 3.3, 3.4, and 3.5.

Table III.3 One-way ANOVA and Duncan's multiple range pairwise analyses for weight loss

C1			C2		
Application rate mean (kg/m^2)	Weight loss mean (kg/m^2)	Duncan's grouping[1]	Application rate mean (kg/m^2)	Weight loss mean (kg/m^2)	Duncan's grouping[1]
0.08	0.32	A	0.08	0.24	C
0.16	0.15	B	0.15	0.26	C
0.21	0.19	B	0.23	0.25	C
p-value (%)		2.03	p-value (%)		16.30
C3			C3D		
Application rate mean (kg/m^2)	Weight loss mean (kg/m^2)	Duncan's grouping[1]	Application rate mean (kg/m^2)	Weight loss mean (kg/m^2)	Duncan's grouping[1]
0.14	0.63	D	0.11	0.58	F
0.19	0.56	D & E	0.16	0.38	G
0.29	0.52	E	0.22	0.34	G
p-value (%)		4.53	p-value (%)		0.46

[1] Duncan's grouping labels (e.g. "A" and "B") are used to show groups of different statistically significant means. Results with the same letter are statistically similar. Where two letters are reported then the mean could belong to either group. Each table shows a separate analysis and is not meant to be comparable. This means that an "A" label in one table is not comparable to the same label in another table.

Table III.4 One-way ANOVA and Duncan's multiple range pairwise analyses for max curling

C1			C2		
Application rate mean (kg/m^2)	Max curling mean (mm)	Duncan's grouping[1]	Application rate mean (kg/m^2)	Max curling mean (mm)	Duncan's grouping[1]
0.07	2.58	A	0.08	5.11	B
0.16	2.26	A	0.15	4.50	B
0.21	2.58	A	0.23	4.14	B
p-value (%)		92.55	p-value (%)		49.02
C3			C3D		
Application rate mean (kg/m^2)	Max curling mean (mm)	Duncan's grouping[1]	Application rate mean (kg/m^2)	Max curling mean (mm)	Duncan's grouping[1]
0.14	11.66	C	0.11	8.71	F
0.19	9.23	D	0.16	8.36	F
0.29	7.41	E	0.22	6.88	F
p-value (%)		0.11	p-value (%)		8.22

[1] Duncan's grouping labels (e.g. "A" and "B") are used to show groups of different statistically significant means. Results with the same letter are statistically similar. Where two letters are reported then the mean could belong to either group. Each table shows a separate analysis and is not meant to be comparable. This means that an "A" label in one table is not comparable to the same label in another table.

Table III.5 One-way ANOVA and Duncan's multiple range pairwise analyses for curing type

Curing compound	Application rate range (kg/m^2)	Weight loss		Max curling	
		Mean (kg/m^2)	Duncan's grouping[1]	Mean (mm)	Duncan's grouping[1]
C1	0.16-0.21	0.17	A	2.42	A
C2	0.14-0.20	0.25	B	4.32	B
C3	0.15-0.20	0.59	C	7.47	C
C3D	0.16-0.24	0.36	D	10.20	D
p-value (%)		<0.01		<0.01	

[1] Duncan's grouping labels (e.g. "A" and "B") are used to show groups of different statistically significant means. Results with the same letter are statistically similar. Where two letters are reported then the mean could belong to either group. Each table shows a separate analysis and is not meant to be comparable. This means that an "A" label in one table is not comparable to the same label in another table.

3.5 DISCUSSION

3.5.1 Application Rate

Figures 3.3 and 3.4 show that, in general, as the coverage rate increased for a curing compound the weight loss of the samples decreased after 72 hours of drying and so did the magnitude of the ultimate amount of curling of the sample. This improvement in performance is expected as an increase in the thickness of the applied curing compound should more effectively seal the specimen and reduce water loss. With reduced water loss there will be reduced moisture gradients within the sample and therefore less curling. However, C2 showed almost no change in weight loss after 72 hours over all of the coverages investigated. Based on one-way ANOVA, the difference between weight losses with an increase in application rate is significant with 95% confidence level for all curing types except C2. Moreover there is no significant difference between maximum deflections with an increase in application rate for all curing types except C3. Duncan's grouping results based on the significance of difference between averages of weight losses and maximum curling values are in agreement with ANOVA results. This suggests that to

get the best results with the lower performing curing compounds, such as C3, the application rate must be increased.

3.5.2 Curing Compound Type

The weight loss and maximum curling was compared between 0.141 and 0.235 kg/m^2 to statistically determine difference in curing compound performance. Based on ANOVA and Duncan's multiple range pairwise comparison results for coverage rates between 0.14-0.24 kg/m^2 there is a probability of less than 0.01% that the average weight loss and maximum curling value for different curing types are the same. This means that the curing type effect on weight losses and maximum curling values is significant.

As seen in Figures 3.3-6, the water-wax based curing compound (C3) showed increased moisture loss and curling followed by the water-resin based curing compound (C2) and the poly-alphamethylstyrene based compound (C1) performed the best at similar coverage rates. The curing compounds with the highest VOC levels performed the best in the testing and the lower VOC levels performed the worst. This finding matches previous work (Taylor, 2013; Whiting & Snyder, 2003).

The improved performance by the solvent based curing compounds C1 is likely due to three different effects. First, the sealing material in the solvent solution is more miscible and so easier to place in suspension. Second, the solvent based curing compounds should provide more uniform coverage due to the improvements in wetting provided by solvents when compared to water based curing compounds. Dhir et al. (1989) have also suggested that solvent-based curing compounds have less vapor permeability than water-based curing compounds which may also be important.

3.5.3 Double Layer Application of Curing Compound

As shown in both Figures 3.3-6, a double application of curing compound C3 showed better performance than a single application for equal amounts of curing compound that is statistically significant based on ANOVA and Duncan's pairwise comparison over the application rates investigated. When compared at the manufacturer suggested coverage the double layer showed a 33% reduction in the weight loss and a 20% reduction in the amount of maximum curling. As the application rate of the curing compound increased then the difference in curling also decreased.

Shariat and Pant (1984) suggested that a single layer of curing compound causes either non uniform coverage or imperfections in the formed membrane. It is possible that the double application allowed imperfections in the first coating to be covered by the second without increasing the amount of material used. This is not surprising as paints and coatings are suggested to be applied with multiple coats in order to get uniform coverage. This seems to also apply to curing compounds. This improvement in curling reduction may not be as beneficial with curing compounds of superior performance such as C1. For example, curing compound C1 did not show improvements in performance with increased coverage and so there may be less imperfection with this curing compound.

3.5.4 The Use of Curing Compounds after Wet Curing

Some specifications have started requiring combined curing methods to try and provide a synergistic effect between the two methods. One common technique is to first wet cure concrete and then provide a curing compound to reduce subsequent moisture loss. By using curing compound C3 after 1-day of wet curing it was possible to reduce the moisture loss and maximum curling compared to a sample that was wet cured for 1-day and then allowed to dry. Figures 3.5 and 3.6 show that samples with only a day of wet curing had 210% more weight loss at 72 hours and 130% higher maximum curling compared to the combined curing method. This means that the external water provided during the wet curing was retained within the sample and was

available to promote hydration in the surface of the concrete. For certain concrete structures the combined method of using wet curing and the subsequent applications of curing compounds has potential to help maintain a high moisture content in the concrete for extended periods and should be investigated further.

3.5.5 Comparison of Different Curing Methods

Figure 3.5 shows that samples that were not cured or received wet or sealed curing for one and three days show significant water loss on removing the curing. Samples with no additional curing showed the maximum weight loss of the samples investigated, most likely due to a higher permeability on their exposed surface (Gowriplan et al., 1990; Ramezanianpour & Malhotra, 1995). The wet cured samples also had a considerable amount of weight loss after 72 hours of drying due to the loss of the extra water added over the curing period. However, as shown in Figure 3.5, this value after 72 hours of drying is still less than the sample that was not cured. This decrease in moisture loss in both wet and sealed curing compared to no cured samples is likely due to the decrease in surface permeability caused by the prolonged curing. This has been discussed previously by Hajibabaee and Ley (2015). All of the samples with curing compounds showed less weight loss compared to other methods. This can be attributed to the formation of a film created by the curing compound on the surface of the concrete or blocking the pores. Both of these phenomenon will reduce evaporation.

When comparing the performance of sealed and wet cured samples in Figure 3.5, the magnitude of the weight loss between different curing periods is high but the deformations caused by drying shown in Figure 3.6 are not. This might be because the extra water provided during wet curing fills the larger pores and can be lost more easily without causing subsequent shrinkage and consequently the curling. Figure 3.6 also shows that increasing the duration of wet or sealed curing increased the maximum curling, as shown with the dashed red box. This has been attributed to the extended curing causing a decrease in the pore sizes (Hajibabaee & Ley, 2015),

increase in saturation of the microstructure at a given moisture content (Hajibabaee, Grasley, et al., 2016; Hajibabaee & Ley, 2016), and then a subsequent increase in the ultimate pressures upon drying according to Eq. (3.1). This differential shrinkage in the specimen leads to increased curling according to Eq. (3.2). Samples that used curing compounds had the lowest amount of curling of the specimens investigated, as shown in Figure 3.6. This is likely due to the curing compound reducing the moisture loss in the sample. If little moisture was lost in the sample, this means that there was little external drying compared to uncured or wet cured samples after exposure to drying. Therefore, according to Eq. (3.1), the relative humidity h does not change significantly, i.e. remains high, and the capillary pressure p_c does not considerably increase the one-dimensional drying shrinkage ε_d. Therefore, there was little differential drying shrinkage and so little curling. In an ideal curing method, such as a sample that is continuously sealed as shown in Figures 3.5-6, the external drying is ceased, and so the external moisture loss and curling from differential drying does not occur. This observation explains the superior performance of curing compound C1, as this material has the biggest reductions in drying.

As shown in Figure 3.5-6, C3 had 340% more weight loss and 380% more curling than C1 at the recommended application rate of 0.2 kg/m2. Curing compound C2 showed 150% more weight loss and 170% more curling than C1 at this same rate. This suggests that C1 may be used at a lower application rate and achieve similar performance while also reducing costs.

3.5.6 Cost Comparison

Using the chosen regression models Figure 3.7 shows the maximum curling of curing compounds for coverage rates of equal costs. For comparison, the cost of curing compound C3 at the manufacturer's recommended dosage has been used as unity. This was chosen as C3 was the least expensive and the lowest performing product. Data points are also shown for costs that are 30% and 60% more. This was done to allow one to compare the performance of the curing compounds

at equivalent costs or to find the costs at equivalent performance between curing methods. The double layer application was assumed to cost 1.5 more than a single layer. This cost increase was for the increase in labor for the second layer. The data shows that certain curing compounds perform better than others at comparable costs. It also shows that increasing the coverage of C3, the water-wax based curing compound, in one or two layers has some increase in performance, but not as much as when a better performing curing compound is used.

By quantifying the interplay between curling and curing compound application rate, it may help users justify the use of higher cost curing compounds where high quality curing is needed. The data also shows that lower application rates of C1 may be able to be used to save costs while still providing a similar or improved performance over other curing compound types.

This work shows that a double application of the curing compound is able to improve curling performance without increasing the amount of material or cost, at least according to the assumptions in this paper. This would be a simple way to decrease moisture loss and curling without significantly increasing material costs.

3.5.7 Practical Implications

In the 23 °C and 40% RH drying conditions investigated, the ability of the curing compounds to reduce moisture loss was shown. This performance is beneficial to reduce the moisture gradient and subsequent volume change of the concrete.

It was also shown that not all curing compounds are equivalent. The research showed that the poly-alphamethylstyrene based curing compound provided the best moisture retention of the curing compounds investigated. However, this material is roughly 300% more expensive than the wax based compounds and 150% more expensive than the compound with resin base. However, this work showed that poly-alphamethylstyrene continued to show superior performance at lower

application rates or the same level of cost. This may be a way to reduce the cost of the curing compound and still achieve outstanding performance.

A double layer application of curing compounds showed an increased effectiveness of water retention without increasing the amount of material used. This is a useful finding and supports the recommendation that a double layer of curing compound should become common practice much like it is with paint and other coatings.

It should be noted that all the specimens investigated were paste beams that were prepared in the laboratory and so the curing compound was applied on a smooth surface. Field concrete may have a rough surface with tines, broom finish, or carpet drags. This increase in surface texture makes the required amount of curing compound more challenging to predict. Imprecise equipment and wind can also cause non uniform coverage. Because of these issues, greater coverage rates and a larger number of applications may be needed to provide satisfactory performance and should be investigated for other applications. However, it is expected that the trends from this work would still hold.

The use of wet curing followed by the usage of a curing compound did not show the rapid drying that is typically observed with wet cured specimens after the curing is removed. This means that the curing compound helped keep this additional water in the concrete and promote hydration. This in turn would create a dense and low permeability pore structure that should improve the durability and strength of the surface of the concrete.

3.6 CONCLUSIONS

This work examined the impact of different curing compounds at different application rates on paste samples that were stored in a 23 °C and 40% relative humidity environment. All samples were only allowed to dry through the cured surface to evaluate the ability of the curing method and paste to retain moisture and resist volume change from differential drying. Different curing

compound types at different application rates were investigated and compared to samples that were wet, sealed, and not cured. Investigations were also done with double layers of curing compounds and combinations of wet curing followed by a curing compound. A statistical analysis was used to evaluate the significance of the measured differences between results for application rate and curing type. A number of useful conclusions can be made:

- At the manufacturer recommended application rate the Type 2-Class-B poly-alphamethylstyrene curing compound (C1), had the least weight loss and dimension changes, followed by the Type 2-Class B water-resin curing compound (C2), and then the water-wax based curing compound (C3).

- This same order of performance was found when the curing compounds were applied at a comparable cost.

- As the coverage rate increased for the water-wax based curing compound then so did the performance. However, the water-resin and poly-alphamethylstyrene curing compounds did not show statistically significant improvement in performance with increased coverage rates.

- The double application of the water-wax based curing compound with the same coverage rate of a single application was shown to be statistically different and able to reduce weight loss by over 30% and curling by 20% when used at the manufacturer's application rate.

- While curing compounds are in place they limit moisture loss to a greater degree than the paste after wet curing has been removed. This reduction in moisture loss reduces the differential drying shrinkage because of a reduced moisture gradient and therefore reduces the curling.

- Although not as effective at moisture retention as a plastic sheet, curing compounds can stay in place for longer periods of time and continue to retain moisture.

- A combination of wet curing then a subsequent application of curing compound reduces moisture loss when compared to the samples that only have the wet curing.

The work shows that curing compounds can be used on members that are sensitive to drying, such as slabs on grade and pavements, to reduce their moisture loss and subsequent curling. This work shows that curing compounds of different types and costs have statistically different performance. The quantitative nature of this work has allowed performance and cost comparisons to be made that may help justify construction practices or increase expenditures on curing in order to improve moisture retention or reduce curling. Although this work was done with paste specimens, the trends from these findings should hold for concrete samples. While curing is widely agreed to be useful to concrete, more quantitative work is needed to compare the performance of concrete with different levels of surface texture and application procedures.

3.7 ACKNOWLEDGMENTS

The authors would like to thank the Oklahoma Department of Transportation (ODOT 2208) and the Oklahoma Transportation Center (OTCREOS10.1-24) for funding the work. The following individuals also deserved acknowledgement for their help in completing the experiments: Basil Abdulkareem, Jake LeFlore, Nicholas Ley, David Porter, and Paul Field.

CHAPTER IV

IV. THE IMPACT OF WET CURING ON CURLING IN CONCRETE CAUSED BY DRYING SHRINKAGE

4.1 ABSTRACT

This paper examines the impact of wet curing with different durations on differential drying shrinkage of concrete beams. The work shows that in severe drying conditions the magnitude of curling increased with the duration of wet curing of concrete specimens. Testing results are presented along with an explanation for the mechanisms observed. These findings provide guidance for wet curing durations for concrete slabs that must be resistant to volume change from drying.

Keywords Capillary tension; Concrete pavement; Degree of saturation; Drying shrinkage; Wet curing

4.2 INTRODUCTION

It is common in concrete members with large surface to volume areas, such as slabs on grade or concrete pavements, to have vertical movement from differential temperature, moisture, and shrinkage over the depth of the member. This is referred to as curling. The movement is a problem if the edges or middle of a slab curl upward and lose contact with the foundation. This will cause increased stresses from gravity loads and cause cracking, or impact ride quality. This can be a significant problem, as this may lead to premature failures, costly repairs, or unsafe

working conditions for industrial slabs on grade (Darter, Khazanovich, Snyder, Rao, & Hallin, 2001; Hiller & Roesler, 2002; Hveem & Tremper, 1957; Zollinger & Barenberg, 1989).

The moisture distribution in a concrete slab is assumed to be uniform before drying begins and it starts changing as concrete loses moisture (Hedenblad, 1997). Depending on the length of the drying period, external relative humidity, temperature, and the initial water content, the moisture gradient can be quite complicated, resulting in a strain profile from drying. The analysis of this strain profile is even more complicated if the temperature and moisture fluctuate simultaneously and the slab experiences creep strains from its self-weight. Previous studies on concrete pavements showed that a combination of both temperature and moisture have been documented to cause curling (Hveem, 1951). Moreover, if a concrete member is only allowed to dry from one side, then this will in turn lead to a differential shrinkage strain in the member and will cause the edges of the slab to lose contact with the foundation (Ytterberg, 1987a, 1987b, 1987c). This behavior has been observed in the field as moisture barriers placed under concrete slabs were shown to cause problematic curling when drying occurred (ACI-302.1R, 2004; Anderson & Roper, 1977; Nicholson, 1981; Turenne, 1978).

A number of properties of the concrete mixture and construction practice can impact the long-term drying shrinkage of concrete. After placing concrete, it is common to protect the concrete from moisture and temperature loss by curing it with wet coverings. These coverings supply moisture to the surface of the concrete to promote continued hydration. Rapid moisture loss from the surface of a slab can cause plastic shrinkage cracking, reduce strength, increase permeability and lead to harmful impacts on the long-term durability and abrasion resistance. Therefore, prolonged wet curing is thought by many to provide only improvements in concrete performance, and it has been recommended for fresh concrete (ACI-302.1R, 2004; Aïtcin, 1999; Kosmatka et al., 2011). However, not all work has shown that extended wet curing is beneficial. For example, Perenchio (1997) observed an increase in drying shrinkage when concrete was wet cured for up to

seven days. The authors have also shown that extended wet curing of thin paste specimens can lead to increased curling when allowed to dry only from their surface (Hajibabaee & Ley, 2015).

The drying shrinkage of the cement paste is typically six to eight times greater than the amount observed in concrete (Bisschop, 2002). The shrinkage can be decreased by reducing the paste content and increasing the aggregate content (Tazawa, Miyazawa, & Kasai, 1995). Therefore, the shrinkage of the concrete ε_c is highly affected by the shrinkage of the cement paste ε_p, and the aggregate volumetric fraction g, which is typically between 60% and 80%. Pickett (1956) has suggested

$$\varepsilon_c = \varepsilon_p (1-g)^n, \qquad \text{Eq. (4.1)}$$

in which a constant n with values of 1.2 to 1.7 is used to fit the data.

One of the driving forces for shrinkage of an element is the capillary forces during drying within the pore network (Scott, Lane, & Weyers, 1997). Drying causes the loss of moisture in the pores and the formation of menisci on the walls. The formation of the menisci and generation of the capillary tension p_c can be related, according to the Young-Laplace equation (Adamson and Gast 1967; Radlinska et al. 2008)

$$p_c = -\frac{2\gamma}{r} = \frac{2\gamma\cos(\theta)}{a}, \qquad \text{Eq. (4.2)}$$

where γ is the surface tension of pore fluid, r is the radius of the curvature of the meniscus, θ is the liquid-solid contact angle, and a is the radius of cylindrical pore. When the pore structure is finer, the radius of the pore and the radius of curvature of meniscus will be smaller. The solid surfaces or pore walls will be pulled together by this negative pressure, causing the volume change or shrinkage.

Shrinkage of the paste ε_p can be defined as a function of capillary tension p_c, liquid water saturation S_l, bulk modulus of porous body with empty pores K_p, and bulk modulus of solid phase comprising the skeleton of the porous body K_s (Bentz et al., 1998; Mackenzie, 1950)

$$\varepsilon_p = \frac{S_l}{3} p_c \left(\frac{1}{K_p} - \frac{1}{K_s}\right), \quad \text{Eq. (4.3)}$$

$$S_l = \frac{\phi_l}{\phi} = \frac{w\rho_s}{\phi\rho_l}, \quad \text{Eq. (4.4)}$$

where ϕ_l is the volumetric content of liquid water, ϕ is the total porosity, w is the water content mass, ρ_s is the apparent density of the material, and ρ_l is the density of liquid water.

Due to the generation of hydration products and associated self-desiccation of the pore structure of the cement matrix, autogenous shrinkage occurs. This component is more important for concrete mixtures with w/c less than 0.40 (Tazawa, 1999). The autogenous shrinkage in concrete increases by reducing the w/c and increasing the cement fineness since the capillary tension mechanism will cause higher tension in the pore water of the finer structures (Bentz et al., 2001; Jensen & Hansen, 1996). These effects may increase the external drying previously described. This may lead to greater internal stresses and increased levels of cracking.

When concrete is exposed to external drying, the relative humidity is a controlling parameter. According to the Kelvin-Laplace equation, capillary tension is also related to the internal relative humidity (Adamson & Gast, 1967; Bentz, 2008)

$$p_c = -\frac{\rho_l RT}{M_v} \ln h = -\frac{RT}{V_m} \ln h, \quad \text{Eq. (4.5)}$$

where R is the universal gas constant, T is the absolute temperature, M_v is molar mass of water, V_m is the molar volume of water ($\approx 1.82\times10^{-5}\ \frac{L}{mol}$), and h is the internal relative humidity with values between 0 and 1. In this work, V_m is assumed to be constant. It should be noted that, for a constant temperature, decreases in relative humidity h will lead to increases in capillary tension. This will be discussed later in the paper.

It has been suggested in previous studies that the ultimate value of drying shrinkage should be multiplied by terms, like $1-(\frac{h}{100})^3$ (Bazant & Baweja, 2000) or $1-1.18(\frac{h}{100})^4$ (Gardner, 2000), to predict the drying shrinkage of the concrete at a certain relative humidity h . However, through a macro-level model based on the theory of nonlinear poroelasticity (Baroghel-Bouny et al., 1999; Coussy, 1995; Coussy et al., 1998), one can predict the one-dimensional drying shrinkage of cement or concrete as a function of relative humidity and a few physical properties. This model uses capillary pressures to predict for both drying and autogenous shrinkage for conditions of 44% relative humidity and above (Baroghel-Bouny, 1997). Other models and mechanisms may become more important below 44% relative humidity (Wittmann, 1973). This means that one-dimensional drying shrinkage strains ε_d can be predicted by using the capillary curve, the desorption isotherm S_l , and the bulk modulus K_0

$$d\varepsilon_d = \frac{1}{3}\frac{RT}{K_0 V_m}\frac{S_l}{h}dh. \qquad \text{Eq. (4.6)}$$

Several phenomenon are known to have an impact on the curling of concrete elements such as daily temperature and moisture gradients, built-in temperature gradient, creep, and differential drying shrinkage (Rao & Roesler, 2005). This work focuses specifically on how different

durations of wet curing can impact the drying shrinkage gradient and the consequent curling of the element when it is dried from only one surface. The mechanisms are then discussed and practical recommendation is provided for practitioners.

4.3 EXPERIMENTAL INVESTIGATIONS

4.3.1 Materials

The cement used in this test is type I, according to ASTM C150 (2011), and its chemical analysis is shown in the Table 4.1.

Table IV.1 The oxide analysis of the cement and its phase concentrations.

chemical test results (%)					
SiO_2	Al_2O_3	MgO	Fe_2O_3	CaO	SO_3
20.77	4.57	2.37	2.62	62.27	3.18
Na_2O	K_2O	TiO_2	P_2O_5	SrO	BaO
0.19	0.32	0.34	0.14	0.22	0.07
phase concentrations (%)					
C_3S		C_2S	C_3A	C_4AF	
52.13		20.22	7.68	7.97	

Samples were made with dolomitic limestone aggregate and natural river sand used commercially in concrete. An ASTM C618 (2008) class C fly ash was also used. The chemical analysis is shown in Table 4.2.

Table IV.2 The oxide analysis of the fly ash used in the testing.

chemical test results (%)						
K_2O	BaO	MgO	SrO	CaO	SO_3	Na_2O
0.58	0.72	5.55	0.39	23.12	1.27	1.78
SiO_2	Al_2O_3	MnO_2	P_2O_5	Fe_2O_3	TiO_2	
38.71	18.82	0.02	1.46	5.88	1.35	

4.3.2 Mixture Proportions and Procedures

In the mixtures investigated a water to cement ratio (w/cm) of 0.42 was used. All of the aggregate, both coarse and fine, were brought into the temperature controlled mixing facility at least a day before and their batch weights were corrected for the moisture content. The aggregates were charged into the mixer along with approximately two-thirds of the mixing water. The combination was mixed for three minutes. Next any clumped fine aggregate was removed from the walls of the mixer. Then the cement and fly ash was loaded into the mixer, followed by the remaining mixing water. The mixer was turned on for three minutes. Once this mixing period was complete, the mixture was left to "rest" for the following two minutes while the buildup of material along the walls was removed. Next the mixer was allowed to run for three minutes. The slump (ASTM-C143/C143M, 2010), unit weight (ASTM-C138/C138M, 2010), and the air content (ASTM-C231/C231M, 2010) were measured. The mixture proportion used for a cubic meter is presented in Table 4.3.

Table IV.3 The mixture proportions used in this experiment per cubic meter.

cement (kg/m^3)	fly ash (kg/m^3)	course aggregate (kg/m^3)	fine aggregate (kg/m^3)	water (kg/m^3)
267	66.7	1094.7	736.1	136.8

4.3.3 Sample Preparation, Casting and Curing

The specimens used for this work are a simplified version of much larger beam tests by Hansen et al. (2007), Springenschmid et al. (2001), and Hajibabaee (2011). By studying these smaller elements it was possible to investigate a greater number of samples and variables more economically. Also, it allowed the mass change to be measured in addition to the strain and relative humidity. This is not possible with the larger beam tests previously investigated.

For this work all drying is assumed to originate from the top surface of the slab. To ensure this, a waterproof membrane is used on all faces of the sample except for the finished surface. An overview of these beams is shown in Figure 4.1.

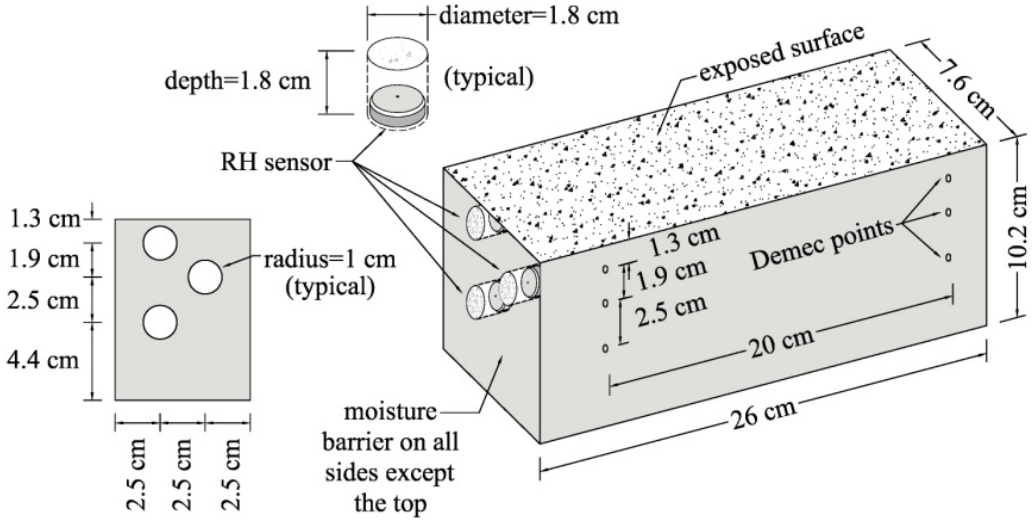

Figure IV.1 An overview of the sample investigated for this testing

For this testing, all specimens were cast and stored in an environmental chamber at 23 °C and 40% relative humidity. In this experiment the specimen was 7.6×10.2×26 cm. The moisture barrier was used as a form liner during casting. This material had a plastic waterproof membrane on one side and fibers on the other. The fibers were oriented so that they bonded to the wet concrete and provided a tight fit of the water proof layer on the outside of the beam.

This specimen was carefully demolded 24 hours after casting, and the interfaces between the membrane and the concrete were sealed by wax. Specimens were prepared with no-curing and 7 and 14 days of wet curing with wet burlap and a plastic tarp. While drying, the beams were flipped on their side and placed on wooden dowels to minimize the impact of the self-weight on the curling measurements.

4.3.4 Test Procedure and Measurement

4.3.4.1 Deflection and strain measurements

The strain of the beam was measured at 3 different depths, as shown in Figure 4.1. Surface mounted stainless steel gage points were glued to the beams. This was done by first burning through the membrane in a localized area and then gluing one of these gage points. Each gage point had a machined cone in the surface that fit within a hand held mechanical strain gage. The accuracy of this gage was 4 microstrain.

4.3.4.2 Relative humidity

The relative humidity of the beams was measured at 1.3 cm, 3.2 cm, and 5.8 cm from the finished surface starting four days after the termination of curing. This was done by using the DS1923 Hygrochron Temperature/Humidity Logger iButtons. The sensors were placed into the side of the concrete in 1.8 cm deep holes with 1.8 cm diameter that were cast into the sample. These sensors were programmed to take relative humidity measurements every hour. The gages were inserted after four days of curing to prevent failure due to the high amount of moisture in the concrete. After demolding, the holes were sealed with water poof tape.

The relative humidity sensors were calibrated according to ASTM E104 (2012) with four different salt saturated solutions. The relative humidity calibration range was between 57.6% and 97.3%. This was chosen in order to cover the ranges of humidity expected inside the concrete during the testing. A specific calibration was generated for each sensor before testing and applied to all subsequent measurements.

4.3.5 Beam Deflection

While the measurements of differential shrinkage are helpful, the focus of this work is on determining the impact of this phenomenon on the curling of concrete members. By using regression analysis with $0.96 \le R^2 \le 1$, the strain function $\varepsilon(y,t)$ is fitted to measured

shrinkage values at certain time t and different heights y . Then the maximum deflection $\delta_{\max}$ of the concrete beam is estimated by Euler-Bernoulli equation

$$\delta_{\max}(t) = \frac{3l^2}{2L^3}\int_0^L \varepsilon(y,t)\,y\,dy, \qquad \text{Eq. (4.7)}$$

assuming spatial variations in the mechanical properties are negligible. In Eq. (4.7), l is the length of the idealized concrete beam that is 26 cm and L is the thickness of the concrete beam which is 10.2 cm. This thickness matches the size of the tested specimens. This helps minimize artifacts caused by size effects in the analysis. Other effects such as base friction or support were not accounted for in this analysis.

4.4 RESULTS

Figure 4.2 shows the percentage of mass change of the beams after casting for different curing techniques.

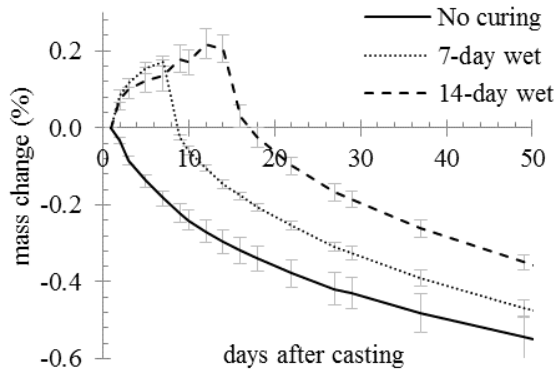

Figure IV.2 The percentage of mass change after casting; the first 7 and 14 days show the mass gain in wet cured specimens.

Figures 4.3a-b show the strain and relative humidity profiles over the depth of different specimens for no-curing, 7, and 14 days of wet curing. The mass change, strain, and relative

humidity values are the average amounts from the three samples used for each method. The profiles in Figure 4.3 are shown for 5, 10, 25, and 50 days after exposure to drying to make it easier to observe the trends in the data.

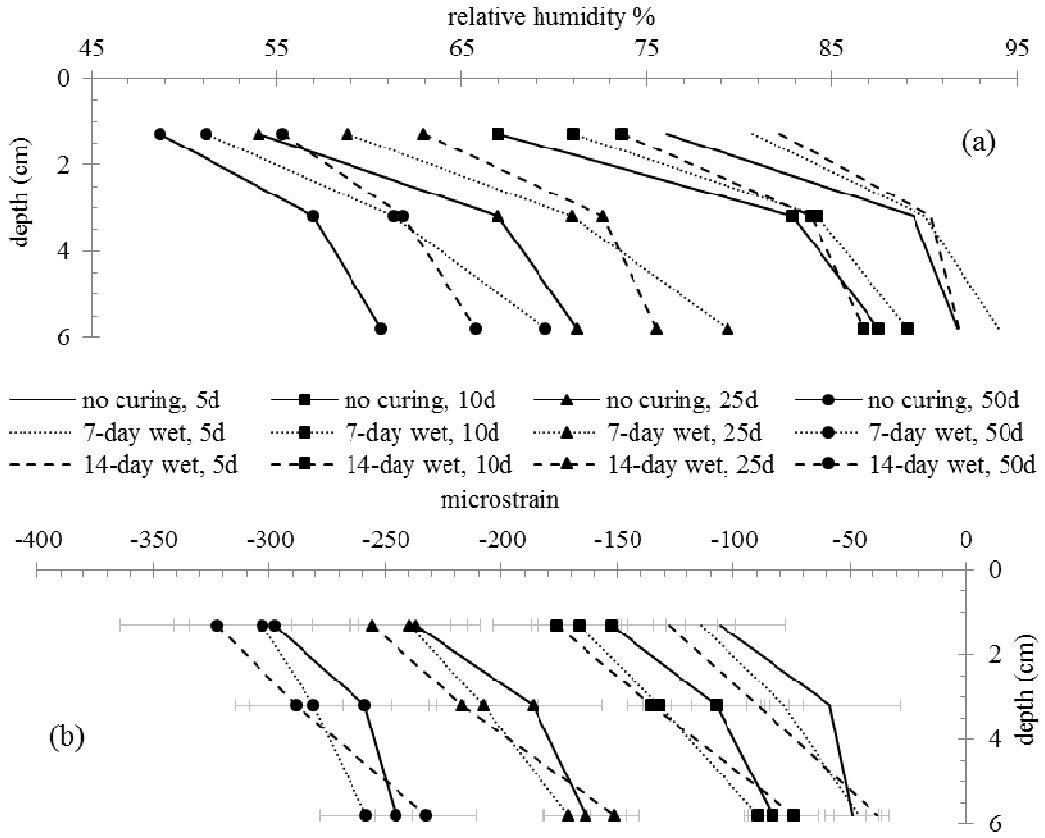

Figure IV.3 (a) The relative humidity and (b) the strain profiles for 5, 10, 25, and 50 days of drying.

While Figure 4.3 contains data at a few days, all of the collected data is shown in Figure 4.4. The strain versus the relative humidity at depths 1.3 cm, 3.2 cm, and 5.8 cm is shown in Figure 4.4. The data from 10 and 25 days after exposure are shown with empty and filled markers respectively. The R-squared values in the graph are for linear regression between relative humidity and strain.

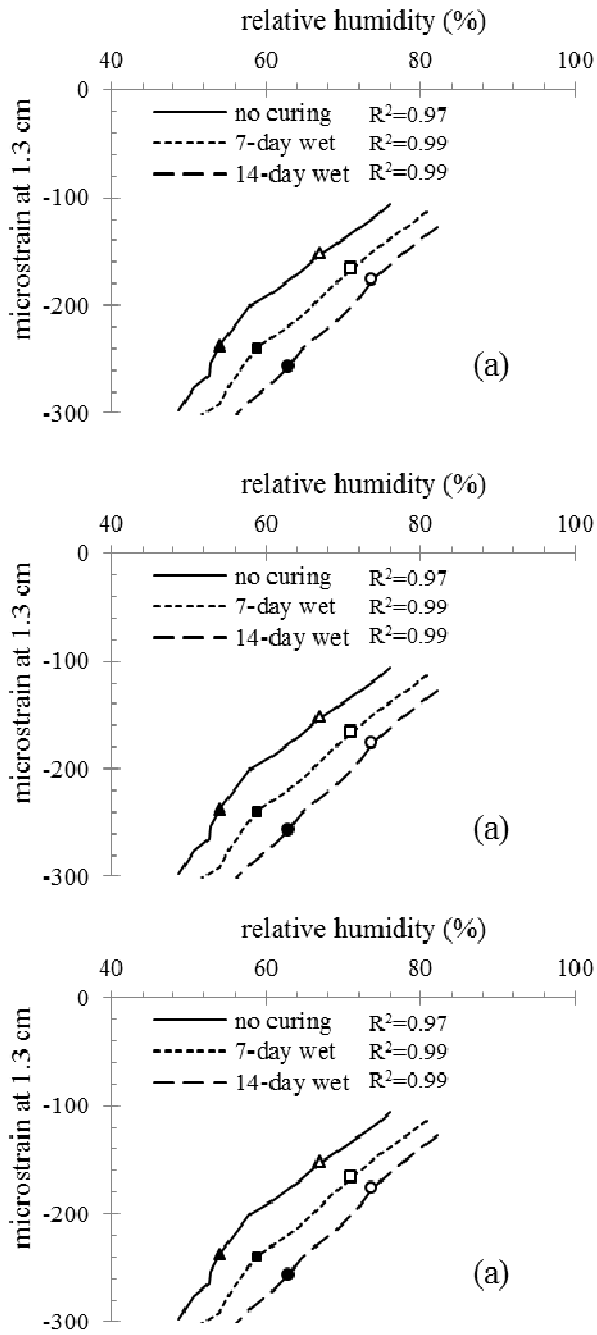

Figure IV.4 The strain versus relative humidity at depths: (a) 1.3 cm, (b) 3.2 cm, and (c) 5.8 cm. The empty and filled markers show 10 and 25 days of drying respectively. R-squared values are for linear regression.

The comparison between the degrees of saturation of cured versus uncured samples is shown in Figure 4.5. Again, R-squared values are calculated to show the linear relation between the $\ln h$ and drying shrinkage ε_d.

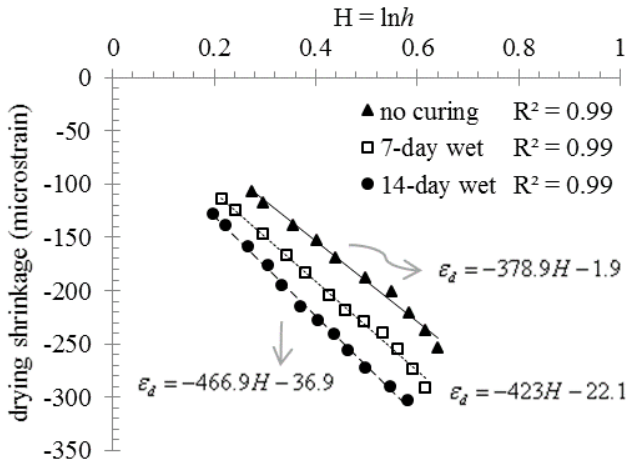

Figure IV.5 The shrinkage vs. $\ln h$ relation according to Eq. (4.7); R-squared values are for linear regression.

The predicted deflection from the measured shrinkage is shown in Figure 4.6. The markers show the calculated deflections up to 50 days by using the measured strain profiles in Eq. (4.7). The dashed markers after this period show the peaks of deflections, which are calculated by extrapolation with second degree polynomial regressions. The R-squared values show the suitability of the model chosen.

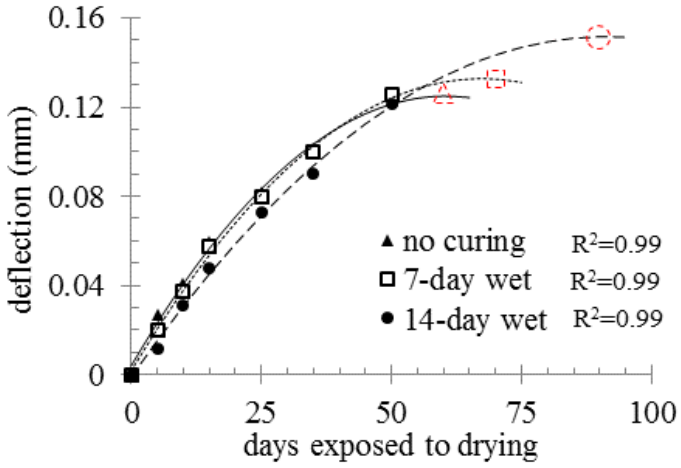

Figure IV.6 The calculated deflection of the concrete beams using their measured shrinkage

4.5 DISCUSSIONS

4.5.1 Mass Change from Wet Curing and Subsequent Drying

As seen in Figure 4.2 the wet cured samples increased in mass from the additional water that was supplied from wet curing. However, when these specimens were dried they quickly lost the extra mass gained from the wet curing. When comparing wet cured samples with the uncured one, even though the drying rates are similar, the wet cured samples have a higher saturation level at a comparable amount of drying for the time period investigated. This is caused by the additional moisture added from the wet curing.

While wet curing causes a smaller total porosity ϕ due to the generation of more hydration products, the volumetric content of liquid water ϕ_l will be larger due to the existence of more water filled pores. According to Eq. (4.4) the degree of saturation will be larger for the cured samples. This higher saturation level of the cured samples will be quantitatively verified again later in the paper. Therefore, according to Eq. (4.3), a higher saturation level will produce higher shrinkage in the paste if capillary tension p_c and the bulk modulus values are assumed to be

similar between samples. While there are other mechanisms that could be contributing to these observations, this seems to be an important one.

4.5.2 Relative Humidity and Strain Profiles

As shown in Figure 4.3a, the relative humidity was lower at the surface for all of the samples investigated. This is expected as the boundary conditions of the samples only allow moisture loss from the surface. This differential in moisture leads to differential shrinkage over the depth of the sample and causes subsequent curling. This is the same phenomenon that happens with concrete pavements and floors in the field.

For a given amount of drying the no curing sample had the lowest relative humidity, followed by the 7 and 14 day wet curing. This is expected because, by using extended wet curing, the samples should have improved levels of hydration and decreased permeability and hence lose less moisture at comparable times. At 5 and 10 days of drying the relative humidity at a depth of 3.2 cm and 5.8 cm of all samples were similar while there was a greater difference on the surface. This suggests that the water loss was occurring first on the surface and did not have a major impact on the relative humidity over the depth of the samples. Greater differences in the relative humidity profiles over the depth were observed after 25 and 50 days and between the relative humidity profiles of the samples cured for different durations. The sample that was not cured showed lower relative humidity at virtually all places in the specimen for all of the compared drying periods.

As shown in Figure 4.3b and Figure 4.4, despite the internal relative humidity being consistently lower for the no curing samples, these samples showed the lowest shrinkage strain closest to the surface. This means that despite the no curing samples losing more moisture their shrinkage was smaller than that of the wet cured samples. For the wet cured samples there was little difference in shrinkage strain for the first 10 days of drying, but these differences became more pronounced

with increased drying. At 25 and 50 days of drying the sample cured for 14 days showed increased amounts of shrinkage at the surface and mid depth. The development of the strain gradient is expected to continue as long as an imbalance between the internal and external relative humidity exists. Maintaining the liquid-vapor equilibrium is a slow process due to the very fine pore structure and will stop upon a balance between the ambient and internal relative humidity (Baroghel-Bouny et al., 1999). Therefore, the evaporation of the liquid water within the pores and the movement of moisture from the bottom to top surface of the beam are the slowest in 14-day wet curing followed by 7-day wet curing and no curing, respectively. This is likely due to the slower drying rate of the wet cured samples caused by their finer pore network.

While Figure 4.3 shows measurements of samples at four discrete drying periods, Figure 4.4 shows the combination of relative humidity and shrinkage for a larger number of measurements. Markers are included to show measurements at comparable drying times. This plot shows that for comparable amounts of relative humidity there was a significant difference in the amount of drying shrinkage that occurred with an increase in the wet curing of the samples. This was more pronounced on the surface of the sample as well as with increased amount of drying. These same trends were observed in the previous work that investigated cement paste elements (Hajibabaee & Ley, 2015).

As observed in Figure 4.4 there is a linear relation between the relative humidity and the measured shrinkage with R-squared values between 0.97-0.99. This is similar to observations by Baroghel-Bouny et al. (1999). The work in this paper verifies this and shows that this linearity exists at three different depths. This suggests that within the relative humidity range investigated that capillary tension is quite significant for drying shrinkage as suggested by Eq. (4.6). This linear relation between strain ε_d and relative humidity h could be due to the linearity of $\frac{S_l}{h}$ in Eq. (4.6) (Coussy et al., 1998). This again suggests that capillary tension appears to be the

dominant contributor to this phenomenon. It is possible that mechanisms like creep or differences in material properties for different curing conditions may also play an important role in these strains. However, for these materials and storage conditions it appears that the capillary tension caused by the increased degree of saturation is dominant.

It is expected that the permeability of the wet cured specimens is less than that of no cured samples due to the decrease in connectivity and the sizes of the pores from the increased degree of hydration caused by the curing (Gowriplan et al., 1990; Ramezanianpour & Malhotra, 1995). This lower permeability caused a slower rate of moisture loss with drying. This is supported in the data as the wet cured samples took longer to lose their moisture for a comparable amount of drying, which is verified with the higher relative humidity of wet cured beams at comparable times to the no cured specimens. Also, since these pores are smaller this will lead to an increase in the degree of saturation S_l. As per Eq. (4.3) and Eq. (4.6) this leads to a greater degree of shrinkage on drying of the sample assuming the other parameters in the equations are equal for different specimens. Consequently, when concrete is wet cured the decrease in porosity will cause a larger amount of drying shrinkage if the pores are emptied. Despite all of these changes occurring in the paste, Eq. (4.1) shows that shrinkage in the concrete is related to shrinkage in the paste (Pickett, 1956).

Figure 5 shows the relation between $\ln h$ and ε_d at the top surface for the three different curing conditions and so different degrees of saturation S_l. Assuming bulk modulus K_0 is similar between the samples, the integration of Eq. (4.6) can be written as

$$\varepsilon_d = \alpha S_l H + \beta, \qquad \text{Eq. (4.8)}$$

where $\alpha = \frac{1}{3}\frac{RT}{K_0 V_m}$ is a constant, $H = \ln h$, and β is the fitting parameter. Therefore, the slope αS_l of uncured beam divided by that of cured one can help find a relationship between degrees of saturations of different beams. As shown in Fig. 5 the cured specimens have higher degrees of saturation at the top at any given relative humidity, or at any fixed ages, as $S_l^{uncured} = 0.9S_l^{7-day\ wet} = 0.8S_l^{14-day\ wet}$ or $S_l^{uncured} < S_l^{7-day\ wet} < S_l^{14-day\ wet}$. According to Eq. (4.3), this increase in saturation means that the negative pore fluid pressure is essentially acting on a larger fraction of the solid skeleton, which results in more shrinkage at the same capillary pore pressure.

The findings from these experiments that the capillary tension and degree of saturation is important for one-dimensional drying of concrete are in agreement with proposed nonlinear poroelastic model by Coussy (Coussy, 1995; Coussy et al., 1998). Other mechanisms such as the differences of surface energy of the solid phase (W. Hansen, 1987; Young, Mindess, & Darwin, 2002), disjoining pressure (Powers, 1968), and poroviscoelastic responses (Grasley & Leung, 2011) have been suggested to be important and need further investigation. The combined effects of these mechanisms and their involvement in the global drying process are not well known (Baroghel-Bouny et al., 1999; Coussy et al., 1998). Additional effects of creep and differences in material properties could also be important. Work by the authors to further investigate the combined effects of these mechanisms is underway and will be reported in future publications.

4.5.3 Strain Profiles and Curling

As seen in Figure 4.6, Eq. (4.7) suggests that as the differential shrinkage increases then so will the deflection of the beam. The uncured specimen had slightly larger deflection in the beginning; however, the increase in differential shrinkage of wet cured beams caused the samples to have larger deflections at later ages. The rate of deflection from curling is slower in the cured samples

because of reduced rates of moisture loss (Hajibabaee & Ley, 2015). However, with continued drying the amount of curling of these samples are expected to be higher. The data in Fig. 6 shows that at 50 days of drying that the samples have almost the same amount of curling; however, at 95 days the 14 day wet cured samples have the most deflection, followed by the 7 day wet cured, and then the sample that is not cured. These calculations show that this differential shrinkage between the top and bottom of the specimen can lead to curling in the field that is possibly problematic. These observations match previous work with paste beams (Hajibabaee & Ley, 2015) and large-scale concrete beams (Hajibabaee, 2011). This supports findings by Nicholson (1981) where curling from shrinkage gradient was shown for concrete slabs cast on an impermeable base.

4.5.4 Practical Implications

While this paper has shown that wet curing will increase the shrinkage in concrete for a given amount of drying, care should be taken to not misapply these results. Adequate curing is important to minimize the early age cracking and stresses while the concrete gains strength. Also, the samples investigated were exposed to severe drying on one side without rewetting and no moisture loss on the other side. In some cases, such as a slab on grade not allowed to dry from the bottom in a 40% relative humidity drying environment, the results of this paper may apply. However, in structures where slabs on grade are rewetted, if the drying environment is not as severe, or if the decrease in permeability from the wet curing is able to sufficiently reduce the rate of drying, then this will reduce the amount of observed shrinkage and, therefore, curling. It should also be mentioned that it is not clear what boundary conditions exist in the field for in-place concrete. If some moisture loss is allowed on the bottom of a slab then the shrinkage gradient will not be as extreme and therefore the curling will be decreased. However, these measurements are helpful to understand and model the long-term volume change of concrete from drying. Understanding this phenomenon is becoming more important in the design of

volume change sensitive structures such as pavements, slabs on grade, and concrete dams. This data can provide significant insight into the design of these structures and provide explanations on observed behaviors.

4.6 CONCLUSIONS

This work investigated the impact of wet curing duration on concrete samples that were dried in a 23 °C and 40% relative humidity environment. These samples were only allowed to dry through the exposed surface. The following observations were made:

- The samples that were wet cured had a higher degree of saturation when compared to the uncured samples at any fixed age.
- The samples that were not cured showed the lowest relative humidity and shrinkage strain for comparable drying periods.
- As the wet curing period increased, the resulting drying shrinkage strains increased.
- A predictive model based on capillary tension by Coussy (1995) closely matched the results from this work. This suggests that capillary tension is a prominent mechanism in the curling caused by differential one-dimensional drying.
- A linear relationship was found between the internal relative humidity and drying shrinkage strains at a number of different depths. This supports findings by Baroghel-Bouny et al. (1999).
- Samples that were cured longer showed a greater shrinkage gradient over their depth; through calculations this was shown to suggest greater curling deflections at later ages.

Due to the wet curing process, the surface of concrete will have a finer pore-structure, which will reduce the permeability and porosity. This reduction in porosity will lead to a higher degree of

saturation and smaller pore sizes, which in turn suggests that greater capillary tension induced strain on drying. Calculations were used to show that this differential drying shrinkage could be problematic.

In all of the tests presented, a one-dimensional drying front was used through the use of impermeable boundaries. Care should be taken before extending the use of these findings to slabs with different boundary conditions, support, restraint, temperature, or drying conditions. These findings are useful to understand the drying shrinkage in concrete under severe drying and provide needed data to improve current modeling efforts.

4.7 ACKNOWLEDGMENTS

The authors would like to thank the Oklahoma Department of Transportation (ODOT 2208) and the Oklahoma Transportation Center (OTCREOS10.1-24) for funding the work. The following individuals also deserved acknowledgement for their help in completing the experiments: Basil Abdulkareem, Travis Ebisch, Jake LeFlore, Nicholas Ley, David Porter, Paul Field, and Shardul Kadam. We would also like to thank Dale Bentz and Zach Grasley for their helpful comments on the manuscript.

CHAPTER V

V. MECHANISMS OF DIMENSIONAL INSTABILITY CAUSED BY DIFFERENTIAL DRYING IN WET CURED CEMENT PASTE

5.1 ABSTRACT

This paper examines the mechanisms of wet curing and subsequent drying at 23 °C and 40% *RH* influencing the curling of cement paste, plate-like beams. Both experimental and model results show that as the duration of the wet curing is increased, the member peak deflection also increases from one sided drying. Experiments suggest that the extended wet curing causes a pore structure refinement resulting in greater saturation and consequently greater shrinkage. A simplified 1-D, drying diffusion and shrinkage model is able to adequately predict experimentally measured peak curling deflections, and confirms the effect of saturation on curling. The results provide important insight into the volume stability of slabs and the potential negative impact of wet curing on slab curling.

Keywords: curling; degree of saturation; drying diffusion; shrinkage; wet curing

5.2 INTRODUCTION

Wet curing with saturated wet coverings maintains moisture and temperature, promotes hydration, and has the potential to improve durability, strength, water-tightness, and abrasion resistance of concrete (ACI-308R, 2001; Dhir et al., 1991; Gowriplan et al., 1990; Kosmatka et al., 2011; Montgomery et al., 1992).

Concrete shrinkage occurs due to removal of pore water (desiccation). Desiccation of pore water occurs because of both external moisture loss (diffusive drying) and internal chemical reactions (self-desiccation). Regardless of the source of drying, negative pore fluid pressures (i.e., suction) occurs and menisci forms within pores (Bentz et al., 1998; Coussy et al., 2004). As drying occurs pores of decreasing size will begin to empty leading to increased pore fluid pressure magnitude. In general, shrinkage from desiccation is mainly considered to be due to the following driving forces:

- capillary pressure,
- disjoining pressure, and
- interface induced pressure.

By using the Kelvin-Laplace equation one can approximate the changes in pore fluid pressure associated with capillary effects and disjoining pressure (Grasley, Lange, & D'Ambrosia, 2005; Powers, 1968), while interfacial effects that are noticeable at lower *RH* are due to changes in surface free energy. All three mechanisms are included in an effective pore pressure that can be applied with poromechanical constitutive functions to calculate the shrinkage of cement-based materials (Coussy et al., 2004).

Prolonged wet curing is thought by many to strictly provide only improvements in concrete performance, and it has been recommended for fresh concrete of importance. Suprenant (2002) has suggested that longer curing has little effect on curling. However, not all work has shown that extended wet curing is beneficial. For example, Perenchio (Perenchio, 1997) observed an increase in drying shrinkage when concrete was wet cured for up to seven days. Hedenblad (Hedenblad, 1997) observed that a shorter curing time will result in a faster drying rate, which may minimize internal moisture gradients and subsequent curling. Furthermore, results from previous experiments by Hajibabaee and Ley (Hajibabaee & Ley, 2015, 2016) showed that increasing the

length of wet curing caused the free curling deflection of paste and concrete beams to increase. Based on this previous work it appears that conflicting results have been reported in the literature.

While it was shown in previous research (Hajibabaee & Ley, 2015, 2016) that wet curing increases curling, this work aims to verify the mechanisms by using additional experiments and a 1-D drying diffusion and shrinkage model implementing common simplifications from the literature. This model is not meant to be fully predictive, but rather to provide insight into the mechanisms by which wet curing increases peak curling deflections. In particular, it is hypothesized that wet curing affects the desorption isotherm gradient through surface pore refinement, which accentuates curling; the model is utilized to evaluate this hypothesis. A thorough understanding of the mechanisms by which wet curing increases curling of slabs will provide a basis for judging under what circumstances wet curing (which is widely considered to be strictly beneficial) could result in greater curling and risk of subsequent cracking.

5.3 METHODOLOGY

The magnitude and rate of shrinkage for concrete is dependent on the amount of shrinkage in the paste, amount and type of aggregate used, the specimen geometry, and environmental conditions (Browne, 1967; T. C. Hansen & Mattock, 1966; McDonald & Roper, 1993; Pickett, 1946). To simplify the experiments reported herein, paste specimens were used with a volume to surface ratio of 12.7 mm in order to obtain rapid results. Other studies that use concrete and a number of different sample sizes have been used to validate the effect of wet curing on curling of concrete (Hajibabaee, 2011; Hajibabaee & Ley, 2016), and we are thus confident the results of this work may be utilized to better understand curling in all classes of cementitious materials.

5.3.1 Desorption Isotherm Measurements

The Portland cement used in this study meets the requirements of both a type I and II cement, according to ASTM C150 (2011) and AASHTO M85 (2012). The oxide analysis and the

estimated phases are given in Table 5.1. The paste mixutures in this experiment had a w/c 0.42, and were prepared according to ASTM C305 (2011).

Table V.1 Cement oxide analysis, blaine fineness, and phase concentrations

Oxide mass fractions (%)					
SiO_2	Al_2O_3	MgO	Fe_2O_3	CaO	SO_3
20.23	4.77	1.90	3.23	64.15	2.52
Phase mass concentrations (%)				Blaine	
C_3S	C_2S	C_3A	C_4AF	(cm^2/g)	
63.56	10.05	7.18	9.83	3713	

Paste cylinders with 12.7 mm (0.5 in) thickness and 12.7 mm (0.5 in) diameter, shown in Figure 5.1, were manufactured and wet cured on the exposed surface for 0, 1, 3, 7, and 14 days with saturated wet burlap that was sealed in plastic. After curing and then demolding, samples were marked at one third from the top and the bottom surfaces. Each sample was then polished with a rotating diamond lapping plate to abrade away portions of the sample and isolate the top, middle, or bottom of the sample. The progressive polishing was done as cutting the samples would cause the material to shatter. The approach implemented here allowed the samples to be cured and then individual sections of the sample (i.e., depths from the cured surface) to be examined in order to quantify gradients in the desorption isotherm that are associated with the pore size distribution. Three samples were used for each curing duration; therefore, nine pieces (three for each depth) were made for each wet curing duration.

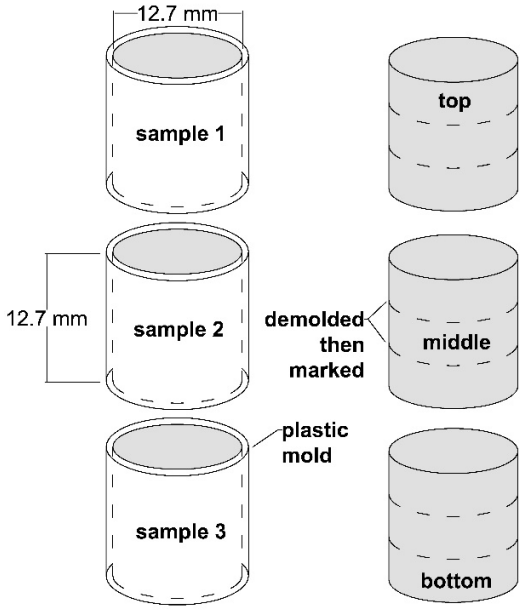

Figure V.1 Typical paste cylinders used to measure the degree of saturation

The sectioned samples were stored in sealed containers above saturated salt slurries at 23 °C according to ASTM E104 (2012). The storage relative humidities (generated by the salt solutions) were 86%, 72%, 50%, and 40%. Two *RH* sensors were used for each container to monitor and verify the *RH*. The samples were placed in the container and their mass was measured daily until there was less than 1% change in mass loss over a 24 hour period, at which time it was presumed that the state of moisture in the pore networks had sufficiently equilibrated with their environment. The samples were then dried in an oven, weighed, and then submerged in water and weighed again. All measurements were recorded after the mass change was less than 1% in a 24 hour period with a scale of 0.0001g precision.

5.3.2 Curling of Paste Beams from Differential Drying

The materials, mixture proportion, and curing methods used in this experiment were the same as the desorption isotherm experiments. Three paste beams with dimensions of 100 cm × 6.1 cm × 1.3 cm, as shown in Figure 5.2, were consolidated in plastic molds from each mixture. This plate-

like paste beam geometry had been first developed by Berke and Li (Berke & Li, 2004) and later used by Hajibabaee and Ley (Hajibabaee & Ley, 2015) to investigate the impact of wet and sealed curing on paste beams. After casting, all specimens were cured with wet burlap on the finished surface for 24 hours at 23 °C and then demolded.

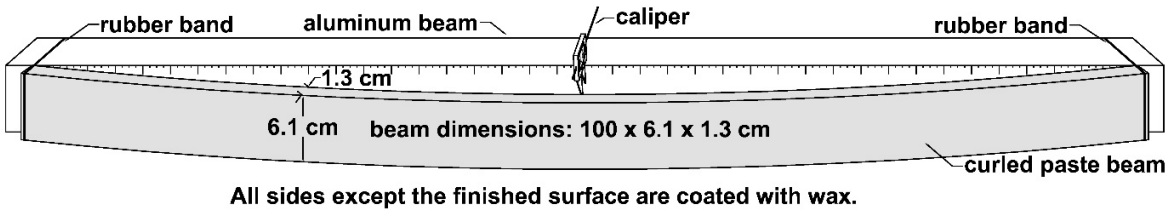

Figure V.2 Typical paste beam used in the testing and the curling measurement configuration

After demolding, the specimens were weighed and then sealed with wax on all sides but the finished surface (the face with dimensions of 100 cm × 6.1 cm) and weighed again. The finished surface of the beams was wet cured for 0, 1, 3, 7, or 14 days in saturated wet burlap sealed in plastic and maintained at 23 °C. These are the same curing durations as were used in the desorption isotherm experiment. After the specified wet curing period, the burlap was removed from the sample. The sample was then stored in a 23 °C and 40% relative humidity environmental chamber. As the member lost moisture from the unsealed surface it caused a moisture gradient in the sample that then led to differential shrinkage that caused curling of the member.

To measure the curling, rubber bands were used to hold the ends of the specimen to a flat aluminum beam with the drying surface of the specimen facing the beam, as seen in Figure 5.2. The distance between the aluminum beam and the specimen was measured at regular locations along the length with a caliper of 0.0127 mm accuracy. The curling of the beams was symmetric with a maximum at the middle of the beam. The loss of moisture of the sample was measured

through the mass loss over time with 0.1 g accuracy. More details about this experiment can be found in Hajibabaee and Ley (Hajibabaee & Ley, 2015).

5.3.3 Modeled Diffusion, Shrinkage, and Peak Curling Deflection

In order to predict the shrinkage gradient and resulting peak curling of the cement paste beams it is necessary to quantify the spatially and time dependent effective pore pressure. This pore pressure is a function of both the local internal *RH* and the local degree of liquid saturation, *S*. As *S* may be expressed as functionally dependent on *RH* via a constitutive function (i.e., the desorption isotherm), we need only define that function for each material and then determine the spatial and time dependence of the internal *RH*. In order to achieve the latter, the 1-D drying of the plate-like paste beams was modeled via drying diffusion whereby *RH* was utilized as the driving gradient; this is a common simplification in the drying of cement paste and other porous materials (Bazant & Najjar, 1971, 1972; Bolander & Berton, 2004; Bramhall, 1995; Gao, Zhang, & Luosun, 2014; Holmes & West, 2013; A. J. Hunter, 1993; Kim & Lee, 1999; Mu & Forth, 2009; Thorpe, 1981; West & Holmes, 2005; Xi, Bazant, Molina, & Jennings, 1994; Zhang, Gao, & Han, 2011). Thus, we first approximated that the drying process of cement paste may be approximately expressed according to the governing equation

$$\frac{\partial RH(x,t)}{\partial t} = \frac{\partial \left(D_i(x,t) \partial RH(x,t)/\partial x \right)}{\partial x}, \qquad \text{Eq. (5.1)}$$

where *t* is time, *x* is the spatial position coordinate through the drying thickness. Based on available experimental data and the goals of this paper, Eq. (5.1) was linearly approximated as

$$\frac{\partial RH(x,t)}{\partial t} = D_i(t) \frac{\partial^2 RH(x,t)}{\partial^2 x}. \qquad \text{Eq. (5.2)}$$

It should be noted that Eq. (5.2) is not only a linearized approximation, but neglects osmotic effects (Grasley & Rajagopal, 2012), source terms (e.g., self-desiccation), and energy associated

with interface development during drying (Grasley, Rajagopal, & Leung, 2011). Although this equation is a simplification, it is still useful for evaluating hypothesized mechanisms influencing the peak measured curling deflections. To solve the governing equation, we prescribed the initial condition as $RH_{initial}$ as described in the appendix. The boundary conditions were prescribed as

$$\frac{\partial RH(-L/2,t)}{\partial x} = 0 \text{ and}$$
$$RH(L/2,t) = RH_{bound}, \qquad \text{Eq. (5.3)}$$

where the beam thickness is L (with the drying surface x coordinate $L/2$ and the sealed bottom surface $-L/2$), and RH_{bound} is the ambient RH surrounding the specimen. An approximate solution to Eq. (5.2) and Eq. (5.3) was determined in the Laplace Transform domain.

The constitutive function for $S(RH)$ was prescribed as[1] (K. K. Hansen, 1986)

$$S = (1 - \frac{1}{\beta}\ln[\frac{RH}{RH_i}])^{-\alpha d} \qquad \text{Eq. (5.4)}$$

where α and β are fit coefficients and

$$d = 1 - \lambda x / L \qquad \text{Eq. (5.5)}$$

is a depth factor that allows the constitutive function to have a spatial dependence due to a gradient in the pore size distribution associated with curing conditions. The expression in Eq. (5.4) was chosen as it was verified as able to accurately fit the measured experimental

[1] In addition to the extra parameter d to account for variation with depth, Eq. (5.4) is a simplified form of that given in the original, cited reference where the sorption isotherm is given as

$$S(RH, x) = \text{Exp}\left[-\alpha \times \ln\left(1 - \ln\left(\frac{RH}{RH_{initial}}\right)\Big/\beta\right)\right].$$

desorption data. Note that, according to Eq. (5.5), we have approximated a linear variation in the sorption isotherm with depth where λ is a constant fit coefficient. In order to determine the fit coefficients for each material tested, desorption data were fitted from slices along the center of the sample first (since $x = 0$ and thus $d = 1$ at this location) to determine α and β for the given material. Next, desorption data from slices taken from the top and bottom of the samples were fitted in order to determine λ.

In order to determine the $D_i(\mathrm{t})$ for the materials tested, we utilized the relationship between the spatially averaged liquid saturation ($\langle S \rangle$) and the mass loss ($\delta m(t)$), expressed by

$$\delta m(t) = \left(1 - \langle S(t) \rangle\right) \phi(t) V \rho_w \qquad \text{Eq. (5.6)}$$

where ϕ is the pore volume fraction, V is the mass-loss specimen volume, and ρ_w is the density of liquid water. We note here that $\langle S(t) \rangle$ may be written as a function of $\langle RH(t) \rangle$ via Eq. (5.4); to determine $\langle RH \rangle$, the solution to Eq. (5.2) and Eq. (5.3) (in the Laplace transform domain) was integrated according to

$$\left\langle \overline{RH}(s) \right\rangle = \frac{1}{L} \int_{-L/2}^{L/2} \overline{RH}(x,s) ds = \frac{RH_{initial}}{s} + \frac{\sqrt{D_i}}{Ls^{3/2}} \left(RH_{bound} - RH_{initial} \right) \mathrm{Tanh}\left[\frac{L\sqrt{s}}{\sqrt{D_i}} \right]$$

Eq. (5.7)

where $\overline{RH}$ is the Laplace transformed *RH* and Tanh is the hyperbolic tangent function. The transformed spatially averaged *RH*, $\left\langle \overline{RH}(s) \right\rangle$, given by Eq. (5.7) is not analytically invertible for the drying problem of interest. However, it is noted that $\mathrm{Tanh}(z) \to 1$ as $s \to \infty$ such that Eq. (5.7) may be approximated as

$$\left\langle \overline{RH}(s) \right\rangle = \frac{RH_{initial}}{s} + \frac{\sqrt{D_i}}{Ls^{3/2}}\left(RH_{bound} - RH_{initial}\right) \qquad \text{Eq. (5.8)}$$

for small *t*. Eq. (5.8) inverts to

$$\left\langle RH(t) \right\rangle = RH_{initial} + \frac{2\sqrt{D_i}\sqrt{t}}{L\sqrt{\pi}}\left(RH_{bound} - RH_{initial}\right) \qquad \text{Eq. (5.9)}$$

which provides a very close approximation to the numerically inverted exact solution to Eq. (5.7) over the range of drying times of interest. Substituting Eq. (5.9) into Eq. (5.6) yields the function by which the mass loss data were fitted to determine $D_i(t)$ for each material. Note that in the solution of Eq. (5.2) and Eq. (5.3), the time-dependency of D_i was neglected in the Laplace transformation; this approximation was deemed acceptable since the mass loss data was fit at each time step. Thus, $D_i(t)$ was essentially approximated as constant only over each time step, which were on the order of one day. Furthermore, once drying initiates, hydration rate (and thus pore structure evolution) slows substantially, which means any change in the spatially averaged D_i with time after drying initiation is likely minimal.

With the constitutive parameters $D_i(t)$ and $S(RH, x)$ determined for each material, the effective pressure is able to be calculated utilizing $RH(x,t)$; however, the exact solution for $\overline{RH}(x,s)$ determined in the Laplace transform domain is not analytically invertible to the time domain. The exact solution contains the term $\left(1+\text{Exp}\left[2L\sqrt{s}/\sqrt{D_i}\right]\right)$, which reduces to $\text{Exp}\left[2L\sqrt{s}/\sqrt{D_i}\right]$ when s is large (i.e., at small *t*). This simplification allows inversion of $\overline{RH}(x,s)$ to the time domain to obtain the approximate solution

$$RH(x,t) = RH_{initial}\left(1+\text{Erf}\left[\frac{L}{\sqrt{D_i t}}\right]\right)+\left(RH_{bound}-RH_{initial}\right)\left(\text{Erf}\left[\frac{L-2x}{4\sqrt{D_i t}}\right]+\text{Erf}\left[\frac{3L+2x}{4\sqrt{D_i t}}\right]\right)$$

Eq. (5.10)

where Erf is the error function.

Based on the above analysis, $RH(x,t)$ and $S(x,t)$ were determined for each material and then the capillary pressure was calculated through

$$P_c(x,t) \approx \frac{-RT}{v_l^w}[\ln(\frac{RH}{100})+\ln(1+\frac{n_l^{diss}}{n_l^w S})],^{2} \quad \text{Eq. (5.11)}$$

in which P_c is the capillary pressure, n_l^{diss} is the concentration of dissolved species in the pore fluid, n_l^w is the molar concentration of pure water, v_l^w is the molar volume of water, *R* is the universal gas constant, and *T* is the temperature. Then, the additional pressure induced by interfaces was calculated by

$$U(S(x,t)) = \int_S^1 P_c(S')dS', \quad \text{Eq. (5.12)}$$

in which S' is the dummy saturation variable of integration (Coussy et al., 2004). The effective pressure ξ in the pore network was calculated according to

$$\xi(x,t) = SP_c + U \quad \text{Eq. (5.13)}$$

[2] The second logarithmic term is valid at the dilute limit and thus approximately accounts for the effect of changing dissolved species concentration during drying; the term is reasonably accurate above about $S(RH) = 0.5$.

Finally, free strain and deflection of the beam were calculated. The infinitesimal axial strain, ε, of cementitious materials accounting for both capillary and interface induced pressures is approximated by (Grasley & Leung, 2011)

$$\varepsilon(x,t) = \int_0^t \frac{1}{3}\frac{\partial \xi(t')}{\partial t'}(3(1-2v_p)J_p(t-t') - \frac{1}{K_s})dt', \qquad \text{Eq. (5.14)}$$

where v_p is the Poisson's ratio of the porous body (assumed to be time independent), K_s is the bulk modulus of the solid phase (also assumed to be time independent), and J_p is the uniaxial viscoelastic compliance of the porous body. J_p is calculated through the inverse Laplace transform of $\bar{J}_p$ where

$$\bar{J}_p = \frac{1}{s^2 \bar{E}_p(s)}, \qquad \text{Eq. (5.15)}$$

in which $\bar{J}_p$ is the Laplace transformed uniaxial viscoelastic compliance of the porous body, *s* is the transform variable, and $\bar{E}_p(s)$ is the Laplace transform of $E_p(t)$, which is the viscoelastic Young's modulus (i.e., the uniaxial relaxation modulus) of the porous body. Assumptions for $E_p(t)$ are shown in the appendix. It should be noted that the same function for $E_p(t)$ was utilized for each specimen when in fact such a constitutive function should vary between materials, as a function of age, and even as a function of spatial position within each material. The 10% relaxation presumed in the function for $E_p(t)$ was based on the observation by Grasley et al. (Grasley & Leung, 2011) that elastic models on average tended to under predict shrinkage by around 10%.

The cement paste beams were approximated as Euler-Bernoulli beams, with spatial variations in the mechanical properties neglected. Thus, the axial shrinkage strain given in Eq. (5.14) was utilized to calculate the midpoint deflection of the paste beams according to

$$\delta_{\max}(t) = \frac{3l^2}{2L^3} \int_{-L/2}^{L/2} \varepsilon(x,t) x dx \qquad \text{Eq. (5.16)}$$

Where l is the length of the beam. The preceding expression was derived by the induced thermal moment and beam kinematics (Hetnarski & Eslami, 2009) with deflection boundary conditions $\delta(x=0,t) = \delta(x=l,t) = 0$.

The model used in this study helps more easily discern the mechanisms behind the observed behavior from a prolonged wet curing. This model could be made more precise if it is modified to incorporate aging of the mechanical properties, self-desiccation and changing pore structure, and nonlinearity. While the importance of considering nonlinearity of the diffusivity is examined in subsequent sections, it is not within the scope of this study to develop a highly accurate predictive model incorporating every possible variable. The purpose of this work is mainly to investigate the mechanism of the general impact of the wet curing length on the curling performance of the paste beams, especially the peak of this deflection. Improvements in the model should primarily impact the strain prediction after the peak deflection. Therefore, comparisons will be restricted to the strains until the peak deflection. More information on methods to incorporate aging into shrinkage prediction can be found in Grasley and Leung (Grasley & Leung, 2011).

5.3.3.1 Nonlinear diffusion model

The results of the simplified, linearized approximate analytical model was compared to predictions acquired via a fully nonlinear diffusion model. In the nonlinear diffusion model, the diffusivity was expressed as (Bazant & Najjar, 1972)

$$D_i(RH) = D_{i0}\left(\alpha_0 + \frac{1-\alpha_0}{1+\left(\frac{100-RH(x,t)}{100-H_0}\right)^n}\right), \qquad \text{Eq. (5.17)}$$

where D_{i0}, α_0, H_0 and n are empirical constants. This diffusivity term was used in Eq. (5.1), which was then solved numerically subject to the boundary conditions given in Eq. (5.3). To assess the influence of the degree of nonlinearity on the predicted deflections, various parametric values were used for α_0, H_0 and $n\alpha_0$, H_0 and n, and an inverse algorithm was utilized to fit the nonlinear solution (via adjusting D_{i0}) to the measured mass loss data for the samples with no curing, 3, and 14 day wet curing. As with the approximate, linearized solution, the nonlinear solution made use of expressions Eq. (5.4) - Eq. (5.6) and Eq. (5.11) - Eq. (5.16).

5.4 RESULTS AND DISCUSSION

Figure 5.3 shows the desorption isotherm of the paste cylinders for the top 4 mm for different wet curing lengths. The change in degrees of saturation for the entire depth is shown in the saturation profiles in Figure 5.4.

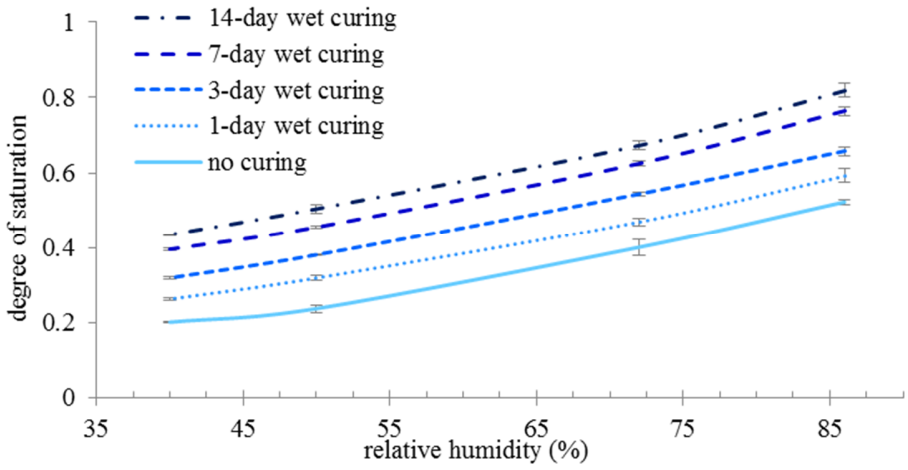

Figure V.3 Measured desorption isotherm for the top 4 mm of the specimens

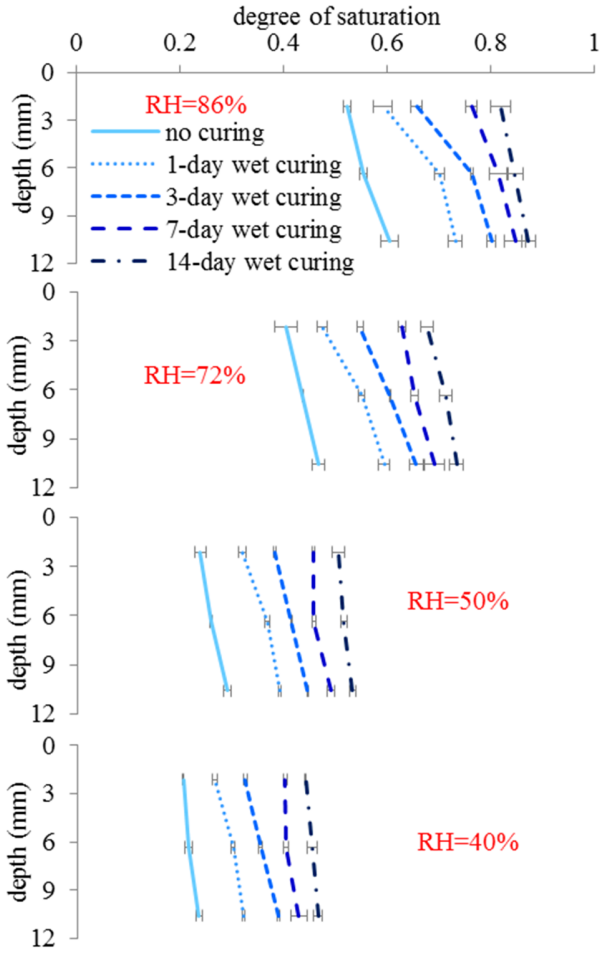

Figure V.4 Measured degree of saturation profiles at different RH and for different wet curing lengths

The degree of saturation increases with the following: depth from drying surface of the specimen, increased wet curing length, and *RH* of the specimen storage. Therefore:

- The top section of the sample without any moist curing in 40% *RH* has the least degree of saturation measured,
- The bottom of the sample with 14 days of additional wet curing at 86% *RH* has the highest degree of saturation measured.

These results are likely due to a finer pore structure caused by wet curing the samples, which promotes hydration and ultimately causes a higher degree of saturation (at a given *RH*) via refinement of the pore network. The gradient in the sorption isotherm is presumably due to a gradient in pore size distribution induced by enhanced hydration from the surface moisture associated with wet-curing.

Figure 5.5 shows the mass loss versus drying time for the paste beams after exposure to 40% relative humidity and 23 °C. Open markers have been added to the graph to highlight the point of maximum curling, which will be shown later.

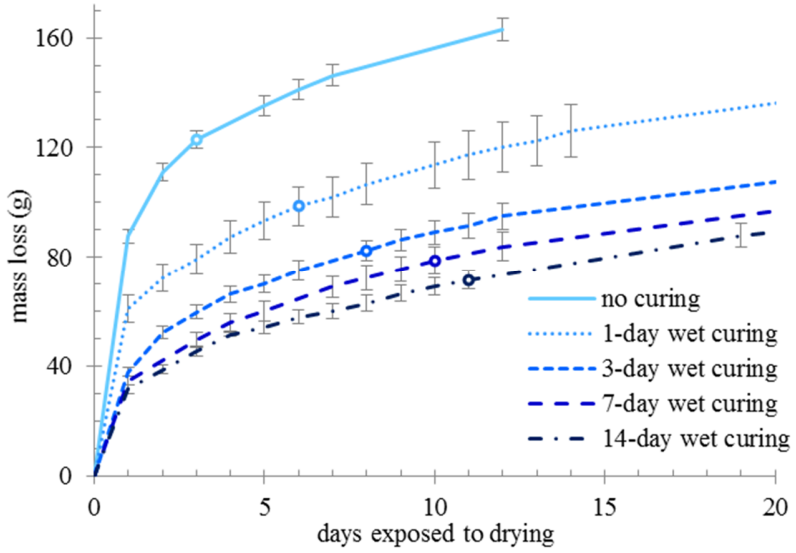

Figure V.5 Measured mass loss of the paste beams after the exposure to drying conditions

Mass loss of the samples in the experiment shows that the sample with no curing lost more moisture than other samples after exposure. Increasing the wet curing refined the pore structure and caused the specimens to lose moisture at a reduced rate. This observation is in agreement with the results found from the degree of saturation/desorption isotherm testing, which also indicated pore refinement caused by extended wet curing.

Figure 5.6 shows the effective pore pressure of uncured, 3-day wet cured, and 14-day wet cured specimens, calculated by Eq. (5.13), over the depth of the member L at different drying times. It should be noted that through depth position is normalized by L; at -0.5L the sample is sealed, while the drying surface is at 0.5L.

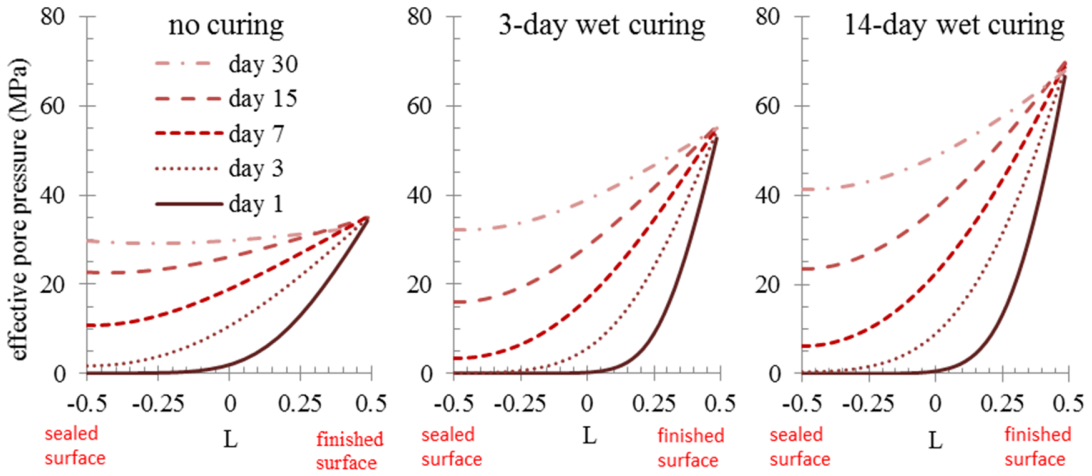

Figure V.6 Simulated effective pore pressure at different depths and drying times. Position 0.5L corresponds to the drying surface and -0.5L corresponds to the sealed surface.

For each curing period and exposure time to drying, the drying surface has the greatest calculated effective pore pressure. Furthermore, of importance to expected curling, the gradient of effective pore pressures is greater for longer durations of wet curing. The magnitude of the gradient in effective pore pressure influences the gradient in shrinkage and thus the curling deflection magnitude. The steeper gradient (and overall higher effective pore pressure at all depths) in the wet cured beams is attributed to the higher degree of saturation (particularly on the drying surface) in these specimens (Coussy et al., 2004).

Figure 5.7 shows the comparison between the deflections of the paste beams versus the deflections calculated by the simplified, linear model. Due to the parabolic shape of deflection and a uniform drying, the maximum curling value can be used to characterize the test results. All

of the curves have a similar shape with different maximum curling value and time periods. The observed deflection is caused by rapid surface drying that causes moisture and shrinkage gradients over the depth of the sample. Because of this differential shrinkage, the sample curls upwards. As shown in Figure 5.5 this point of maximum deflection comes far from where the sample has completely dried. As the sample continues to dry the gradient magnitude decreases, stress relaxation occurs, and the deflection necessarily decreases.

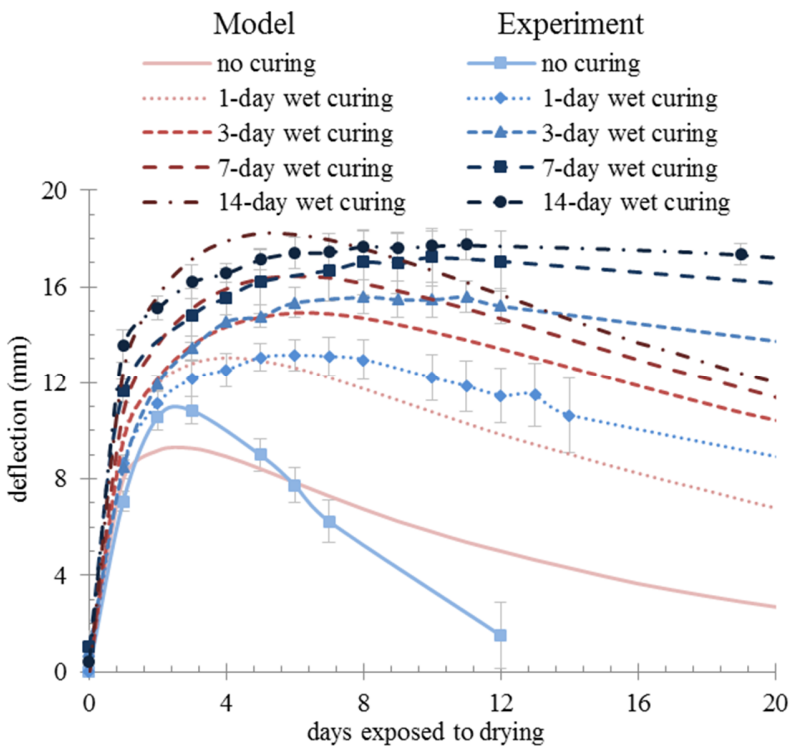

Figure V.7 The comparison between the deflections of the paste beams from the experiment versus the simulated data

Figure 5.7 also shows the impact of curing length on the curling performance of paste beams; longer wet curing caused an increase in deflection and extended the drying time as well. Due to a finer pore structure of the wet cured specimens, a decrease in diffusivity makes it more difficult for a specimen to lose moisture from drying. This is why specimens that were cured longer lost

moisture at slower rates and required more time to reach their maximum curling deflection. The modeled deflections show good agreement with the measured data from the initial drying up until the point of maximum deflection. The post-peak deflection had a lower quality fit. This is likely caused primarily by the lack of consideration of aging, self-desiccation, nonlinearity of the drying diffusion, and gradients in mechanical properties in the model. The focus of this modeling was not accurate prediction of the entire deflection curve at all ages, but an investigation of the mechanisms influencing peak deflection. The model may be refined in the future to more accurately predict the entire deflection history.

Figure 5.8 shows the comparison between the maximum deflection of the paste beams that were calculated by the model and measured in the paste beam experiments.

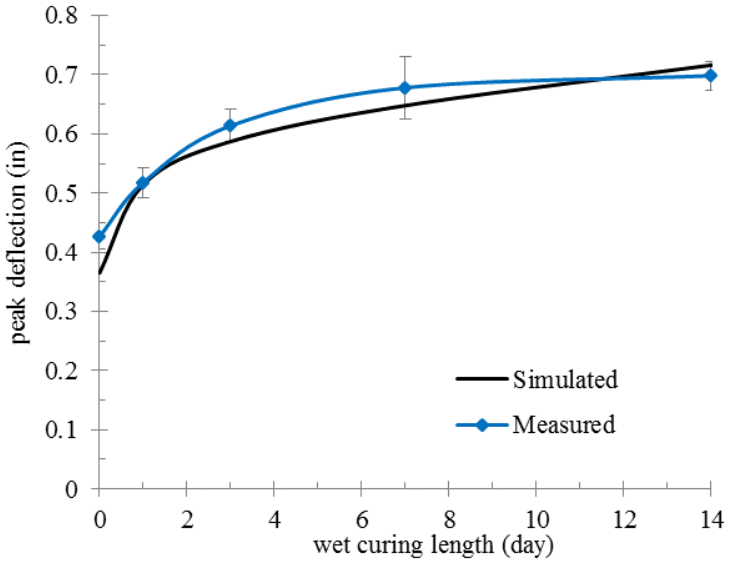

Figure V.8 A comparison between the maximum deflection of the paste beams from the experiments versus the simulated data

Increasing the wet curing length has increased the maximum deflection in both the model and the experiment. The predicted result of the simplified model is close to that of the experiment.

Figure 5.9 shows the deflection of uncured, 3, and 14-day wet cured specimens that were calculated by the linear model, nonlinear model, and our linearized approximate analytical model in comparison with the measured deflection.

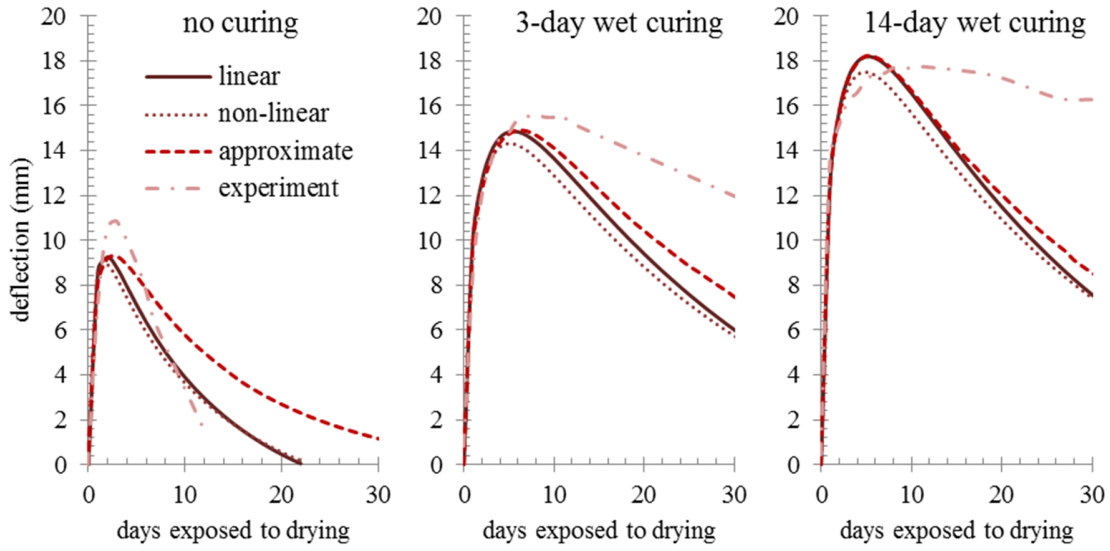

Figure V.9 A comparison between the deflection of the paste beams from experiments versus different models

In general, both the approximate linearized solution and the nonlinear solutions indicate that the beam deflections gradually increase, reach a peak, and then decrease as drying progresses. The models also show that with increased wet curing, the peak is delayed and increases in magnitude. The overall deflection predictions by the approximate linearized models are comparable to the results from the full, nonlinear solution. This indicates that drying diffusion may not be highly nonlinear for the tested samples. This finding could be attributed to factors lacking in the model such as source/sink terms or, more likely, small surface microcracks caused by the rapid exposure to a severe drying condition (Hwang & Young, 1984). Surface microcracking would tend to offset any reductions in the diffusion coefficient associated with lower internal RH values. It also should be mentioned that the nonlinear simulations took approximately 60x more computational

time to complete then the linearized, approximate model suggested in this paper. Therefore, the linearized approximate model was chosen to predict the deflections and discuss the driving forces behind the 1D drying shrinkage problem in the paper.

5.4.1 Mechanisms

When the relative humidity is above about 70% the mechanism related to the capillary pressure and the formation of the menisci becomes important; such capillary pressure may be expressed according to the Young-Laplace relationship (Adamson & Gast, 1967) as

$$P_c = -\frac{2\gamma\cos(\theta)}{r}, \qquad \text{Eq. (5.18)}$$

where γ is surface tension of pore fluid, θ is the liquid-solid contact angle, and r is the circumferential mean radius of the curvature of the meniscus. The negative pressure induces a hydrostatic compression in the surrounding solid phases, which causes their volume to reduce, yielding bulk shrinkage.

When the degree of saturation S is less than 0.6, the mechanism related to the interface induced pressure or the solid surface free energy becomes important as well. A simplified, linearly elastic version of Eq. (5.14) (Bentz et al., 1998) can help explain the impact of S on the linear shrinkage. Such a model is expressed as

$$\varepsilon_p = \frac{S}{3} P_c \left(\frac{1}{K_p} - \frac{1}{K_s}\right), \qquad \text{Eq. (5.19)}$$

where ε_p is the linear shrinkage in the paste and K_p is the bulk modulus of porous body with gas filled[3] pores. As seen in Figure 5.3 for the desorption isotherm, at a given relative humidity,

[3] More precisely, the pores should be filled with a highly compressible fluid.

when the capillary pore pressure P_c is the same between the wet cured and no cured specimens, the increase in the duration of wet curing has increased the degree of saturation *S* due to the refined pore structure. Eq. (5.19) simply shows that this increased *S* increases the shrinkage in the paste assuming all other parameters in the equation, i.e. K_p and K_s, remain unchanged. This increase in saturation means that the negative pore fluid pressure is essentially acting on a larger fraction of the solid skeleton, which results in more shrinkage at the same capillary pore pressure. However, all of these driving forces need to be taken into account via an effective pore pressure ξ, which was shown in Eq. (5.13) (Coussy et al., 2004).

5.5 PRACTICAL SIGNIFICANCE

This work has suggested both experimentally and via a mechanistic model that prolonged wet curing may cause increased magnitude of shrinkage strain gradients and therefore curling. This work focused on 1-D drying that is often prevalent in concrete slabs cast on a substrate that does not allow drying. These structures are commonly used for slab on grade and pavements. The increased strains and deformations caused by this prolonged wet curing may cause increased amount of cracking of these structures. This cracking may impact the strength, stiffness, and long term durability of these structures. Thus, the benefits of decreased permeability and increased strength that is typically promoted by wet curing should be balanced with the risk of increased cracking associated with greater curling magnitude. The developed model can help provide insight into this issue and allow more informed decisions to be made.

5.6 CONCLUSIONS

This work has shown that there is a potential increase in the amount of curling of members that are wet cured and then subject to 1-D drying such as slabs on grade and pavements. This increased curling may cause loss of local support or uneven riding surfaces. In turn, this may lead to premature cracking from edge loading or serviceability issues. This means that in certain

situations the disadvantages of wet curing may be more critical than the anticipated advantages. These findings question the common mantra that wet curing is strictly beneficial for concrete.

Results from 1-D drying experiments and simulations of 0.42 w/c paste beams stored in 40% *RH* showed different degrees of saturation, drying diffusivity, and subsequent deformation from drying. Based on this work the following conclusions were drawn:

- Increasing the wet curing length of cement paste increases the degree of saturation at either a given duration of time after exposure to drying or at a given equilibrium *RH*.
- This increased level of saturation will lead to increased strains when dried to a given *RH*. This effect is particularly prevalent on the wet cured surface.
- Increased duration of wet curing was shown to reduce mass transport (drying) rate.
- The results above in combination will lead to larger moisture gradients and greater curling in wet cured paste samples versus samples that are simply sealed or allowed to dry from casting.

The experiments showed good agreement with a 1-D drying shrinkage model based on those developed previously by Grasley et al. (Grasley, 2010; Grasley & Leung, 2011) when measured desorption isotherms and drying diffusion coefficients were used as inputs in the model. It should be pointed out that the model in this study was not intended to be a predictive tool, but simply to test the hypothesis presented by the authors regarding the mechanism dictating increases in peak curling of wet cured pastes. The model confirms the hypothesis that changes in the desorption isotherm (as alluded to in the aforementioned bullet points) is sufficient to explain the effect of wet curing on peak curling deflections. Further refinement of the model shows promise to be used in more detailed prediction of the shrinkage strains caused by different curing methods, conditions, material properties, and drying, and to determine whether the hypothesized

mechanism for increased curling is not only sufficient but also necessary to explain measured behavior.

5.7 ACKNOWLEDGEMENTS

The authors would like to thank the Oklahoma Department of Transportation (ODOT 2208) and the Oklahoma Transportation Center (OTCREOS10.1-24) and the National Science Foundation (CMMI # 1300024 and CMMI # 1301060) for funding the work. The following individuals also deserve acknowledgement for their help in completing the experiments: Paul Field, Basil Abdulkareem, and David Porter.

CHAPTER VI

VI. MODELING 1D DRYING SHRINKAGE OF CONCRETE

6.1 INTRODUCTION

In chapters 2 to 4 the impact of wet curing was investigated on curling deflection and shrinkage of paste and concrete elements with different curing methods. Next, a mechanistic model was introduced to further investigate the mechanisms that caused the increase in curling deflection of paste elements with extended wet curing. Also, the ability of this analytical model to capture the mechanistic sources of wet curing on peak deflections was evaluated by comparing its predictions to those acquired via a fully nonlinear diffusion model. While both the approximate linearized solution and the nonlinear solutions showed that longer wet curing delayed the peak deflection and increased its magnitude, the overall deflection predictions by the approximate linearized model were in greater agreement with the measured data than with the full, nonlinear solution.

In this chapter the previously presented approximate model will be further adjusted to investigate the ability of the model to predict the shrinkage of concrete elements and to compare to experimental results presented in chapter 4.

This investigation through model adjustments and experimental concrete shrinkage, helps to verify the accuracy or limitations of the model and if further refinement of the model is required to explain measured behaviors.

6.2 METHODOLOGY

In this chapter the same modeling work as chapter 5 is used to find the peak deflections of paste beams. Also, shrinkage results of concrete beams from chapter 4 will be used to verify the simulated shrinkage results of concrete. The model uses the measured relative humidity (*RH*) at different depths of concrete beams. Further information about the model and details of the experiment are shown in chapters 4 and 5. New experiments are also done on paste prisms and concrete cylinders to find the degree of saturation with depth and the instantaneous Young's modulus of the porous body of concrete to improve the simulated results. These will be described in this chapter.

6.2.1 Input Parameters

As shown in the previous chapter for the paste model, assumptions such as the pore volume fraction $\varphi = 0.3$, instantaneous Poisson's ratio of the porous body $\nu_p = 0.2$, viscoelastic Young's modulus of the porous body $E_p(t) = 0.1E_0 e^{-t/\tau} + 0.9E_0$ with instantaneous Young's modulus of the porous body $E_0 = 17.5\,GPa$, viscoelastic relaxation time for the viscoelastic Young's modulus $\tau = 10\ \ days$, and concentration of dissolved species in the pore fluid $n_l^{diss} = 1.91\ \frac{mol}{L}$ were used for all curing methods. However, the relaxation factor 0.1 (or 10% relaxation), relaxation time τ, and also the instantaneous Young's modulus of the porous body E_0 can change with the change in the curing length along with the change in the porosity φ. The implication of adjusting model parameters to fit deflection data is one of the advantages of mechanistic models, as the parameters have real physical meaning. This means the model user has a feel for the adjustments being made to the parameters.

Also, different cements with different oxide compositions can release different amount of alkali ion after hydration and therefore the concentration of dissolved species in the pore fluid can also

be different from the assumed number. Further investigation needs to be done to analyze the behavior of this parameter on shrinkage and the impact of curing on it. This can be done by laboratory testing to accurately measure the concentration of ions at early ages, which is out of the scope of this research.

For the concrete model, the actual shrinkage at the top of the concrete samples at 40±4% RH was used to find the best fit for the simulated shrinkage and to adjust the input parameters as discussed above. These parameters were also used for the middle and the bottom of concrete beams to calculate the drying shrinkage at 40±4% chamber *RH*. For the Young's modulus of the porous body, the 28 day compressive strength of cylinders was first measured according to ASTM C39 (2016) and then the modulus was calculated according to ACI C318 (2014) for normal-weight concrete with Eq. (5.20)

$$E_0 = 4700\sqrt{f_c'} \qquad \text{Eq. (5.20)}$$

where E_0 is the instantaneous Young's modulus of the porous body and f' is the 28 day compressive strength (MPa) to use in the model. Therefore, the cylinders were cured in the fog room for 0, 7, and 14 days after casting. Then they were demolded and stored in the drying room at 23 ℃ and 50±4% *RH* until they were 28 days old for the compressive strength test.

6.2.2 Degree of Saturation Measurements

As shown before, one of the factors that affects the shrinkage is the degree of saturation. Previously sections from paste cores were used to measure this parameter at different storage humidities. The final results were used as functions of degree of Saturation over *RH* to use in modeling work. In this chapter, the same approach has been used to find degree of saturation curves for thicker samples instead of those found before for the thin paste samples to improve the simulation. Paste was chosen to measure the degree of saturation due to experimental challenges

with using concrete. It was assumed that the impact of aggregate on degree of saturation is not very significant, since all mass loss occurs in paste. Further research can be done in future to verify this assumption considering the impact of Interfacial Transition Zones of aggregates on degree of saturation profiles.

For the degree of saturation test, samples had the same mix proportion as shown in chapter 4 except that no aggregate was used in the samples. The cement used in this test was type I, according to ASTM C150 (2011), and its chemical analysis is shown in the Table 6.1. An ASTM C618 (2008) class C fly ash was also used. The chemical analysis is shown in Table 6.2. In the mixtures investigated a water to binder ratio (w/b) of 0.41 and 25% class C fly ash by the weight of cement were used.

Table VI.1 The oxide analysis of the cement and its phase concentrations.

chemical test results (%)					
SiO_2	Al_2O_3	MgO	Fe_2O_3	CaO	SO_3
20.77	4.57	2.37	2.62	62.27	3.18
Na_2O	K_2O	TiO_2	P_2O_5	SrO	BaO
0.19	0.32	0.34	0.14	0.22	0.07
phase concentrations (%)					
C_3S		C_2S	C_3A	C_4AF	
52.13		20.22	7.68	7.97	

Table VI.2 The oxide analysis of the fly ash used in the testing.

chemical test results (%)						
K_2O	BaO	MgO	SrO	CaO	SO_3	Na_2O
0.58	0.72	5.55	0.39	23.12	1.27	1.78
SiO_2	Al_2O_3	MnO_2	P_2O_5	Fe_2O_3	TiO_2	
38.71	18.82	0.02	1.46	5.88	1.35	

The paste mixtures were prepared according to ASTM C305 (2011) and 2 samples were made for each curing length including 0, 7, and 14 day wet curing. Two paste beams with dimensions of

7.62×10.16×40.64 cm^3 (3×4×16 in^3) were consolidated in steel molds from each mixture. After casting, 4 samples of wet curing methods were stored in drying room for 6 h at 23 °C and 50% *RH* until the bleeding water disappeared and then samples were moved to a fog room with the same 23 °C temperature and wet burlaps were put on the samples for 7 d and 14 d under a plastic tarp. Two samples were left in the drying room within the mold for the no-curing method until the next day.

These paste beams had the same thickness as the concrete beams, and were wet cured on the exposed surface. After curing and then demolding, the beams were marked at three different depths on their side, 1.27 cm (0.5 in), 5.08 cm (2 in), and 8.89 cm (3.5 in). Then cores of 1 cm (0.4 in) thick with 1 cm (0.5 in) diameter were taken immediately from the marked area on the sample's side. Cores were quickly polished with a rotating diamond lapping plate to remove debris from coring. The cores were stored in a sealed container above KCl saturated salt slurries at 23 °C for the storage *RH* of 85±1% according to ASTM E104 (2012), and in drying chambers with *RH* of 70±0.5%, 50±4%, and 30±0.5% at 23 °C. Three cores were taken from each depth for each curing and each storage *RH* and their mass was measured daily until there was less than 1% change in mass loss over a 24 hour period, at which time it was presumed that the state of moisture in the pore networks had sufficiently equilibrated with their environment. Finally, the samples were vacuum saturated in water for a day and weighed, and then dried in an oven, and weighed again. All measurements were recorded after the mass change was less than 1% in a 24 hour period with a scale of 0.0001 g precision.

6.2.3 Calculating the Drying Diffusion Coefficient of Concrete

Although the bulk mass loss of thin paste beams was used to calculate drying diffusion D_i in the previous chapter, the measured internal relative humidity *RH* of concrete beams at each depth can also determine D_i of the concrete beams. As shown in chapter 3, *RH* of concrete beams at three

different depths was measured by calibrated RH sensors. This data was not available for the experiment done on paste because the beams were too thin. The measured *RH* data can be used to find the drying diffusion coefficient at each depth as described below. As shown in chapter 5, the following *RH* equation

$$RH(x,t) = RH_{initial}\left(1+\text{Erf}\left[\frac{L}{\sqrt{D_i t}}\right]\right)+\left(RH_{bound}-RH_{initial}\right)\left(\text{Erf}\left[\frac{L-2x}{4\sqrt{D_i t}}\right]+\text{Erf}\left[\frac{3L+2x}{4\sqrt{D_i t}}\right]\right)$$

Eq. (5.21)

was used to estimate the internal $RH(x,t)$ at different drying time *t* and different spatial position coordinate *x* through the drying thickness and the diffusion D_i of paste was found from the measured bulk mass loss through the $\delta m(t)$ equation:

$$\delta m(t) = \left(1-\langle S(t)\rangle\right)\phi(t)V\rho_w \qquad \text{Eq. (5.22)}$$

where ($\langle S \rangle$) is the spatially averaged liquid saturation, ϕ is the pore volume fraction, *V* is the mass-loss specimen volume, and ρ_w is the density of liquid water. However, using the bulk mass loss of concrete to find diffusion is not very accurate, since the concrete beams were 8× thicker than paste beams and the diffusion is not perfectly constant over the depth. Since *RH* was already measured for the concrete samples at different position coordinate *x* at different drying time *t*, then the actual *RH* was used to calculate D_i directly from Eq. (5.21).

By assuming the D_i is constant for each depth over the entire *RH* history of that depth, a *Mathematica* function called *FindFit* was used to find the numerical value of parameter D_i that makes the $RH(x,t)$ expression give the best fit to actual *RH* data as a function of time *t*. The initial *RH* and boundary condition *RH* are 96.64% and 40% as shown before. Also, as mentioned

before, the sensors were not put in the samples due to the very high *RH* in concrete at early ages which could cause erroneous measurements and possible corrosion to the sensors. Therefore, *RH* of the first 4 days after casting has been interpolated using a fitted curve to the actual data for each depth for the uncured specimen.

The assumption of D_i being constant was previously used for paste beams for their entire depth. This simplification was shown in the previous chapter to give good shrinkage predictions comparable to the results from the full, nonlinear solution. This could be caused by microcracking at 40% *RH* boundary condition on the surface of paste beams that can easily affect their entire 0.5 in depth and therefore offset any reductions in the diffusion associated with lower internal *RH* values. This assumption has been used again for concrete to verify the accuracy of the approximate linearized model assuming that the diffusion is constant around any given depth with a measured *RH*, which are 1.3, 3.2, and 5.8 cm from the finished surface as mentioned before.

6.2.4 Drying Shrinkage

After finding the $RH(x,t)$ fit and $S(x,t)$ through the measured degree of saturation data as described in the previous chapter, capillary pressure, additional pressure induced by interfaces, and effective pore pressure are calculated by using Eq. (5.11) - Eq. (5.13) in chapter 5. Finally, free strain of the concrete beams were calculated according to Eq. (5.14) of the previous chapter.

6.3 RESULTS AND DISCUSSION

6.3.1 Paste Beams Curling

The results from simulating the maximum curling deflection of paste beams stored at 40% *RH* are shown in Figure 6.1 with adjustments to the mechanical properties to fit the experimental results:

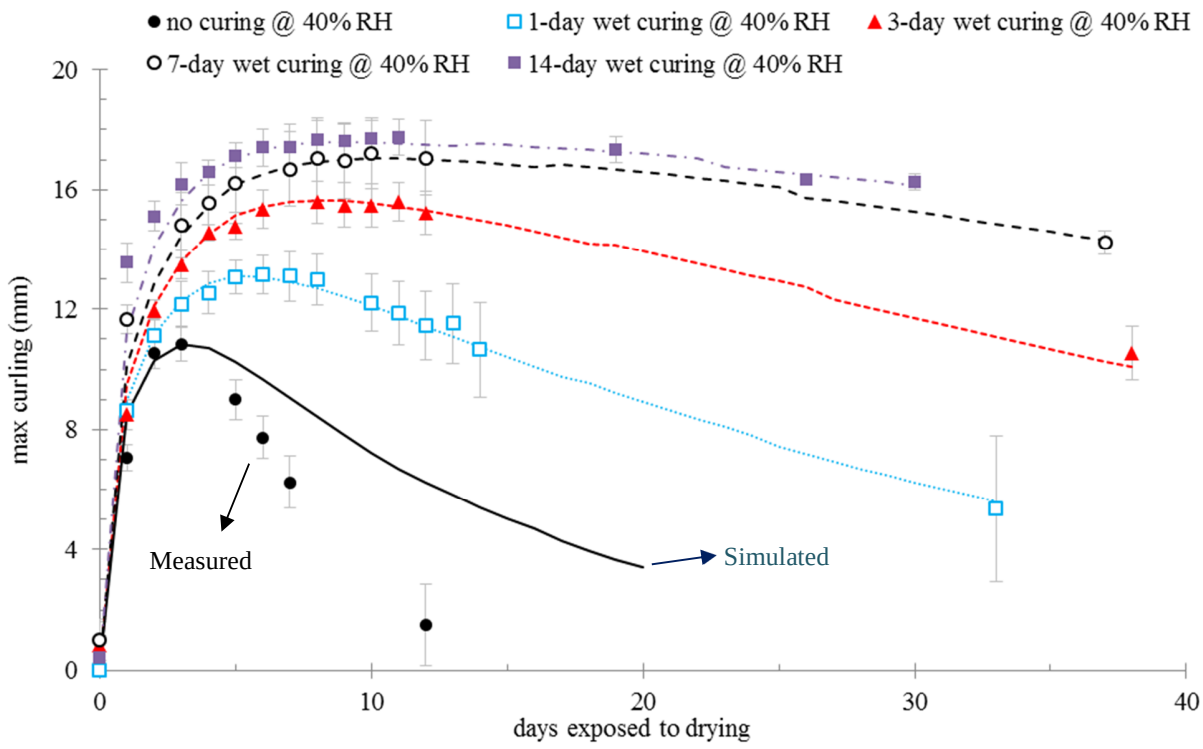

Figure VI.1 The measured max curling shown with markers and error bars versus the simulated one shown with lines

The post-deflection prediction of uncured samples is overpredicted which is possibly due to the unmeasured and uncontrolled mass loss of uncured samples in the mold within the first 24 hours, that results in misleading drying diffusion coefficient. This can also be due to the use of the same concentration of dissolved species for uncured beams in the model as the wet cured specimens, which results in an inaccurate initial *RH*. For thicker paste beams more work needs to be done to verify the linearized approximation of drying diffusion, which is out of the scope of this research. In general, the underprediction of the previously simulated results for paste beams, as seen in chapter 5, were fixed using the shown values in Figure 6.2. These graphs show the trends of mechanical properties of paste affected by the curing duration which were found through the model and verified through the actual deflections. The following assumptions as shown in Figure

6.2 were used to fit not only the peak of deflection but also the post-deflections, which was previously underpredicted in chapter 5:

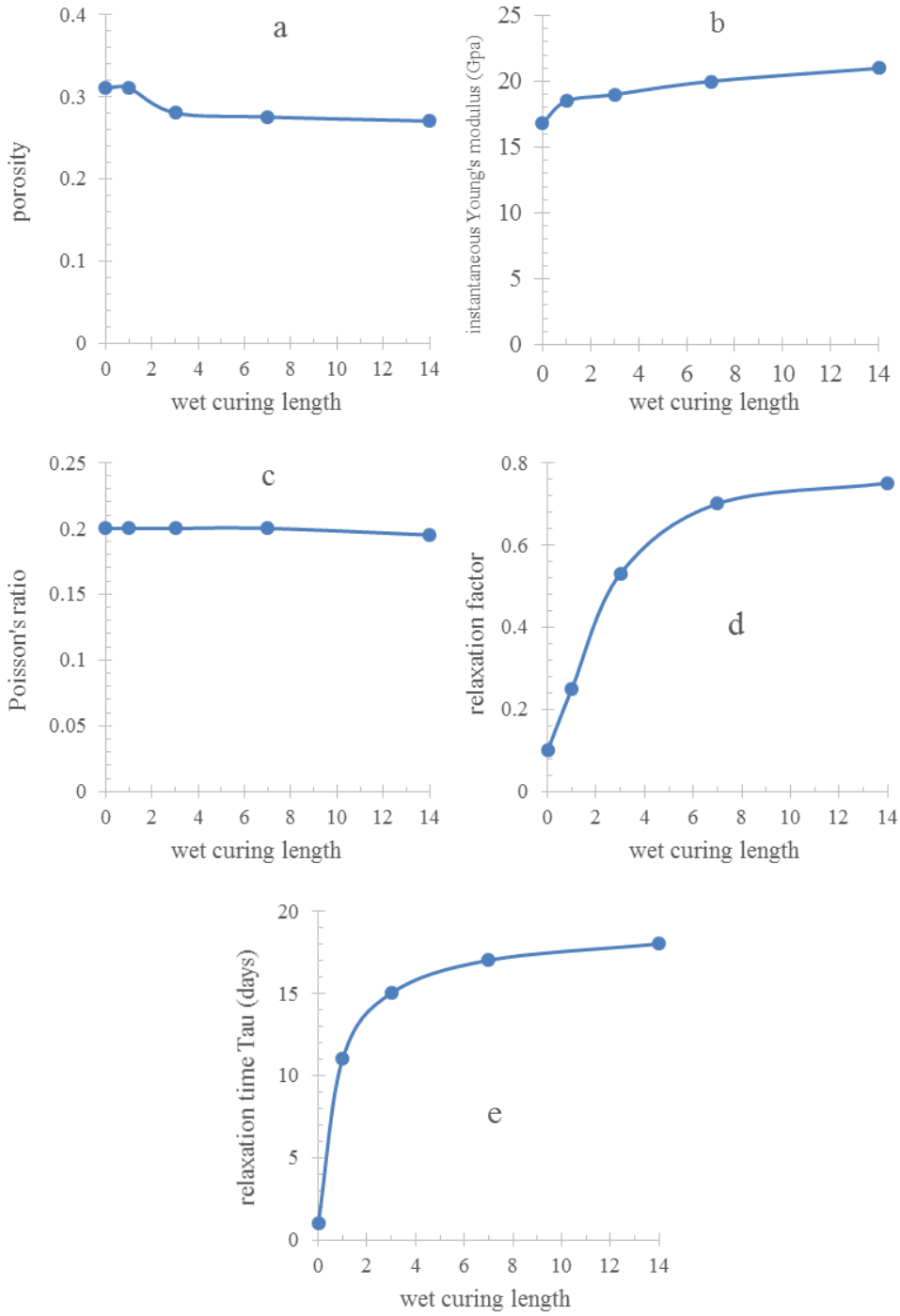

Figure VI.2 Adjusted input parameters for the mechanical properties of paste at 40% RH

For the 3 d wet curing 28% porosity was chosen (Wong & Buenfeld, 2009). The porosity of the paste samples is decreased by increasing the curing length, as shown in Figure 6.2a, which is due to the generation of more hydration products and the refinement of pore structure. This increased the instantaneous Young's modulus as shown in Figure 6.2b (Grasley & Leung, 2011). The reduction in Poisson's ratio as shown in Figure 6.2c is negligible. The 10% relaxation presumed in the function for $E_p(t)$ in chapter 5, which was assumed to be the same for all curing lengths, was based on the observation by Grasley et al. (2011) that elastic models on average tended to underpredict shrinkage by around 10%. However, it is shown here in Figure 6.2d that increasing the curing duration increased the relaxation up to 75% for 14 d wet curing of the thin paste beams, which is due to the larger stresses in longer cured paste samples. Consequently this increased the relaxation time of the paste samples as shown in Figure 6.2e.

6.3.2 Degree of Saturation

The results of the degree of saturation experiment is shown in Figures 6.3 and 6.4 for different storage *RH* values and different depths for 0, 7, and 14 day wet cured specimens, labeled as 0-dwc,7-dwc, and 14-dwc.

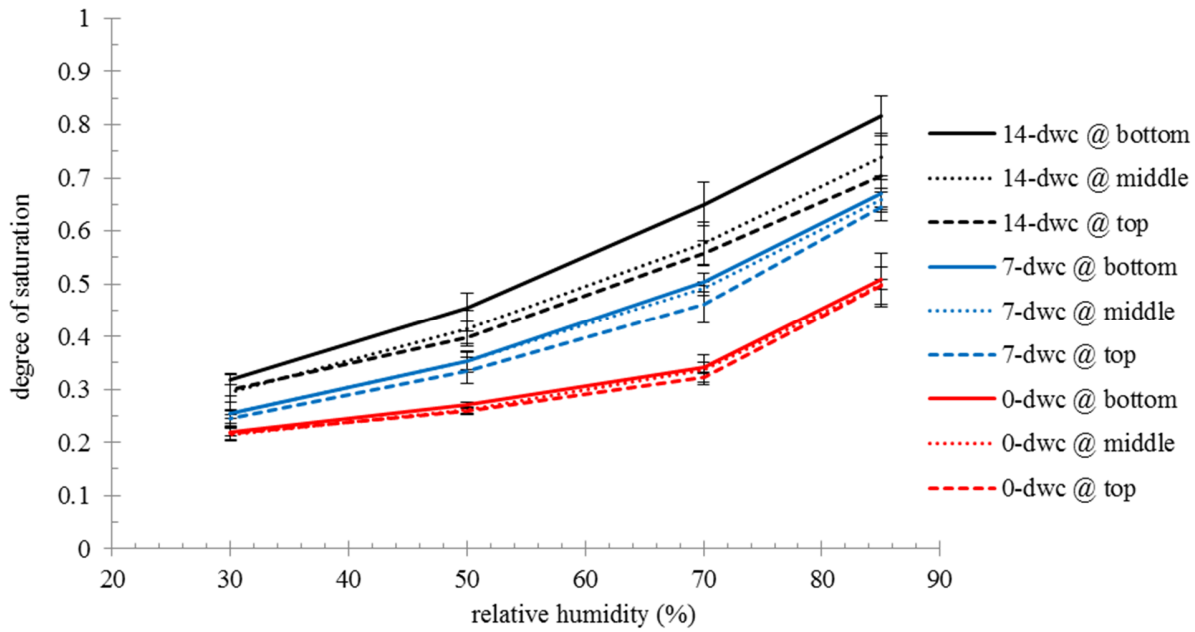

Figure VI.3 Degree of saturation after 14 d of exposure in different *RH* values for different depths and curing lengths

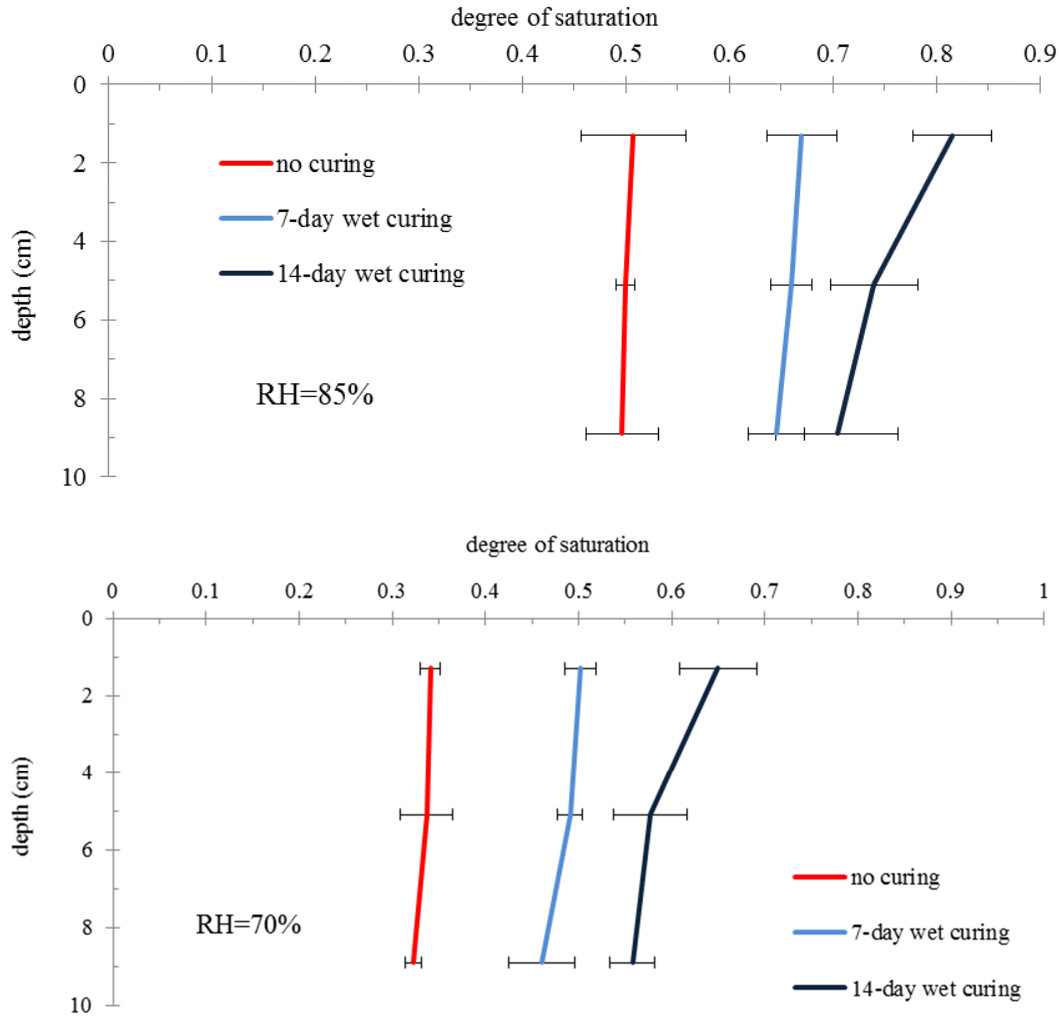
degree of saturation
0
0.1
0.2
0.3
0.4
0.5
0.6
0.7
0.8
0.9
depth (cm)
no curing
7-day wet curing
14-day wet curing
RH=85%
degree of saturation
0
0.1
0.2
0.3
0.4
0.5
0.6
0.7
0.8
0.9
1
depth (cm)
RH=70%
no curing
7-day wet curing
14-day wet curing

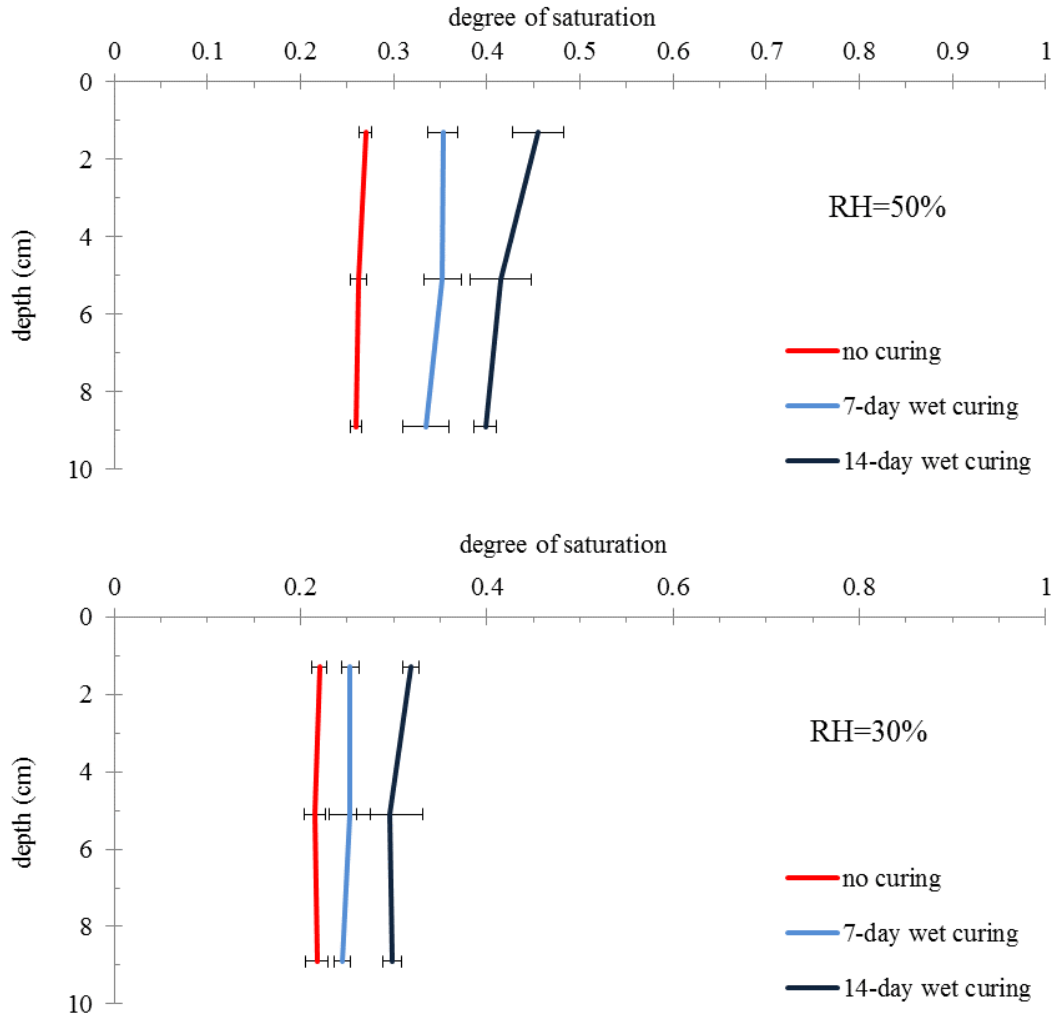

Figure VI.4 Degree of saturation profiles after 14 days of exposure in different *RH* for different depths and curing lengths

The increase in degree of saturation with the depth from drying surface of the specimen is not significant for uncured specimen, but it becomes larger with the increase in curing duration. Also, increasing the wet curing length and *RH* of the specimen storage has increased the degree of saturation. Therefore, the top section of the sample without any moist curing in 30% *RH* has the least degree of saturation measured, while the bottom of the sample with 14 days of wet curing at 85% *RH* has the highest degree of saturation measured. These results are likely due to a finer pore

structure caused by wet curing the samples, which promotes hydration and ultimately causes a higher degree of saturation (at a given *RH*) via refinement of the pore network. The gradient in the sorption isotherm is presumably due to a gradient in pore size distribution induced by enhanced hydration from the surface moisture associated with wet curing.

6.3.3 Drying Diffusion Coefficient

The *RH* fits through the use of Eq. (5.21) are shown for 0 d, 7 d, and 14 d wet curing at different depths in Figure 6.5. The solid line shows the simulation versus the dots that are the measured data from sensors. As mentioned before, the actual *RH* of the first 4 days for uncured beams has been interpolated due to the lack of measured data, since the sensors were put in the samples about 4 days after construction:

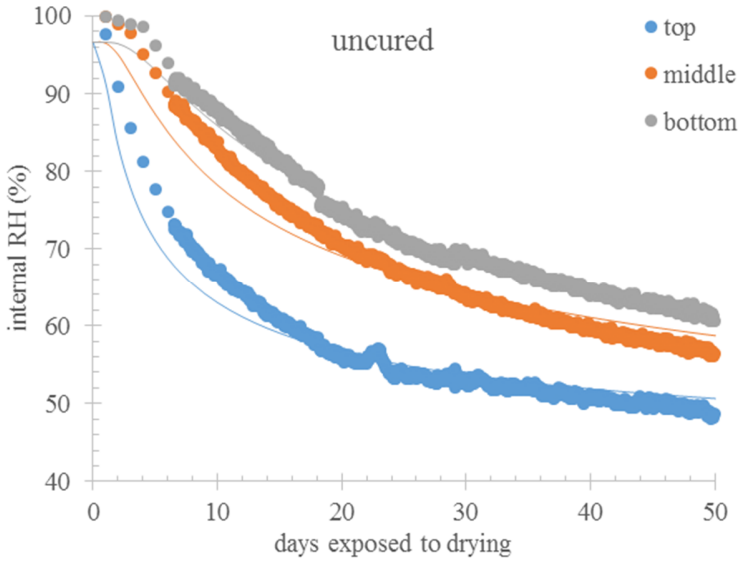

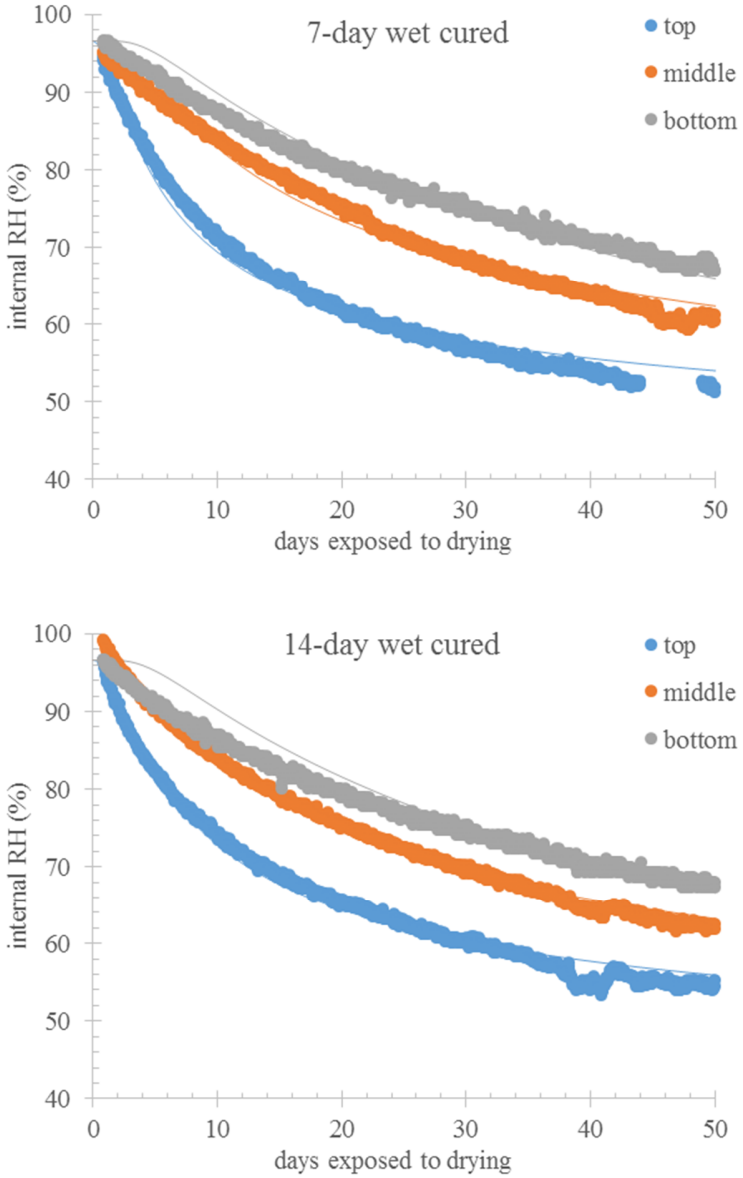

Figure VI.5 *RH* of concrete beams at different depths and curing lengths versus the simulated *RH*

One should use caution to discuss the goodness of the approximated *RH* versus measured data, since:

- The *RH* of beams at the early age was very high and sensors may have had problems measuring this,

- The *RH* of the drying chamber sometimes varied within 4% and this may have impacted the accuracy of the measurement,
- The expression used in Eq. (5.21) is also an estimation and cannot provide exact *RH* values.

If we assume these fits for *RH* are acceptable and that errors of sensors in measuring *RH* are not large, then calculated drying diffusion coefficients for different depths of samples with different curing lengths can be shown in Figure 6.6:

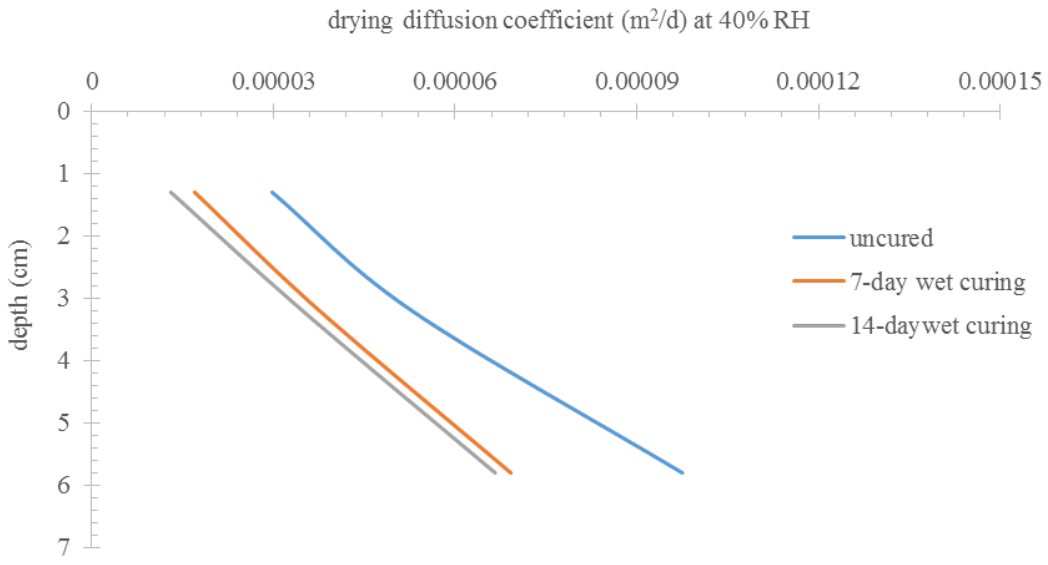

Figure VI.6 Profiles of the drying diffusion coefficient from simulation

Figure 6.6 shows that there is a difference between drying diffusion coefficients at the top (depth = 1.3 cm) versus bottom (depth = 5.8 cm). If the diffusion were perfectly linear, then one would expect no variation in D_i with depth. Therefore, there is a nonlinearity in diffusion, this causes a maximum difference of a factor of 4 difference between the D_i at low versus high *RH* regions in

the samples. Although this shows that the D_i within the considered depth (about 60% of beam's full depth) is close to linear, further experiment is required to measure the *RH* at lower depths. This would be helpful to measure the bottom side of the sample in order to calculate D_i. This may help estimate the magnitude of the nonlinearity of D_i.

6.3.4 Simulating Shrinkage for Concrete

The simulated shrinkage at different depths of the concrete beams is presented in Figure 6.7 for different curing lengths. The markers show the actual measurements according to experimental setup mentioned in chapter 4. The simulated results are shown by solid lines for each depth using the same color as the markers.

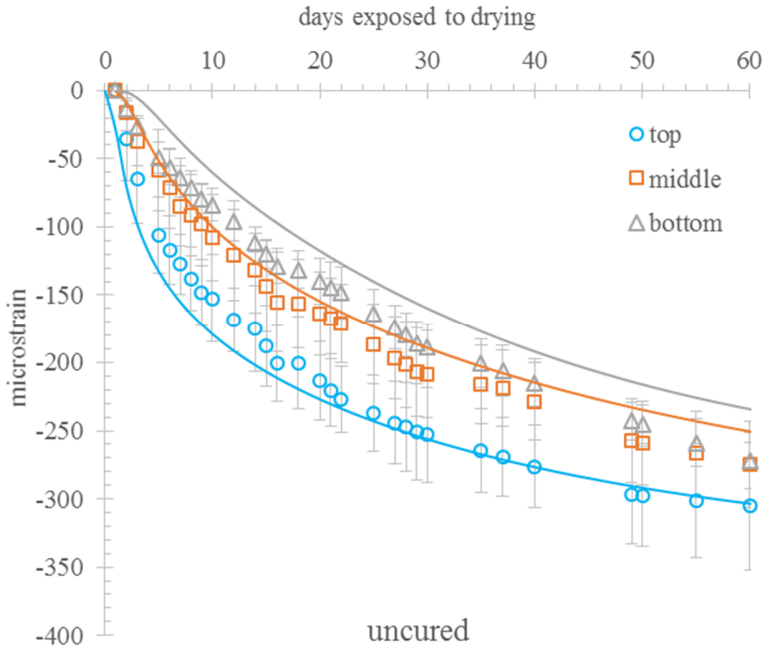

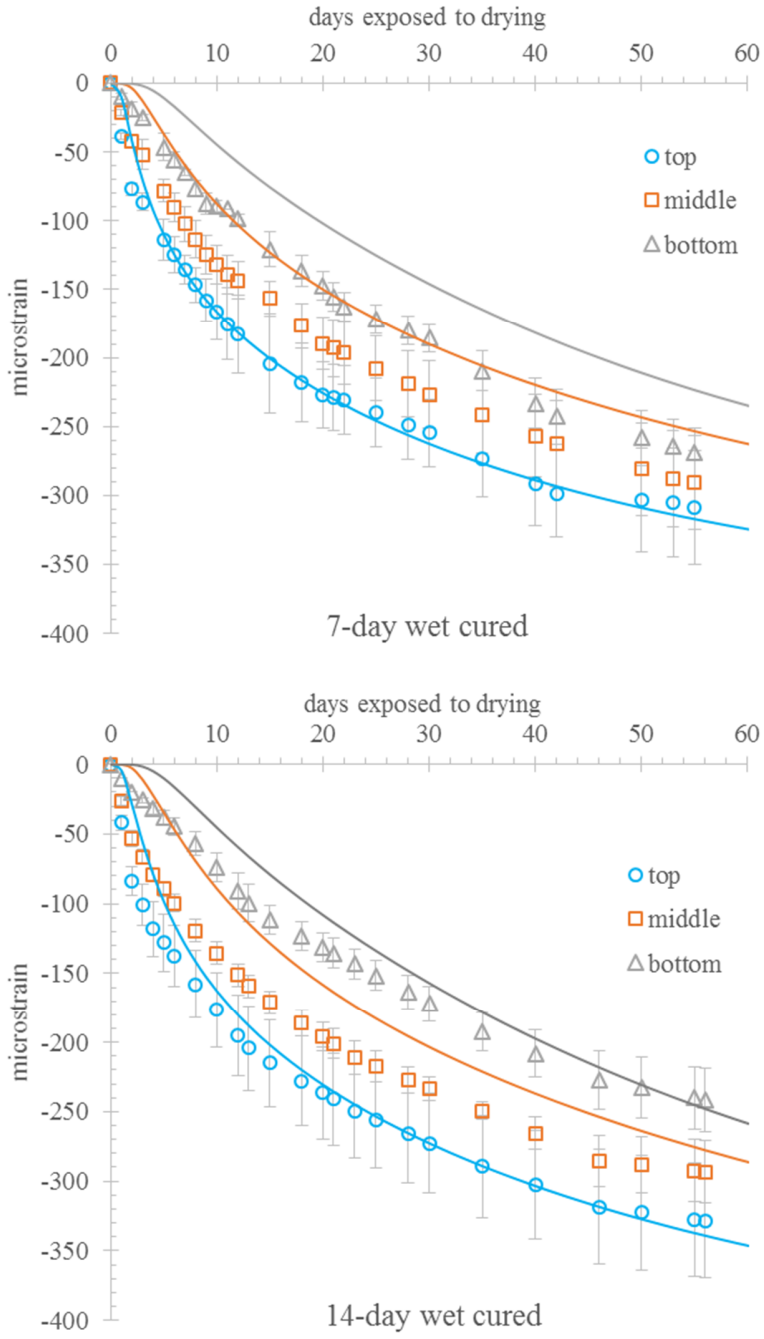

Figure VI.7 Experimental and simulated shrinkage at different depths of concrete beams with different curing lengths

As seen in the simulation for the uncured specimen, there is a small overprediction in shrinkage at the top at early ages which is due to the underprediction of *RH* as shown previously in Figure 6.5 for no-curing. The shrinkage calculation in this method is highly related to the accuracy of prediction of *RH* in the sample, since the underprediction in *RH* causes an overprediction in the calculated pressures and therefore free strain according to Eq. (5.11) - Eq. (5.14) in chapter 5. In general, the shrinkage prediction at the top is good for all curing methods as it is within the error bar range. On the other hand, the model has underpredicted the shrinkage at the middle and bottom of the uncured samples. This underprediction is more significant for wet cured specimens. Although the *RH* at the middle and bottom has been underpredicted like the top *RH*, the shrinkage was not overpredicted like the top one, which could be likely because of using similar input parameters to those found for the top or the nonlinearity of diffusion as shown in Figure 6.6. The input parameters used for concrete beams are shown in Figure 6.8:

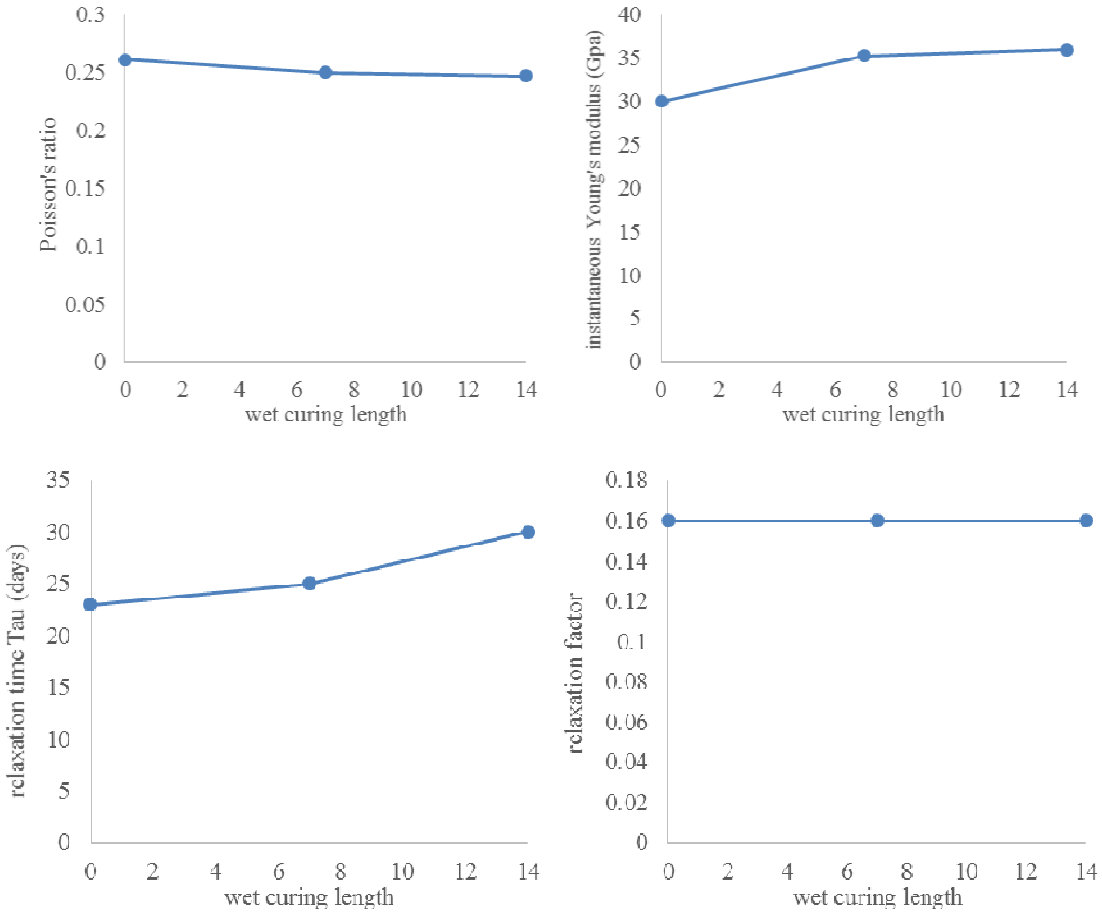

Figure VI.8 Adjusted input parameters for mechanical properties of concrete at 40% *RH*

As mentioned before, to find the best input parameters for the mechanical properties of the concrete beams only the shrinkage near the surface of the beam was used to fit the measured shrinkage and assuming the middle and bottom of the concrete beams have the same properties. In these figures, as shown for the paste at 40% *RH*, the change in Poisson's ratio is minor. The instantaneous Young's modulus has been measured as mentioned before using ASTM C39 (2016). The relaxation time has increased slightly along with 16% relaxation for all curing lengths.

It should be pointed out that the approximate solution for this study was found to be a good shrinkage predictor for the paste beams at 40% and their shrinkage history as shown in Figure 6.1. This could be caused by microcracks at lower *RH* that can reduce the nonlinaerity of diffusion and increase the diffusion. Also, the mechanical properties of thin paste beams are possibly similar at different depths of the paste beams. Therefore, while shrinkage at upper layers of concrete beams, which might have been affected by surface microcracks at 40% *RH*, can be calculated by the approximate linearized solution, shrinkage prediction at lower layers may require a nonlinear solution along with more accurate values for the mechanical properties.

6.3.5 Shrinkage Mechanisms in Concrete

As discussed in chapter 4, the degree of saturation in concrete samples near surface should be higher for wet cured samples comparing to the uncured surface. This is shown through the model in Figure 6.9 for the measured *RH* and degree of saturation. Different line types show the results at different depths (with solid lines for top, dots for middle, and dash for the bottom) and different markers are for different curing lengths:

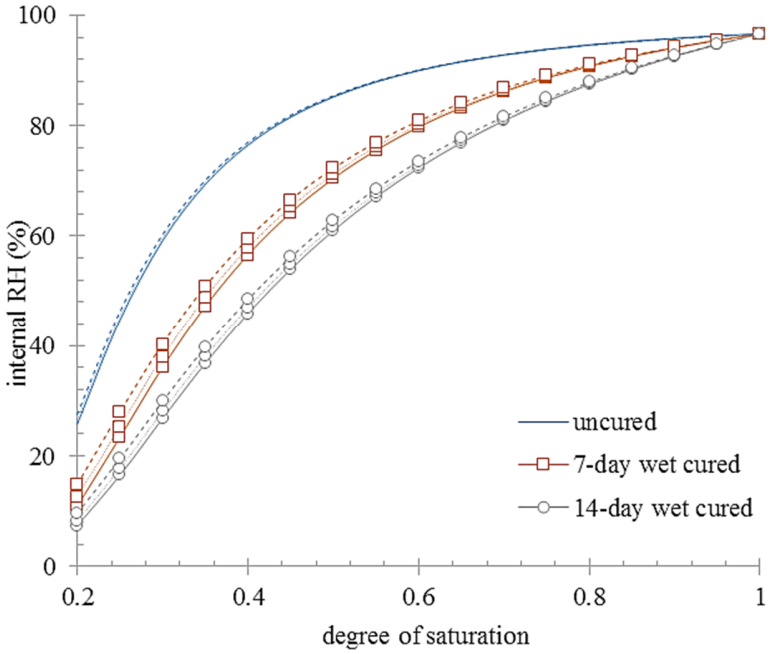

Figure VI.9 Relation between *RH* and degree of saturation for different curing lengths at different depths

This graph shows the degree of saturation at any given *RH* is larger for samples with a longer wet curing length. In other words, it shows that at any given degree of saturation the *RH* is lower in wet cured samples. According to Eq. (5.11) and Eq. (5.12) in the previous chapter a lower *RH* and a larger degree of saturation can cause more tension pressures. This is shown in Figure 6.10. Different line types show the results at different depths (with solid line for top, dots for middle, and dash for the bottom) and different markers are for different curing lengths:

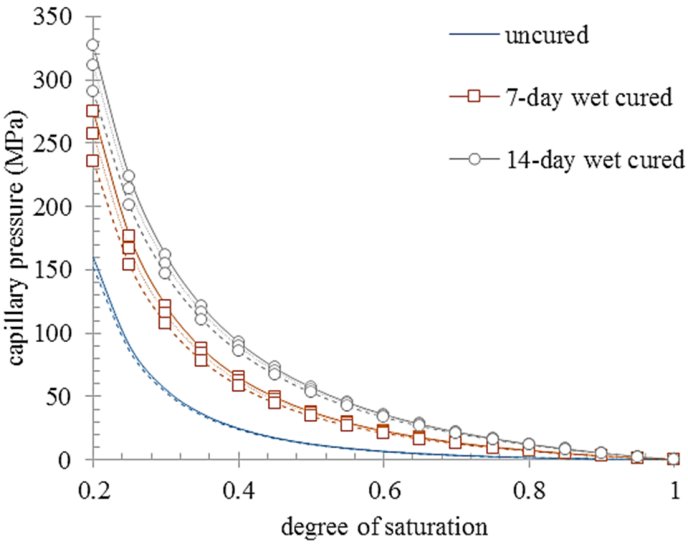

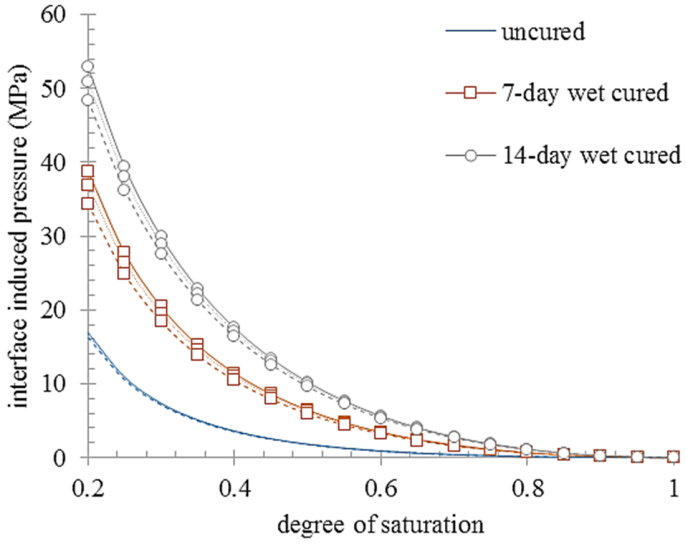

Figure VI.10 The capillary pressure and the interface induced pressure

As shown in Figure 6.10 the capillary pressure and the interface induced pressure are both greater in samples with longer duration of wet curing at any given degree of saturation. These pressures are the main driving forces for the tension occurring in the fine pores of drying paste or concrete and consequently causing a volume change due to the shrinking pores. Since the drying solid surface and liquid films in the pores exert these contracting stresses, the combination of these two pressures as defined by Eq. (5.13), known as effective pore pressure, as well as the rate of effective pore pressure are shown in Figure 6.11:

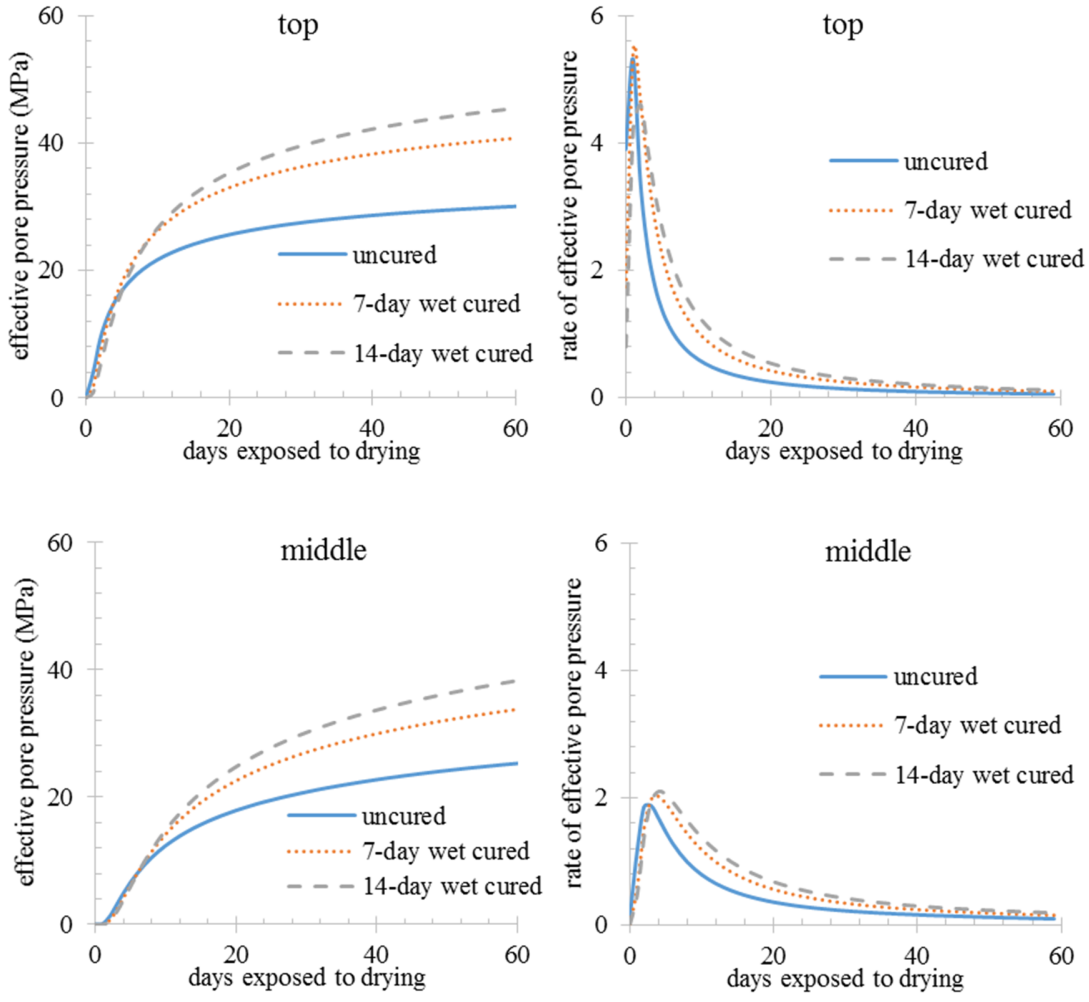

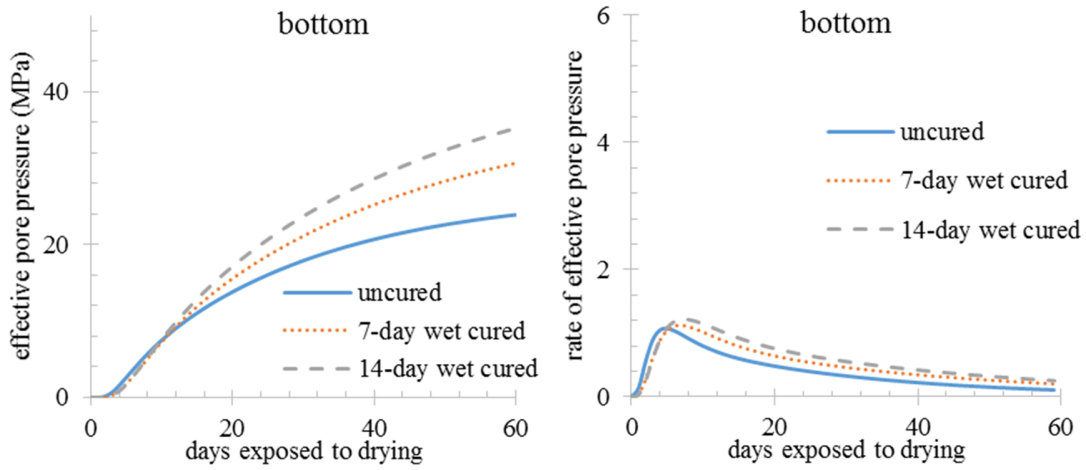

Figure VI.11 The effective pore pressure and its rate for different curing lengths at different depths

The rate of effective pore pressure ($\frac{\partial \xi(t)}{\partial t}$) as shown in Eq. (5.14) is larger in samples with longer curing which consequently caused more shrinkage as shown in Figure 6.8.

6.4 PRACTICAL IMPLICATION

The relation between drying shrinkage and degree of saturation has been investigated in the last 3 chapters. Since the curling of slabs is due to a differential drying shrinkage, then drying shrinkage models can predict the curling by plugging degree of saturation profiles into the model more accurately. Also, accurate mechanical properties of concrete can enable the model to predict shrinkage and deflection more accurately. Since the concrete pavement near drying surface, especially at environments with lower humidities, is more prone to micrcracking, predictions by the introduced simplified linearized model (specifically around the curing affected zones, i.e. the upper layers) will be less affected by the nonlinearity of diffusion. Therefore, the approximate model provides a useful tool to predict the curling of concrete slabs.

6.5 CONCLUSION

In this chapter the previous approximate model, which was verified for fitting the peak deflections of thin paste beams at 40% *RH*, was adjusted further for simulating the concrete shrinkage. It was concluded that:

- Adjusting the model with mechanical properties of cured and uncured paste can help predict the curling response of concrete beams as longer curing increases the relaxation and decreases the porosity.

- Assuming similar values of mechanical properties (input parameters of the model) for both uncured and cured specimens causes underprediction at post deflection for cured samples.

- The presented linearized model is very accurate for dry environemnts and thin samples.

- Regarding the thicker samples, the model is very sensitive to not only the mechanical properties but also *RH* of concrete elements, as shown for a 4” deep sample.

- Predictions are more reliable in lower humidity regions, which can be related to either a more accurate *RH* measurements or surface microcracks which reduce the nonlinearity of diffusion.

- The drying diffusion is not perfectly linear over the entire depth. This nonlinearity was shown by using the approximate model to be a factor of about 4 within 60% of the concrete depth.

- Shrinkage at lower depths of 4” concrete beams was underpredicted by the model. Considering the underprediction for the post deflection of cured thin paste beams due to the use of mechanical properties of uncured thin paste beams, the underprediction of shrinkage at lower depths of thick concrete beams is either due to the use of similar

mechanical properties to those at the top or the high nonlinearity of diffusion at lower depths.

Therefore, while there are very good shrinkage predictions by applying the approximate model, further work needs to be done to improve it for simulation in concrete, thicker elements, and other storage humidities. Also, further investigation near the bottom of specimens (with more precise and durable sensors) is needed to accurately measure RH and diffusion, and shrinkage.

CHAPTER VII

VII. THE IMPACT OF DIFFERENT RELATIVE HUMIDITIES ON DRYING SHRINKAGE

7.1 INTRODUCTION

It was shown in the previous chapters that in 40% relative humidity (*RH*) drying conditions the magnitude of curling increased with the duration of wet curing. This observations were supported by findings from the computer modeling for 40% *RH* as well. The mechanism for this behavior was attributed to the increased curing leading to a decrease in the pore sizes. On drying, the capillary suction in these smaller pores causes increased shrinkage which in turn leads to increased curling. Also, different curing compounds were investigated at a number of different coverage rates in chapter 3. Using statistical analyses this work showed that the poly-alphamethylstyrene (PAMS) performed the best of the curing compounds. Next the resin based and finally the water based performed the worst. Performance with different coverage rates was also investigated (Hajibabaee, Khanzadeh Moradllo, & Ley, 2016).

The work in this chapter examines the curling of cement and concrete samples caused by differential drying in laboratory conditions that are close to the average RH in Oklahoma (~70%). Next modeling work is completed to simulate the shrinkage results at 70% RH. An analytical approximate solution will be used as well to simulate the curling of paste beams at 70% boundary condition.

It should be pointed out that the research in previous and current chapters used laboratory

specimens that were cast and stored in 40 and 70% RH. Therefore, an alternative test is also done to evaluate the performance of these same concrete specimens in the field. One challenge with this work is the variation in temperature, moisture, and wind over time since these samples were stored in the field. This means that all of these variables had to be measured while simultaneously measuring the response of the samples. However, these exposure conditions led to a more realistic environmental condition for field concrete. In order to learn more about the impact of different curing methods on the curling of concrete pavements in the field, 62 different sensors were installed on a continuous reinforced concrete pavement used on Highway I-44 & Lewis in Tulsa, Oklahoma in August of 2013. Therefore, these findings provide guidance for wet curing durations for slabs that must be resistant to volume change in different drying conditions.

7.2 METHODOLOGY

7.2.1 Materials and Mixture Proportions

The Portland cement used for paste beams meets the requirements of both a type I and II cement, according to ASTM C150 (2011) and AASHTO M85 (2012). The cement used for concrete samples is type I, according to ASTM C150 (2011). Samples were made with dolomitic limestone aggregate and natural river sand used commercially in concrete. For both paste and concrete beams the mixutures had a water to binder ratio of about 0.42. More details can be found in chapters 2-4.

7.2.2 Sample Preperation, Test Procedure, and Measurements

7.2.2.1 Paste beams for laboratory condition

As described in details in chapter 2, the paste mixtures were prepared according to ASTM C305 (2011). Three paste beams with dimensions of 39.4×2.4×0.5 in^3 were consolidated in plastic molds from each mixture. Samples were kept in saturated burlap for 1, 3, 7, and 14 days of additional curing after demolding and waxing. The burlap was wetted every day to ensure that it remained saturated. After the curing was removed the specimens were subjected to a 70±4% *RH*

and 23°C drying environment within an environmental chamber. Other samples received no curing after demolding.

To measure the curling, rubber bands were used to hold the ends of the specimen to a flat aluminum plate with the uncoated surface of the specimen facing the plate. The distance between the aluminum plate and the specimen is measured at regular locations along the length with a caliper. The loss of moisture of the sample was measured through the weight loss over time. After finishing the measurements, the specimen is returned to the chamber room until the next measurement. More details can be found in chapter 2.

7.2.2.2 Concrete beams for laboratory and field conditions

In this experiment the specimen was 3×4×10.25 in^3. A waterproof membrane was used on all faces of the sample except for the top. The moisture barrier was used as a form liner during casting. Concrete specimens were demolded 24 hours after casting and the interface between the membrane and the concrete were sealed by wax. The surface strain of the beam was measured at 3 different depths. The *RH* of beams was measured at 0.525", 1.275", and 2.275" from the finished surface starting four days after the termination of curing. The sensors were placed in 0.7" deep holes with 0.7" diameter that were cast into the side of the concrete. The *RH* sensors were calibrated according to ASTM E104 (2012) with four different salt saturated solutions. The *RH* calibration range was between 57.6% and 97.3%.

For the laboratory condition, all specimens were cast and stored in an environmental chamber at 23°C and about 70±4% *RH*. Specimens were prepared with no-curing and 7 and 14 days of wet curing with wet burlap and a plastic tarp. While drying the beams were flipped on their side and placed on wooden dowels to minimize the impact of self-weight on curling measurements. More details can be found in the chapter 4.

For the field condition, specimens were prepared with no-curing, 1, 3, and 7 days of wet curing with wet burlap and a plastic tarp, as well as a number of different curing compound combinations. All curing methods have been summarized in Table 7.1. More details can be found in chapter 3 regarding the curing compound application (Hajibabaee, Khanzadeh Moradllo, et al., 2016).

Table VII.1 All curing methods used before the exposure

Name	Curing methods		
1-day wet	Wet curing with wet burlap for 1 day		
3-day wet	Wet curing with wet burlap for 3 days		
7-day wet	Wet curing with wet burlap for 7 days		
No curing	Exposed to the site without any curing		
Sealed	Sealed with wax and wrapped in plastic before exposure to the site		
Water-wax, S 100%	Single layer	water-wax based curing compound	0.04 lbs/ft^2
Water-wax, S 150%	Single layer	water-wax based curing compound	0.06 lbs/ft^2
Water-wax, D 100%	Double layer	water-wax based curing compound	0.04 lbs/ft^{2*}
Resin, S 100%	Single layer	resin based curing compound	0.04 lbs/ft^2
PAMS, S 100%	Single layer	poly-alphamethylstyrene curing compound	0.04 lbs/ft^2

*The double layer of curing compound was applied in two equal layers of 0.02 lbs/ft2 for each one for a total coverage of 0.04 lbs/ft^2.

A weather station has been used to measure the wind speed, rainfall, temperature, solar radiation, and *RH* during the test. These measurements were taken every five minutes.

7.2.3 Modeling Work

In this chapter the analytical approximate linear model, as defined in chapter 5, was chosen to simulate the curling deflections of paste beams as it gave similar results to nonlinear numerical solution. Since the results were very similar, and that the nonlinear numerical solution was very time consuming, only the results from approximate solution were shown here.

For concrete beams, the approximate model was used as adjusted in chapter 6. The measured internal *RH* of the concrete beams at 3 different depths was used to find diffusion at each depth according to the following expression, Eq. (7.1):

$$RH(x,t) = \left(RH_{bound} - RH_{initial}\right)\left(1 - \mathrm{Erf}\left[\frac{L/2 - y}{2\sqrt{D_i t}}\right]\right) + RH_{initial} \qquad \text{Eq. (7.1)}$$

Then the mechanical properties of concrete beams at the top were used as the input parameters to simulate and compare the shrinkage affected by different curing lengths. More details on the modeling work can be found in the previous chapters.

7.2.4 Field Instrumentation

The following curing methods were investigated as shown in Figure 7.1: wet cure with wet burlap for 5 days, water-wax and PAMS curing compound, and misting provided to the surface of the pavement every hour for 24 hours. Nine strain gages and seven *RH* sensors were used to measure the strain and *RH* profiles of a typical slab.

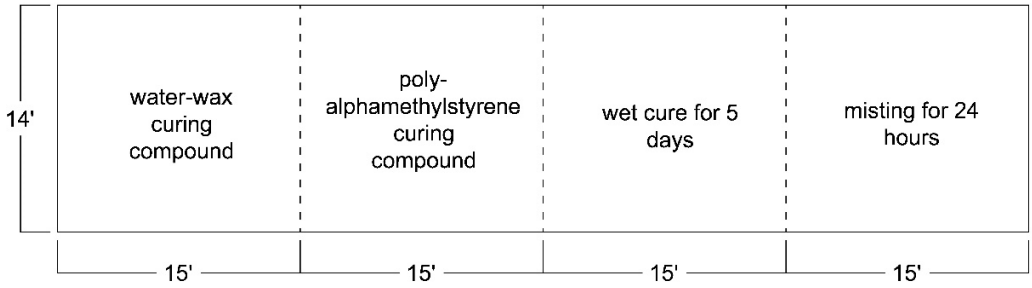

Figure VII.1 Curing materials and methods used on the pavement

Figure 7.2 shows the arrangement of the strain gages and rebar. Each gage can measure strain and temperature simultaneously. These gages were chosen because they were robust and have been used for long term monitoring of concrete structures. These strain gages were tied to a vertical stand with feet at the bottom to help hold the bars in place. This stand was then tied to the traverse reinforcing bars. Care was taken in the field to ensure that each gage was at the reported height from the concrete base shown in Figure 7.2. However, it was not possible to measure these sensors after the fresh concrete was placed and consolidated and so it may be possible that small

changes occurred that were not captured. It should also be noted that the actual pavement constructed was 13” instead of 12” at the point of construction. This slightly changes the strains measured in the pavement but should be able to be overcome in the analysis of the data.

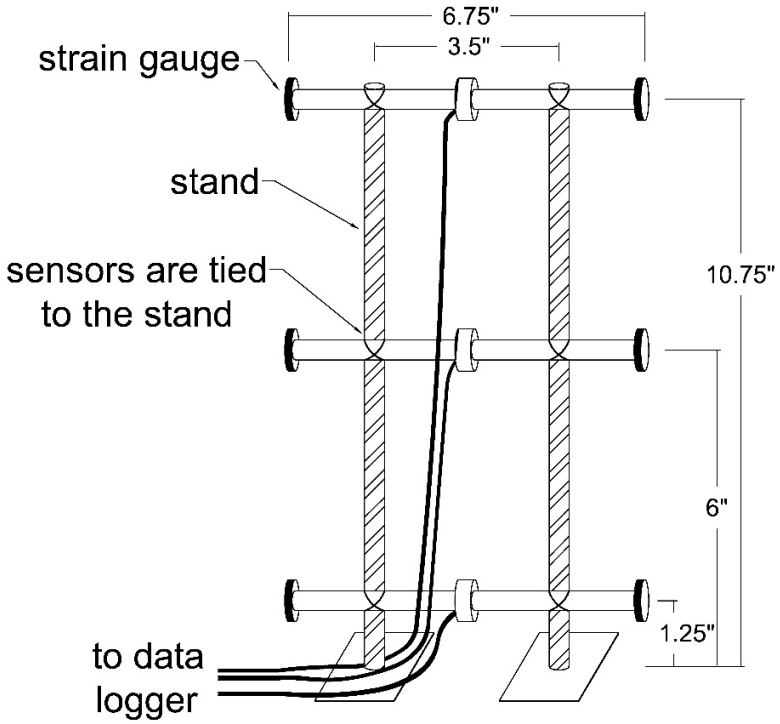

Figure VII.2 A strain gage tied to the steel bars

The RH gages were placed at two different spots, which are the centerline between each two sets of strain gages. RH is measured at different depths: 1”, 3.5”, 6”, and 11” as shown in Figure 7.3.

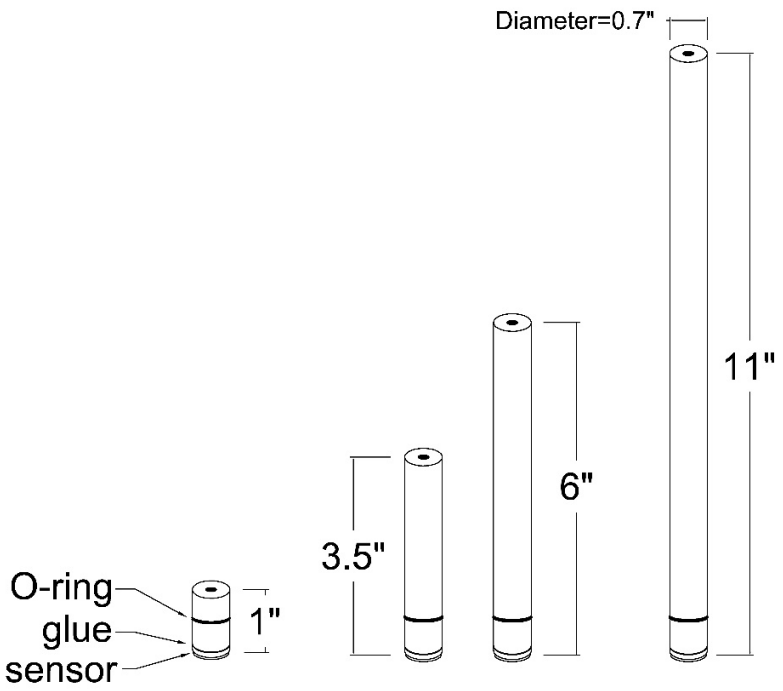

Figure VII.3 *RH* sensors glued to rods

The mentioned depths were drilled in the pavement five days after paving. Sensors were glued to rods that were embedded into the drilled holes. These rods had an O-ring at the end to seal between the concrete and the rod to ensure that the readings were only coming from the concrete near the sensor. Grease and caulk was also used to help seal the rod. A typical installation is shown in Figure 7.3.

Strain gages were embedded in the pavement at three different spots. Nominally the gages were attempted to be placed at the center, edge, and the quarter point of the pavement. Unfortunately because of the rebar layout and pavement vibrators these locations had to be varied slightly. As shown in Figure 7.4 for a typical slab, the gages were oriented in the transverse direction of the pavement in order to measure curling and shrinkage of the pavement. A gage was used at the top and bottom of the pavement so that it could show any differential strain between these two locations. This strain differential will be tied to the amount of curvature or bending that occurs in

the pavement. The strain gage at the center of the pavement will help examine the strain profile and the amount of uniform shrinkage that occurs in the pavement. By combining these measurements with the temperature measurements and humidity, it should be possible to compare the overall strain profiles in the pavement and determine whether these can be attributed to differentials in shrinkage, temperature, or humidity.

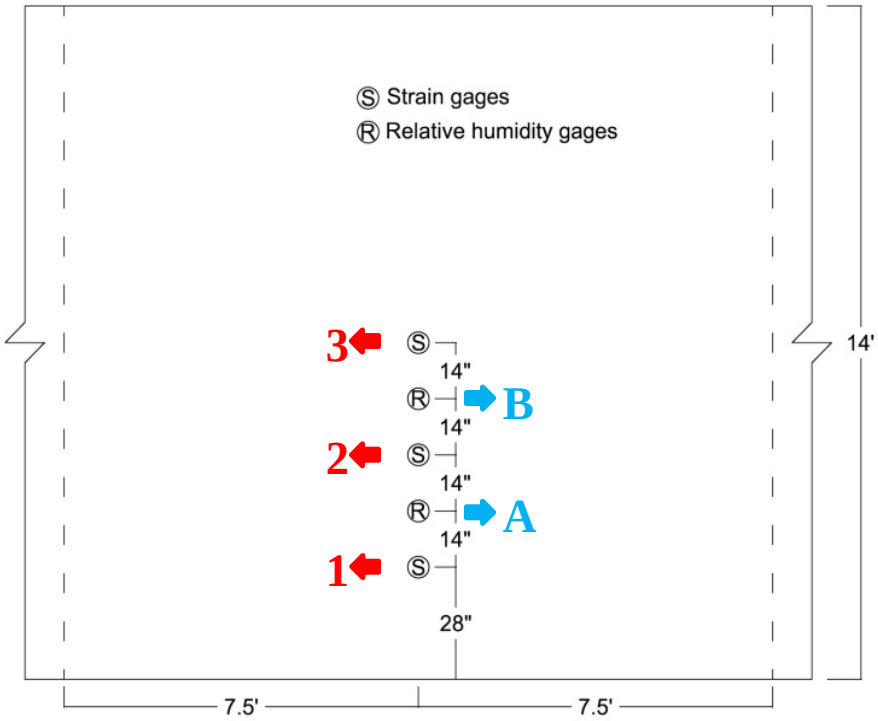

Figure VII.4 Top view of a typical slab to show the coordination of all the gages

Both of the curing compounds were manually applied to the surface of the pavement. The water-wax based curing compound was sprayed manually by the contractor and the PAMS was sprayed by the researchers. For wet curing, five days after paving and before drilling, the curing was terminated and the burlaps under tarp were still moist. The last section of this field experiment was cured by misting. This was done manually every hour for the first 24 hours after placement of the concrete.

7.3 RESULTS AND DISCUSSION

7.3.1 Paste Beams in the Laboratory Condition

The mass loss of the paste samples with different curing lengths in 70% *RH* is shown in Figure 7.5 in comparison with that of samples in 40% *RH* from chapter 2.

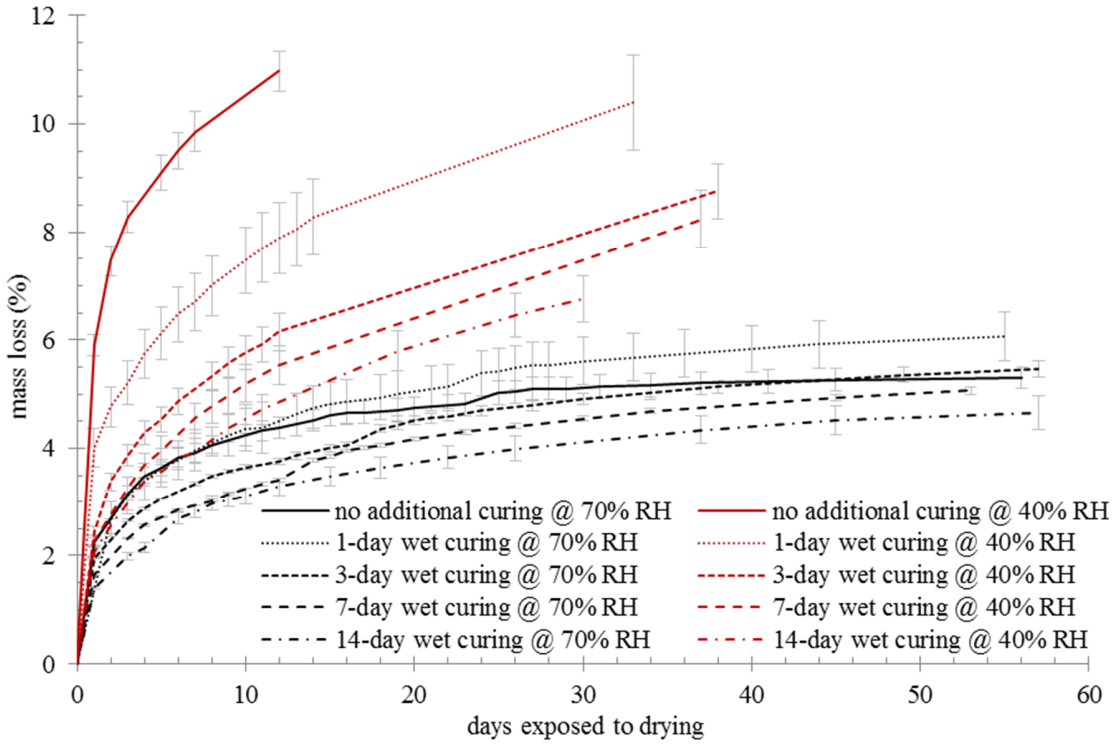

Figure VII.5 Comparison between the mass loss of the paste beams at different *RH* over time

As shown above, the mass loss of the paste samples in 40% *RH* is greater than the samples that were exposed to 70% *RH*. The maximum mass loss of the no curing at 40% *RH* is the most and the least mass loss was observed in 14-day wet curing in 70% *RH*. Also, the difference between mass losses of different curing lengths is less in 70% compared to 40% *RH*'s. Also the increase in the curing length has decreased the mass loss amount. The mass loss of the uncured sample is lower than that of the 1-day wet cured sample for 70%, which is a different observation from the 40% samples. Since it was not possible to measure the mass loss in the first day for uncured

samples that were still molded, then this difference likely happened, while the wet cured samples were covered with wet burlap after 6 hours from casting, i.e. when bleeding water was completely disappeared and paste was hardened, and this caused less erroneous mass loss for wet curing.

In a drier environment the drying rate is faster and samples lose more moisture as it takes more time for samples in 40% *RH* to get to the state of moisture in the pore networks that has sufficiently equilibrated with their environment. Therefore, this mass loss will continue until the internal *RH* reaches equilibrium with the environment. However, because the moisture loss at the top and bottom of the sample is different, there is a differential in shrinkage and so the sample curls. This curling deflection of the paste samples exposed to 70% versus 40% *RH*'s is shown in Figure 7.6:

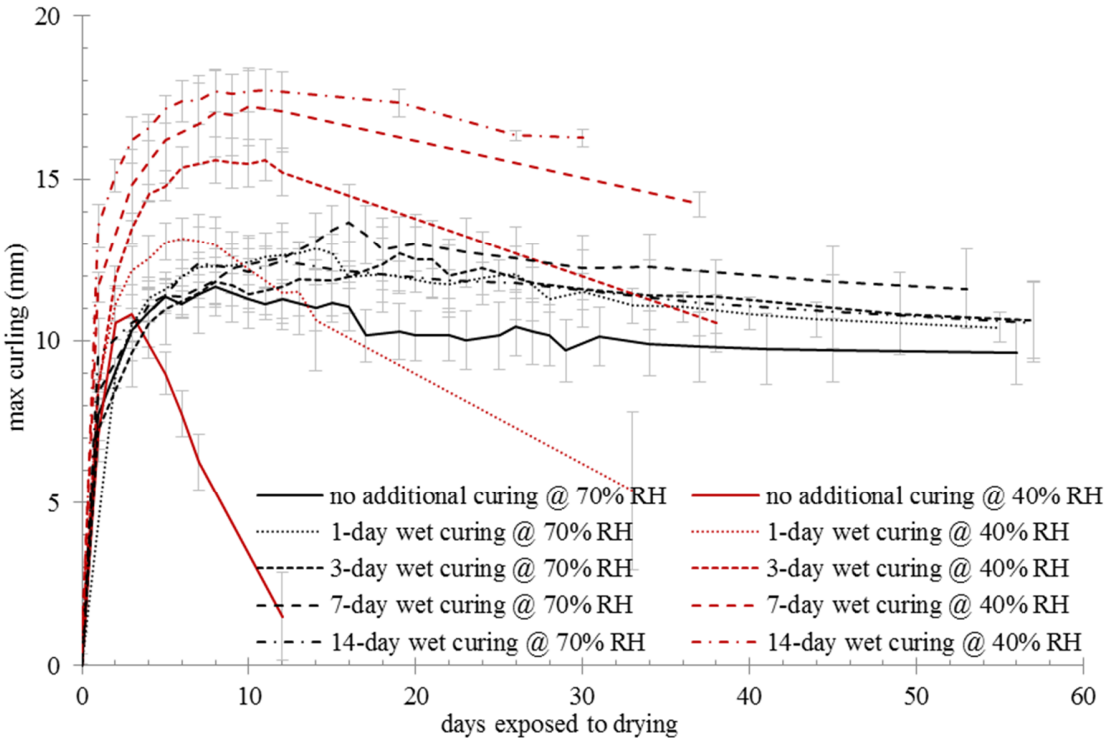

Figure VII.6 Comparison between the maximum curling of paste beams

As shown in Figure 7.6, the samples in 70% *RH* have less curling compared to samples in 40% *RH* and there is a less difference between the maximum deflections of different curing lengths in the more humid environment compared to deflections in the more extreme drying condition. Also the increase in the length of curing has increased the maximum curling. With increased drying, the curl decreases as the material in the bottom of the sample begins to shrink and the differential in shrinkage between the top and bottom is reduced.

Additional curing will sustain hydration and decrease the porosity and permeability of cement paste. Because the pore sizes are smaller for materials with a greater degree of hydration, the degree of saturation will be higher at a given *RH* as discussed in the previous chapter. This increase in saturation may be explained by the Kelvin-Laplace equation, which describes the minimum pore size emptied at a given *RH* at equilibrium. This means that curing will cause a higher level of saturation and will increase the effective pressure in the pore network and, therefore, the shrinkage on drying (Coussy et al., 2004).

Also, the decrease in permeability with extended curing makes it more difficult for a specimen to lose moisture from drying. This is why specimens that are cured longer lost moisture at slower rates, and required more time to reach their maximum amount of curling. Moreover, the additional wet curing may increase the water content of samples, which will increase the length of drying time needed for the samples to reach their maximum curling deflection. A high storage *RH* causes a decrease in the shrinkage gradient and the resulting deflection. Also it delays the drying time required to reach the peaks of deflection as shown above.

The results from simulating the curling of paste beams at 70% *RH* based on the abovementioned mechanisms are shown in Figure 7.7. Since the error bars as shown in Figure 7.6 were large, the results are shown within the 95% confidence and prediction bands:

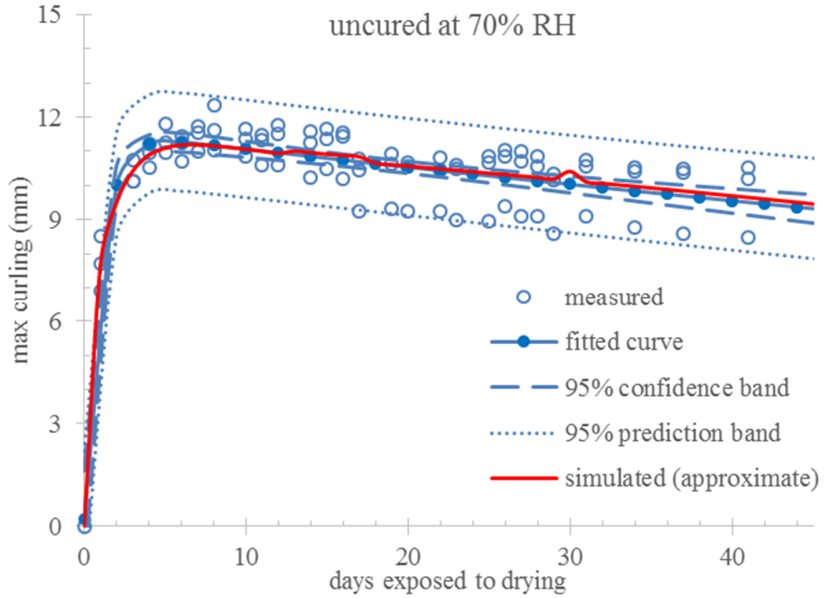
uncured at 70% RH
max curling (mm)
days exposed to drying
measured
fitted curve
95% confidence band
95% prediction band
simulated (approximate)

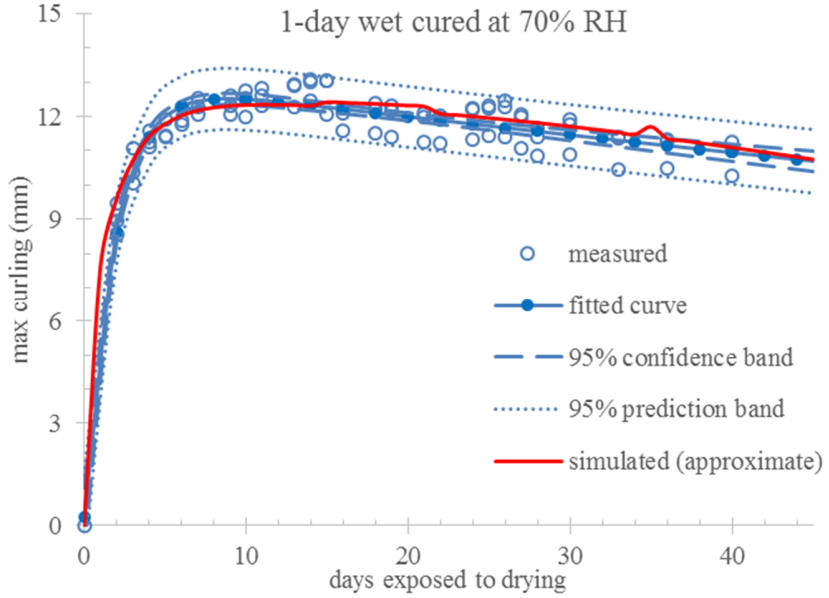
1-day wet cured at 70% RH
max curling (mm)
days exposed to drying
measured
fitted curve
95% confidence band
95% prediction band
simulated (approximate)

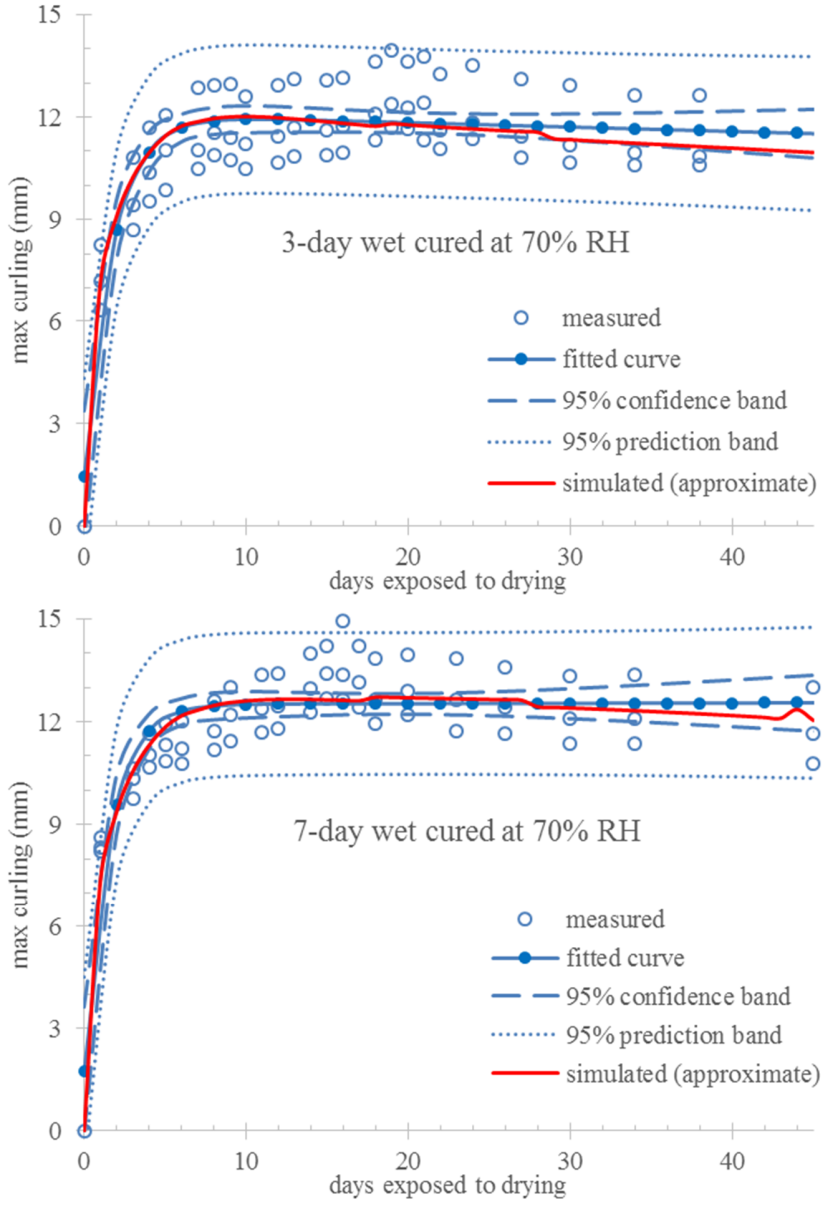
15
12
9
6
3
0
max curling (mm)
3-day wet cured at 70% RH
measured
fitted curve
95% confidence band
95% prediction band
simulated (approximate)
0
10
20
30
40
days exposed to drying
15
12
9
6
3
0
max curling (mm)
7-day wet cured at 70% RH
measured
fitted curve
95% confidence band
95% prediction band
simulated (approximate)
0
10
20
30
40
days exposed to drying

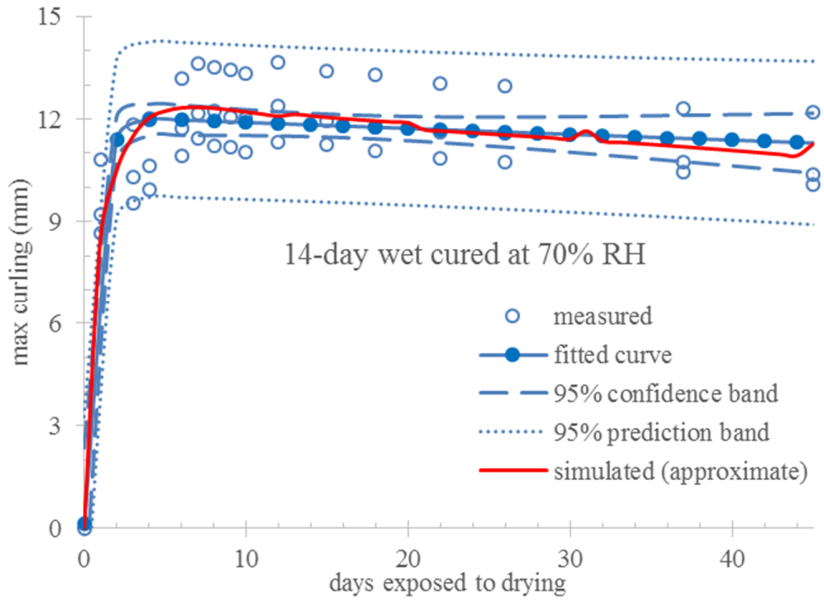

Figure VII.7 Simulated curling results of paste beams at 70% *RH* versus measured data

The simulated curling results in all curing methods are within the 95% confidence band. These results show that the mechanisms discussed above for 1D drying shrinkage and curling of paste beams in 40% *RH* are also valid to explain the curling at higher humidities since the same model has been used for above simulations.

7.3.2 Concrete Beams in the Laboratory Condition

The mass change of the concrete beams in the 40% versus 70% *RH* is shown in Figure 7.8:

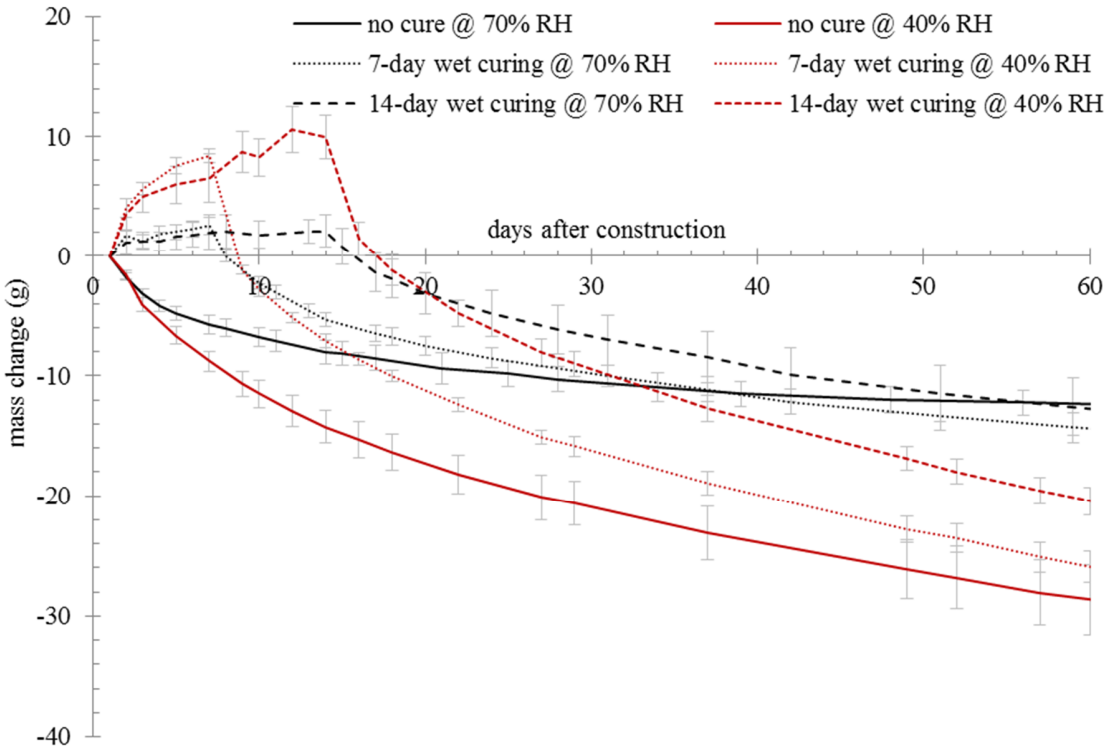

Figure VII.8 Comparison between the mass changes of concrete beams in 40% vs. 70% *RH*'s

The samples stored in 40% *RH* have more mass loss and there is a greater mass loss difference between samples when compared to samples stored in 70% *RH*. The wet cured samples increased in mass from the additional water that was supplied from wet curing. However, when these specimens were dried they quickly lost the extra mass gained from the wet curing. When comparing the first 3 days of drying, the 7 and 14-day wet cured samples had a greater rate of mass loss than the sample that was not cured.

The *RH* profiles within the samples for 5, 25, and 50 days after exposure are shown in Figure 7.9. The *RH* gradient is larger for samples that were exposed to the more extreme drying condition. Also, with extended drying the *RH* decreased faster in the 40% *RH*.

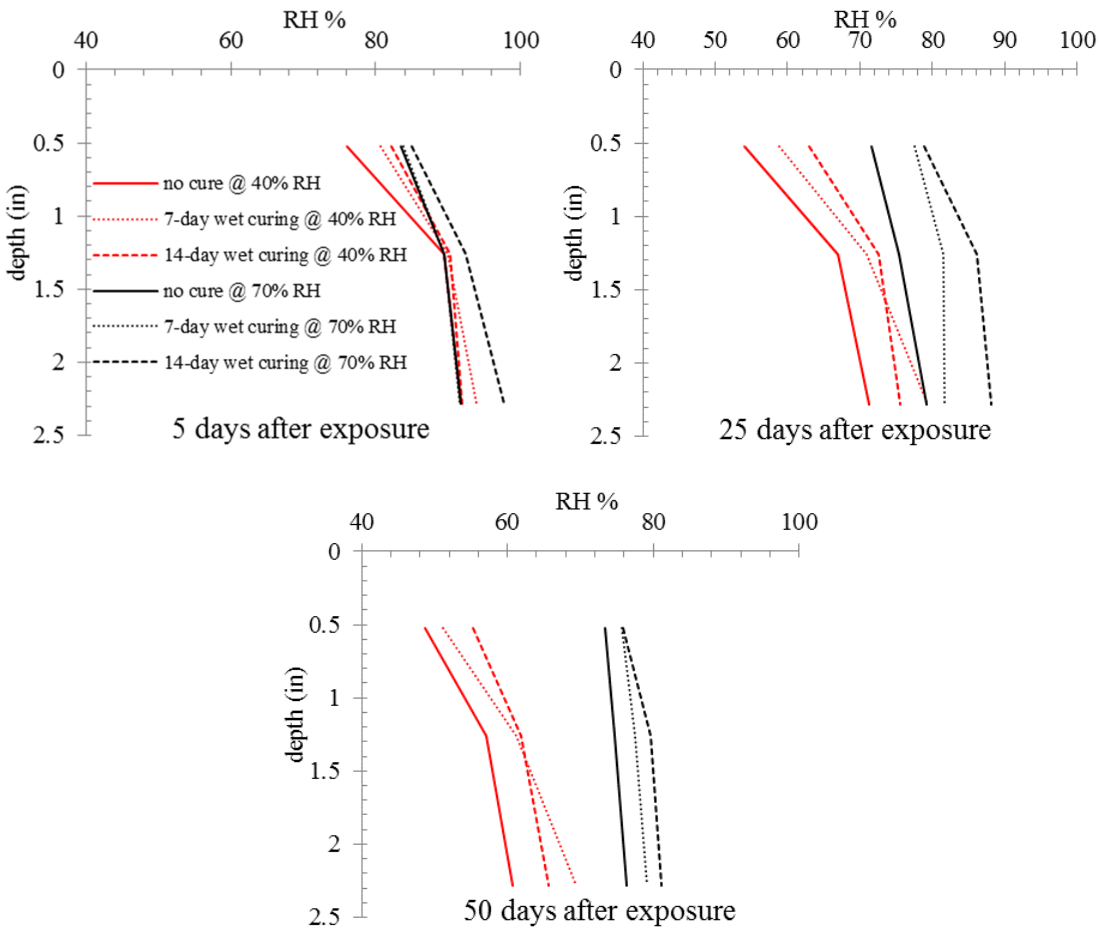

Figure VII.9 Comparison between the RH profiles in 40% vs. 70% *RH*.

Using extended wet curing, the samples should have improved levels of hydration and decreased permeability and hence lost less moisture at comparable times. The water loss occurred first on the surface and did not have a major impact on the *RH* over the depth of samples. The sample that was not cured showed lower *RH* at virtually all places in the specimen for all of the compared drying periods.

The shrinkage of the concrete beams at 0.525" depth (top) is shown in Figure 7.10 for 40% versus 70% *RH*. The shrinkage of the samples in 40% *RH* is greater and as the curing length was

increased then so did the amount of shrinkage that occurred. The rate of shrinkage is greater during the initial drying for the 40% *RH* samples when compared to the 70% *RH*.

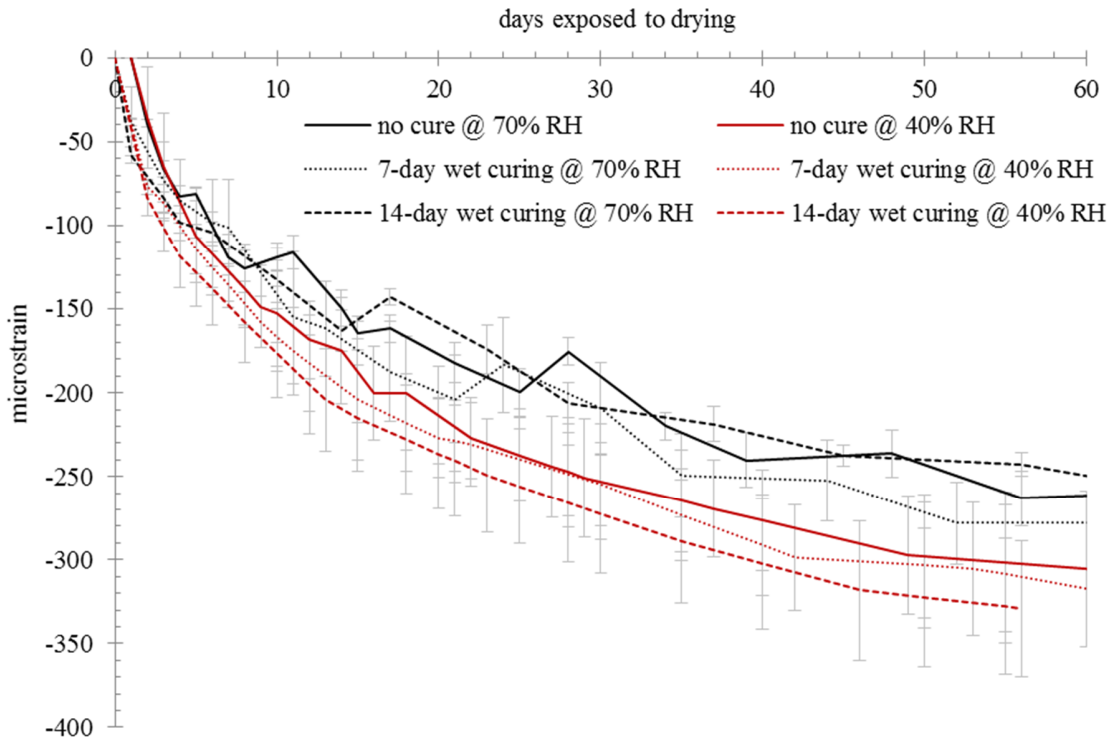

Figure VII.10 Comparison between the shrinkage profiles in 40% vs. 70% *RH*.

The shrinkage profiles within the samples for 5, 25, and 50 days after exposure are shown in Figure 7.11. The shrinkage gradient is larger for samples that were exposed to 40% *RH*. Also, samples exposed to 40% *RH* showed greater amounts of shrinkage.

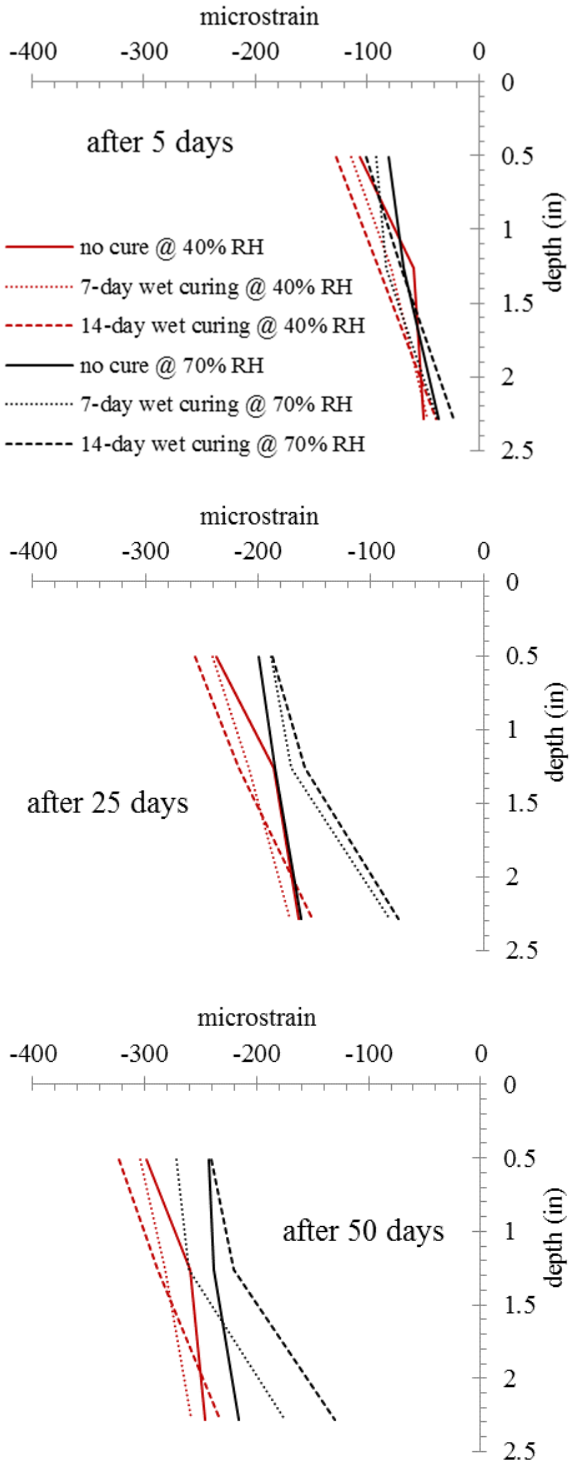

Figure VII.11 Comparison between the shrinkage profiles in 40% vs. 70% *RH*

Despite the internal *RH* being lower for samples with no curing, these samples showed an equal or lower shrinkage strain than the sample with wet curing. This increase in the internal strain gradient is expected to produce a greater amount of curling in the specimen. It is expected that the permeability of the wet cured specimens is less than that of no cured samples due to the decrease in connectivity and the sizes of the pores from the increased degree of hydration caused by the curing. Also, since these pores are smaller this will lead to an increase in the degree of saturation. As seen before for paste beams, this increase in saturation will increase the effective pressure in the pore network and the drying shrinkage (Coussy et al., 2004). Despite all of these changes occurring in the paste, the shrinkage in the concrete is related to shrinkage in the paste (Pickett, 1956).

The results from simulating the drying shrinkage of concrete beams at 70% *RH* based on the abovementioned mechanisms are shown in Figure 7.12. The mechanical properties used for the input parameters of these simulations were found after fitting the modeled shrinkage of the top of the beams with their experimental results. This helps to use different mechanical properties for each curing. The simulated results are shown with solid lines versus the experimental results with markers:

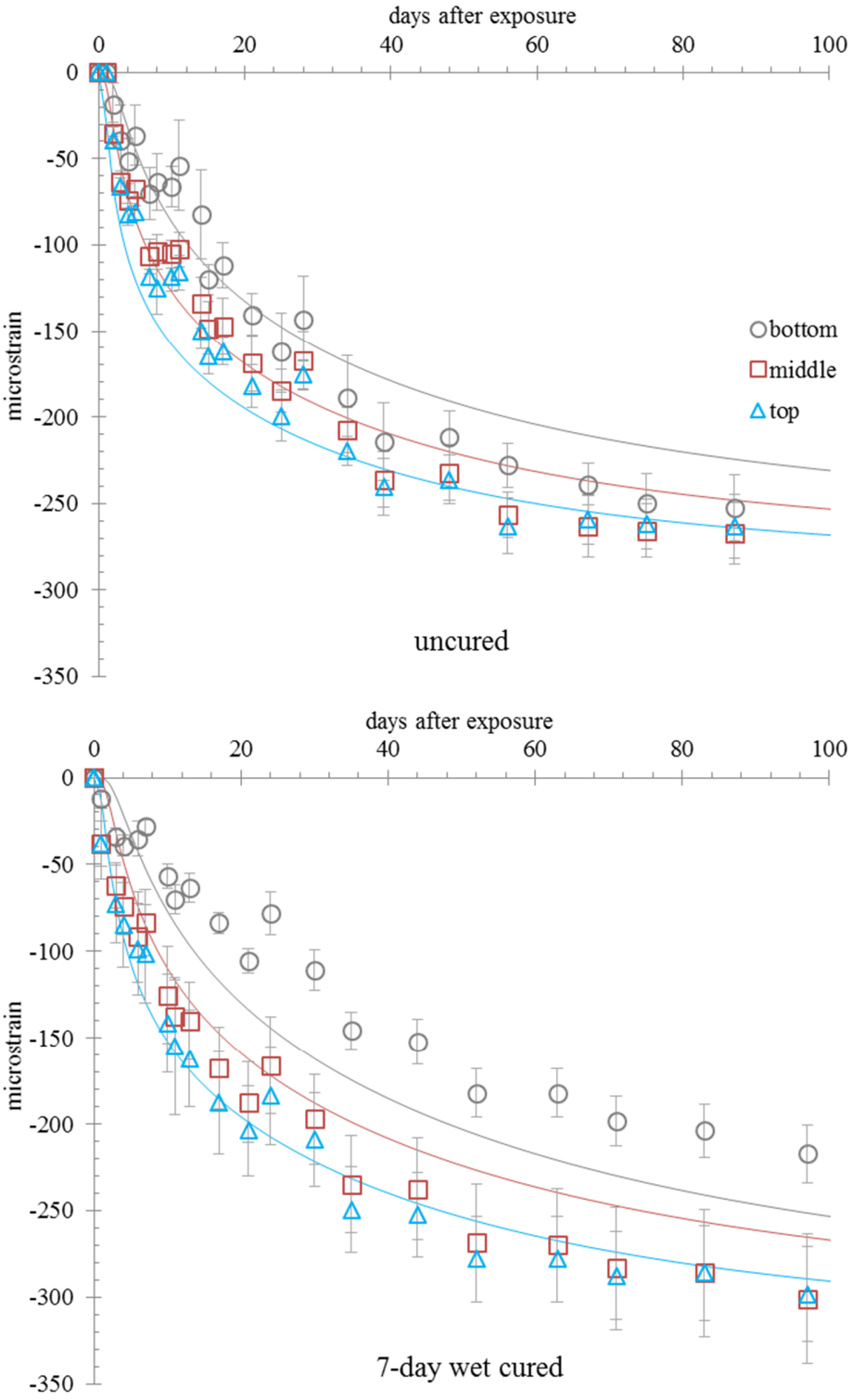
days after exposure
0
20
40
60
80
100
0
-50
-100
-150
-200
-250
-300
-350
microstrain
bottom
middle
top
uncured
days after exposure
0
20
40
60
80
100
0
-50
-100
-150
-200
-250
-300
-350
microstrain
7-day wet cured

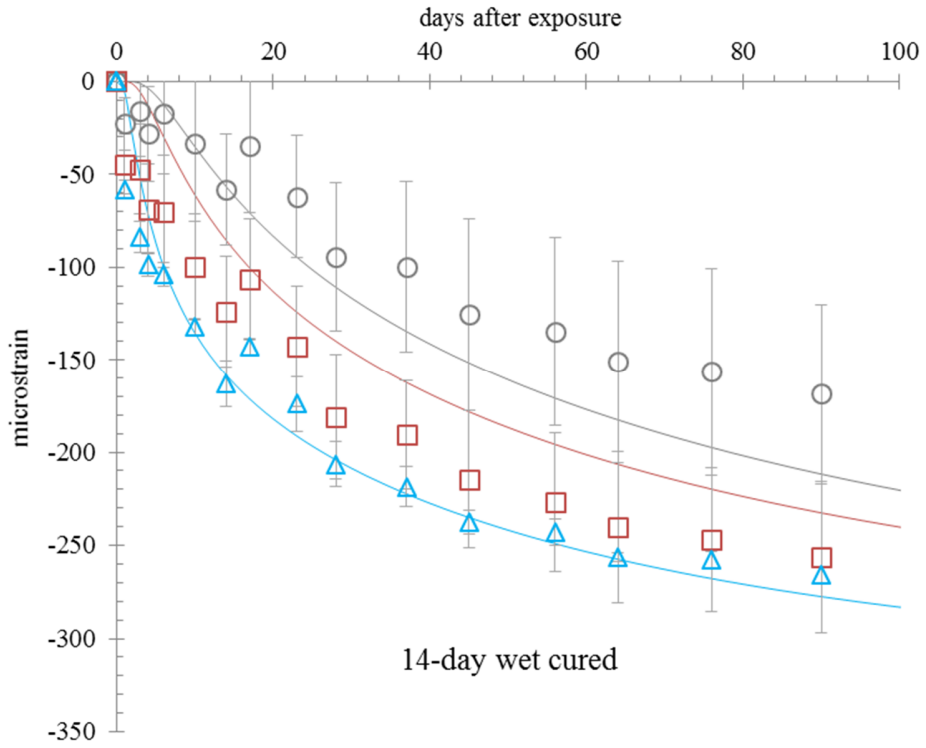

Figure VII.12 Comparison between the shrinkage from the experiment vs simulation in 70% *RH*

The simulated shrinkage at the top, middle, and bottom of the beams had very similar trends to the experimental results as shown in Figure 7.12, however the results for the lower depths didn't fit the measured shrinkage. As shown in the previous chapter for 40%, for higher storage humidities the simulation can have inaccurate prediction as well. This could be related to the assumption of linear diffusion for each depth, or the inaccurate input parameters (using a similar mechanical properties for the entire depth) that need to be measured for an improved prediction. Adjusting the model for the nonlinear diffusion with numerical solution is out of the scope of this study.

7.3.3 Field Investigation

Figure 7.13 shows the monthly average temperature for the last 5 years in Oklahoma City. The average values were calculated using the daily max, min, and average temperature and *RH* data collected from weather website wunderground.

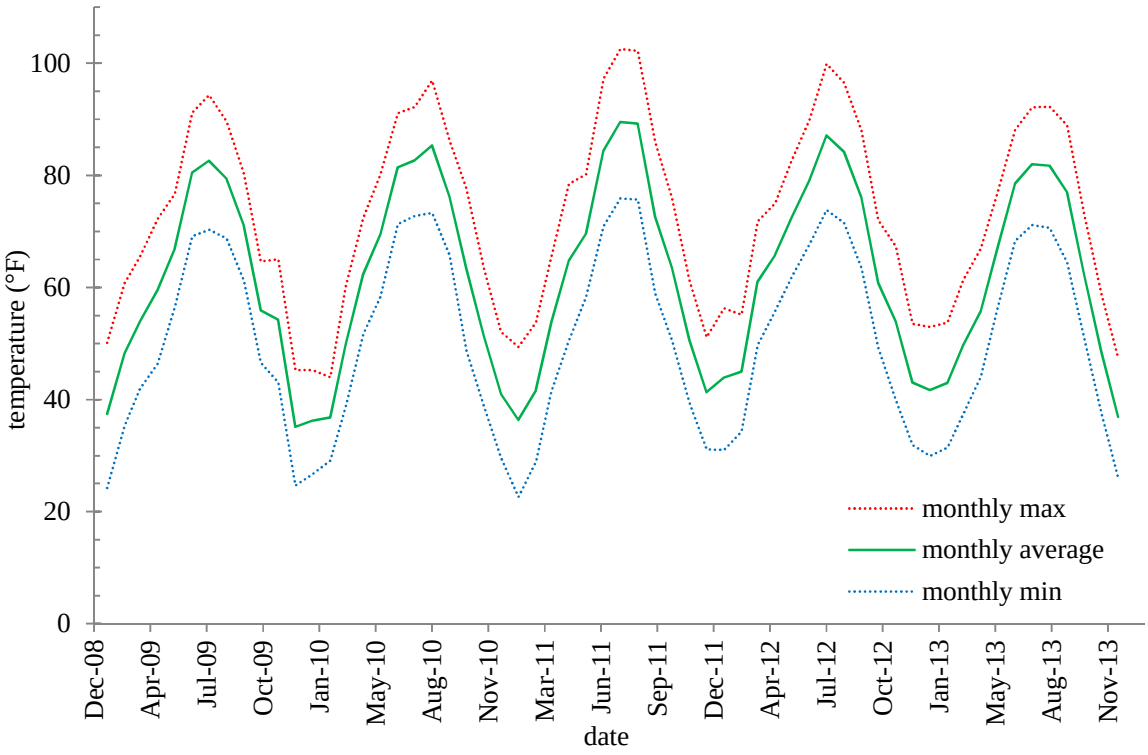

Figure VII.13 The minimum, maximum, and average temperature for each month

As can be seen the average temperature showed an increase over the summer time. The test was started in December 2012 when the weather was colder with considerable amounts of rainfall. Figure 7.14 shows the *RH* for the same duration in this study in Oklahoma City. The average values were calculated using the daily average *RH* data collected from weather website wunderground. The running average was calculated for every 30 days. The precipitation has been shown as well.

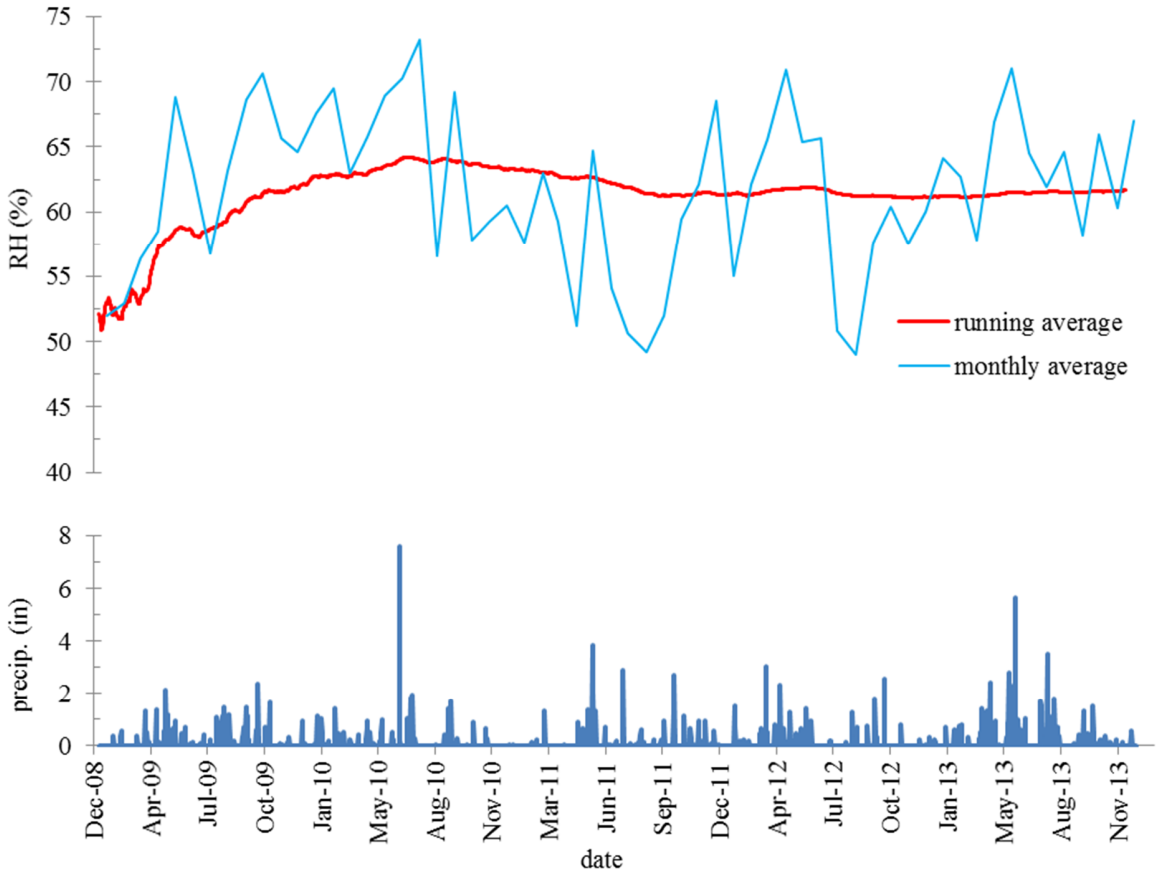

Figure VII.14 Precipitation and the minimum, maximum, and average *RH*

In general, the average *RH* has not significantly changed over the length of the test. Figure 7.15 shows the mass change of the beams and the rainfall events over days exposed to drying. The mass change values are the average from three samples. The positive values of mass change are due to increase in weight after rainfall.

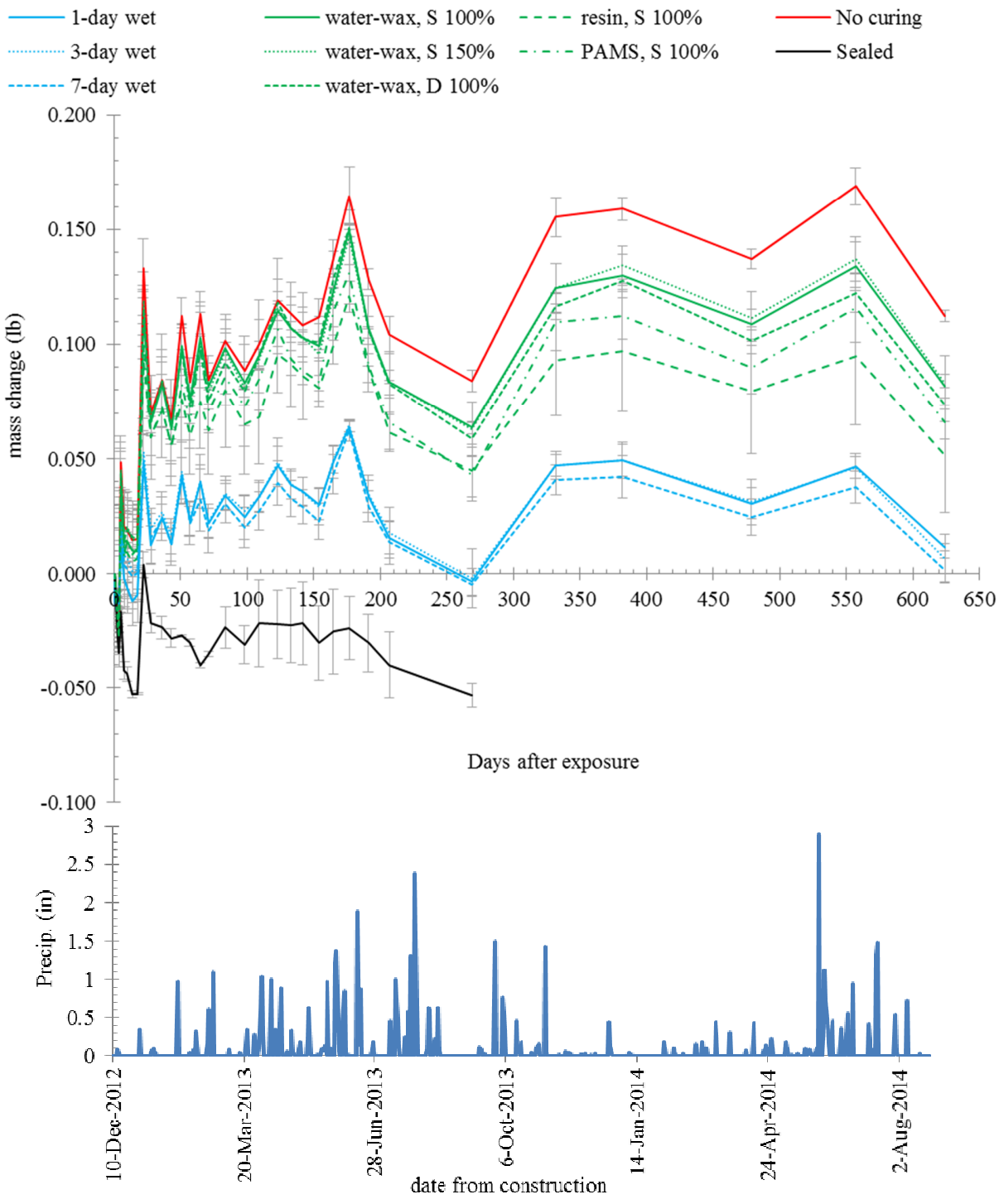

Figure VII.15 The mass change of the concrete specimens and rainfall events at the exposure site

Figure 7.15 shows the weight change of specimens after exposure. There were some problems with the samples sealed with wax. The wax does not appear to be totally effective and the sample started to change in weight. After four weeks the sample was placed in a plastic bag. This was found to be a good solution to stabilize the weight loss of the sample. The mass change of wet cured specimens indicates that they all had similar mass change. Furthermore, the samples with curing compound also showed similar mass loss; however, there was a distinct difference between the results of these two samples. Specimens cured with curing compounds and the specimen that was not cured showed more mass change compared to wet cured and sealed specimens. The permeability of the wet cured specimens is expected to be lower than the no cured specimen and that of specimens cured with curing compounds. Due to a high *RH* in the field it is expected that the pores at the surface have only partially dried and so therefore show a lower amount of shrinkage. On the other hand, the specimen that was not cured has a higher permeability compared to the other specimens and consequently more weight gain after each rainfall, as shown in Figure 7.15.

Specimens that were cured with curing compounds absorbed more water than the wet cured specimens. Specimens cured with water-wax based curing compound and different application rates have a very similar performance. Water-wax based curing compound with different amounts of coverage show statistically similar performance and absorbed more water than the other two curing compounds. This may have happened because it is a water-wax based coating and can be less durable under rain compared to resin and PAMS based materials.

Table 7.2 shows images of the surface of the curing compound samples after 100 and 190 days.

Table VII.2 The surface of cured samples with different curing compounds after 100 and 190 days

After 100 days	After 190 days
Poly-alphamethylstyrene based curing compound	
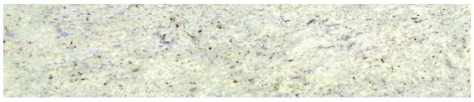	
Resin based curing compound	
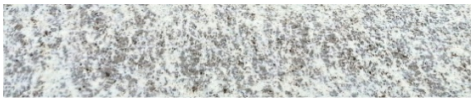	
Water-wax based curing compound (100% double)	
	
Water-wax based curing compound (150%)	
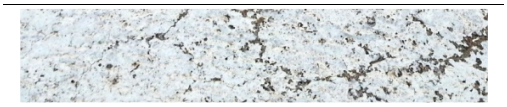	
Water-wax based curing compound (100%)	
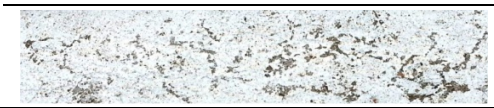	

As shown in Table 7.2, it has been observed after 100 and 190 days that resin and PAMS based curing compounds still remained on the surface, while the water-wax based curing compound has been eroded partially or completely. Moreover, the reason that resin based curing compound look like an eroded surface is due to its high stickiness during application, which makes it more difficult to be applied consistently. However, it has remained on the surface throughout the period investigated.

Figure 7.16 shows the daily average *RH* at the top of the specimens over days exposed to drying in the field for different curing techniques. The bottom figure shows the rainfall amounts and the dates that they occurred.

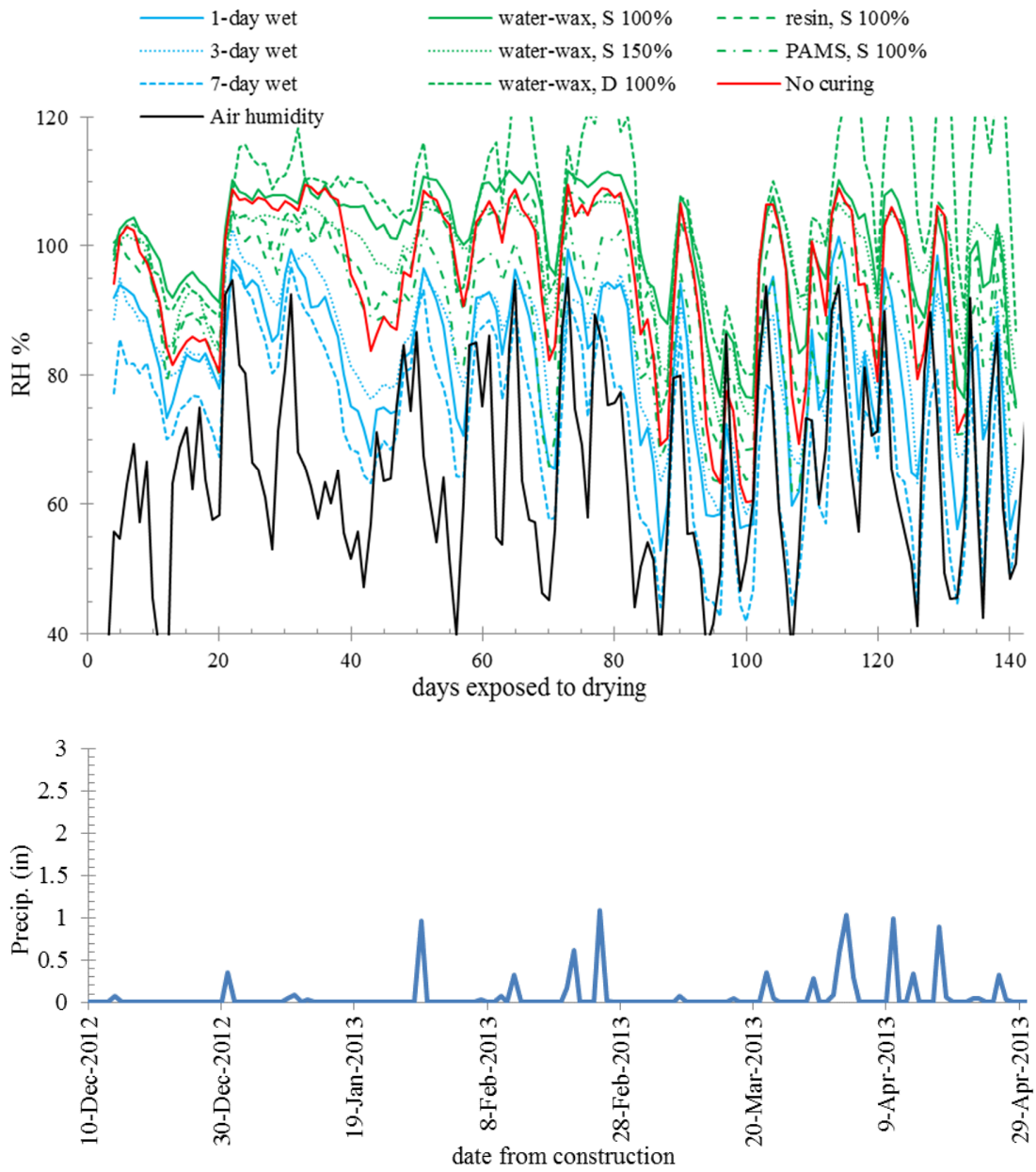

Figure VII.16 The average *RH* at the depth 0.525" and the rainfall events

Figure 7.16 shows the *RH* at the top of specimens (depth 0.525"). The general trend between the beginning and the end of five-month exposure shows very little change in *RH* within the concrete. It should also be noted that the *RH* at the surface of the concrete follows the atmospheric *RH* but is a little higher. Because the concrete does not appear to be drying this suggests that the negative

impacts of moisture gradients and their intensities should be minimized. This means that differential curling from drying shrinkage is not expected to be a major problem in a *RH* close to 65% as was observed during this testing period. High *RH* in the field together with precipitation can maintain the moisture in the samples. For this test this also seems to diminish the expected differences between the effectiveness of different curing methods. However, even with the higher *RH* the wet cured samples have the highest shrinkage.

Figure 7.17 shows the RH profiles over the depth in the middle of three months December, February, and April.

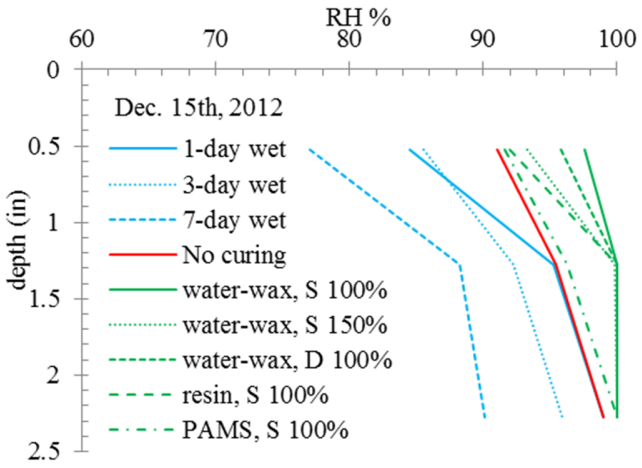

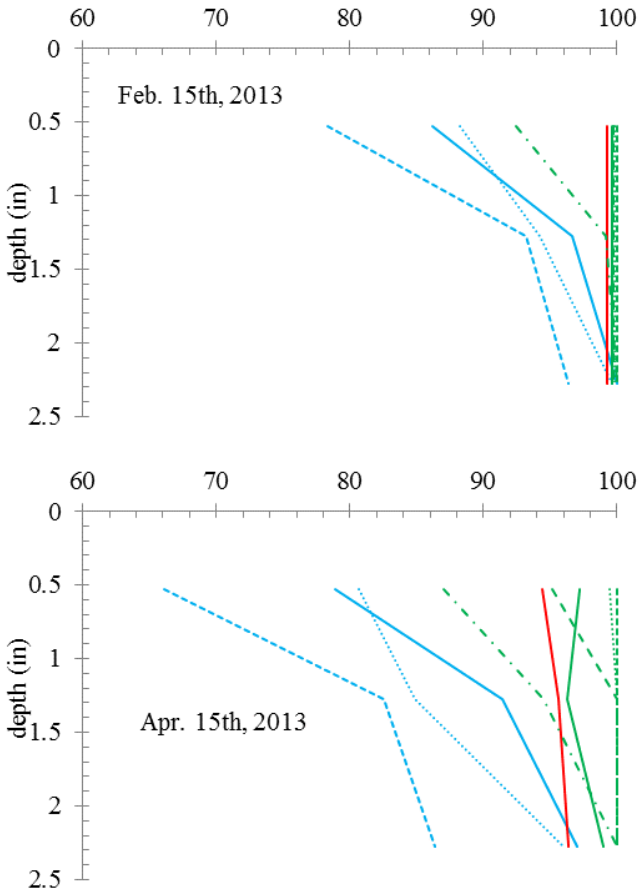

Figure VII.17 Average *RH* profiles for different curing methods

Figure 7.17 shows the *RH* profiles of the specimens at the middle of December 2012, February 2013, and April 2013; the red line shows the profile for specimens without curing. As discussed above, wet cured specimens have less internal humidity compared to specimens with curing compounds. The lower permeability of the wet cured specimens should be the main reason for this difference. Curing compound specimens have a very high internal humidity (above 90%) and less moisture gradients compared to wet cured specimens due to more moisture gain after each rainfall.

Figure 7.18 shows the strain at 0.525” from the surface over time outside. It should be noted that negative values show the shrinkage while the positive values are the amount of swelling or

expansion in the beams. The strain values are the average amounts from the three samples used for each method. Also, the graph shows the strain from the moisture gradient, which is the total measured strain excluding the strain due to the differential temperature. A thermal expansion coefficient 5.5×10^{-6} in/in °F has been used to make this correction.

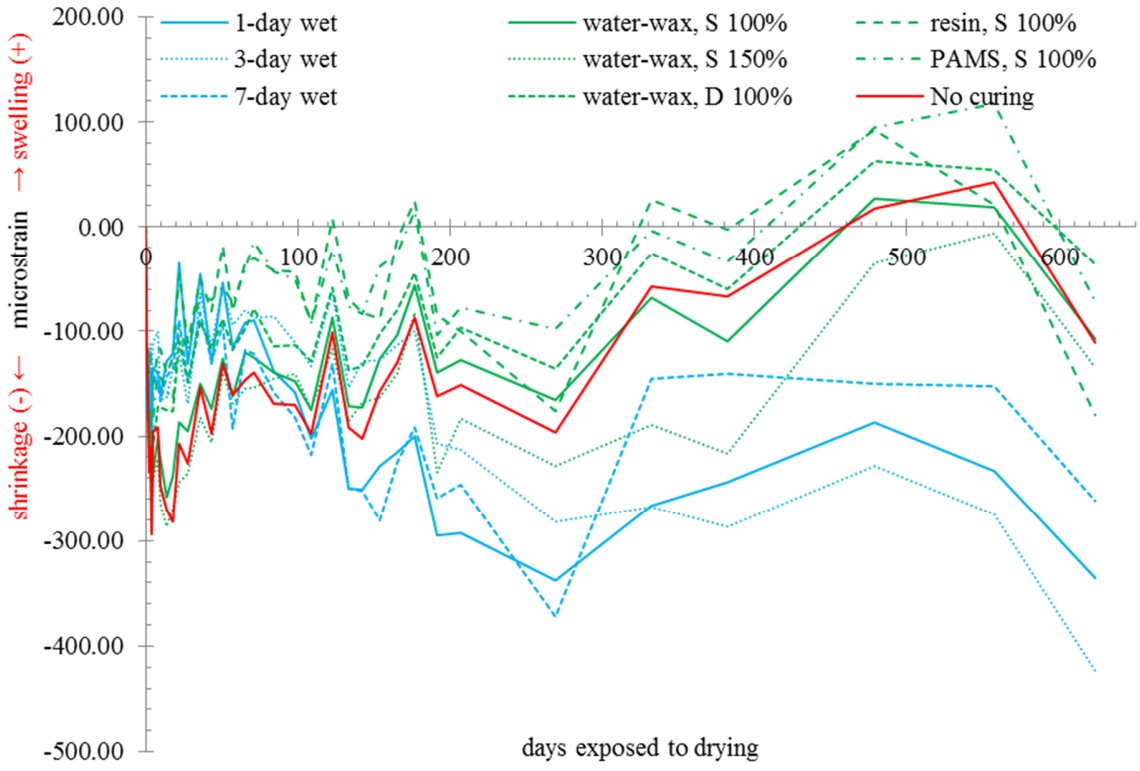

Figure VII.18 Strain at a depth of 0.525" of the concrete after being exposed

Figure 7.18 shows strain changes at the top of specimens where the positive values show swelling and negative values show shrinkage. The thermal strain has been removed from the total strain in this figure. The strain fluctuates at different periods of time because of the rainfall events as shown below the graph. The specimens in general tend to swell due to an increase in moisture after each rain.

Figure 7.19 shows the strain profiles over the depth at every six months for the strain values modified with the thermal strain as mentioned above.

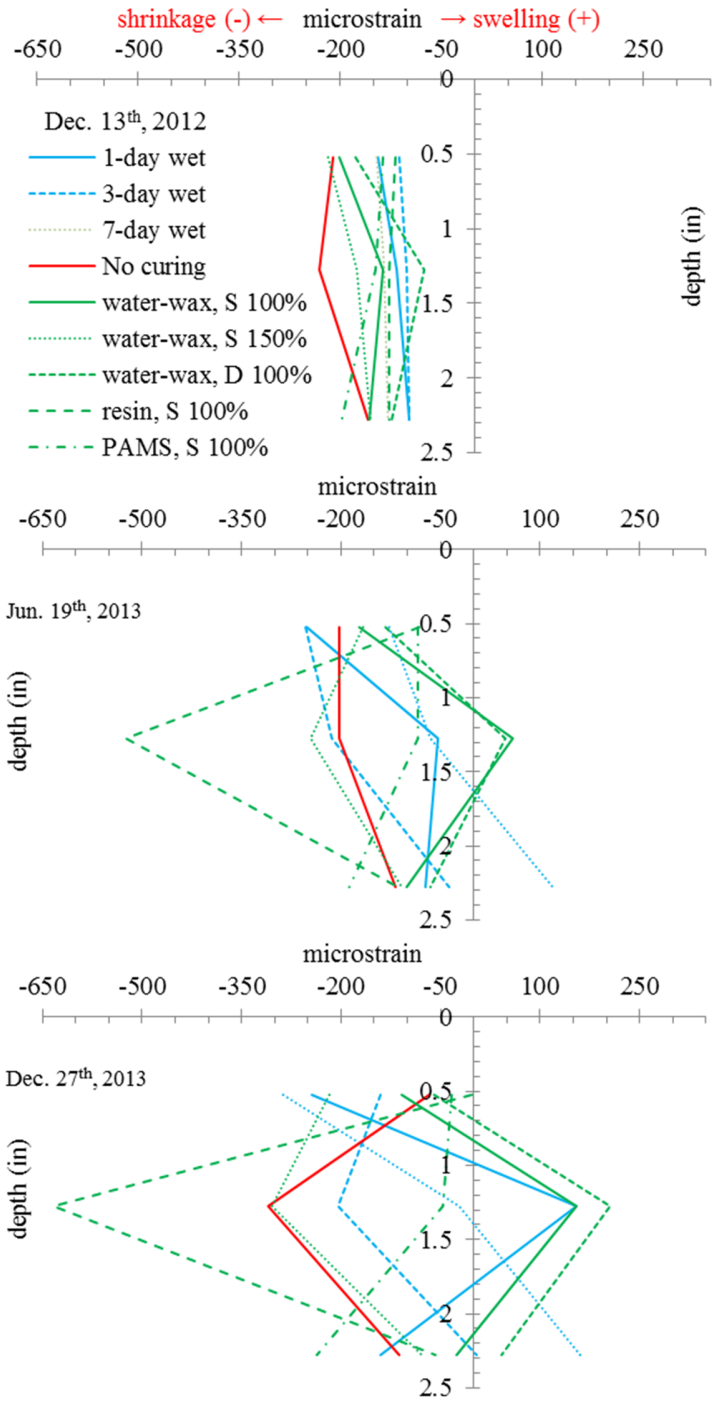

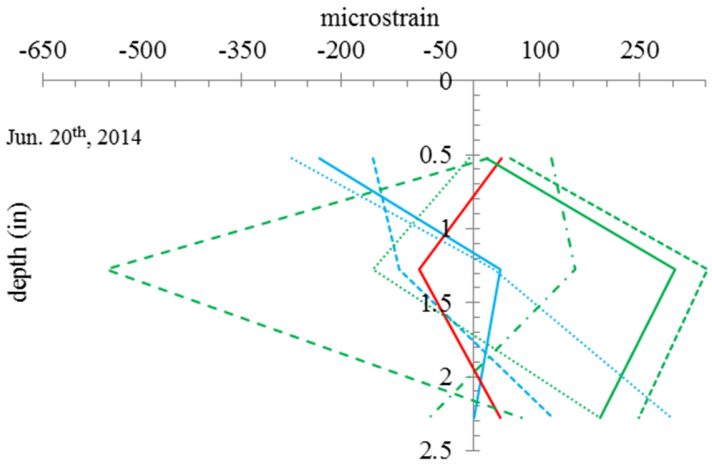

Figure VII.19 Average strain profiles for different curing methods

Figure 7.19 shows the strain profiles every six months during the test; the strain gradients of specimens cured with curing compounds are not as large as the slopes of wet cured specimens, which might be caused by a finer pore structure at the surface of the wet cured specimens that makes them more impermeable to external water. This leads to a less moisture gradient in curing compound samples, as seen in Figure 7.17.

7.3.4 Full Scale Pavement Investigation

Using a running average for every 6 hours from paving the temperature profiles have been calculated from the measured data. The running average has been used to reduce the fluctuations of the data measured with the strain gages over the time. Temperature profiles of the slab are shown in Figures 7.20-22 respectively for locations 1, 2, and 3 in Figure 7.4. These locations are at 28”, 56”, and 84” from the edge of the slab, respectively. The profiles are for ages 0.1, 30, and 100 days after paving.

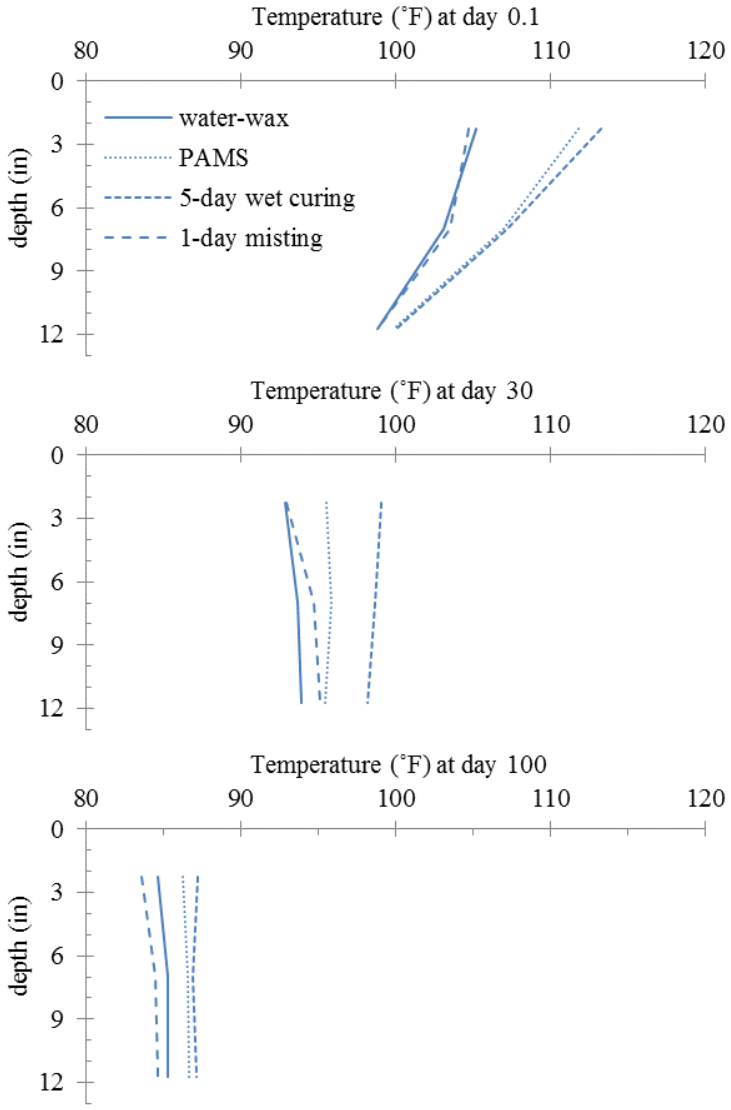

Figure VII.20 Temperature profiles for location 1 at 0.1, 30, and 100 days after paving

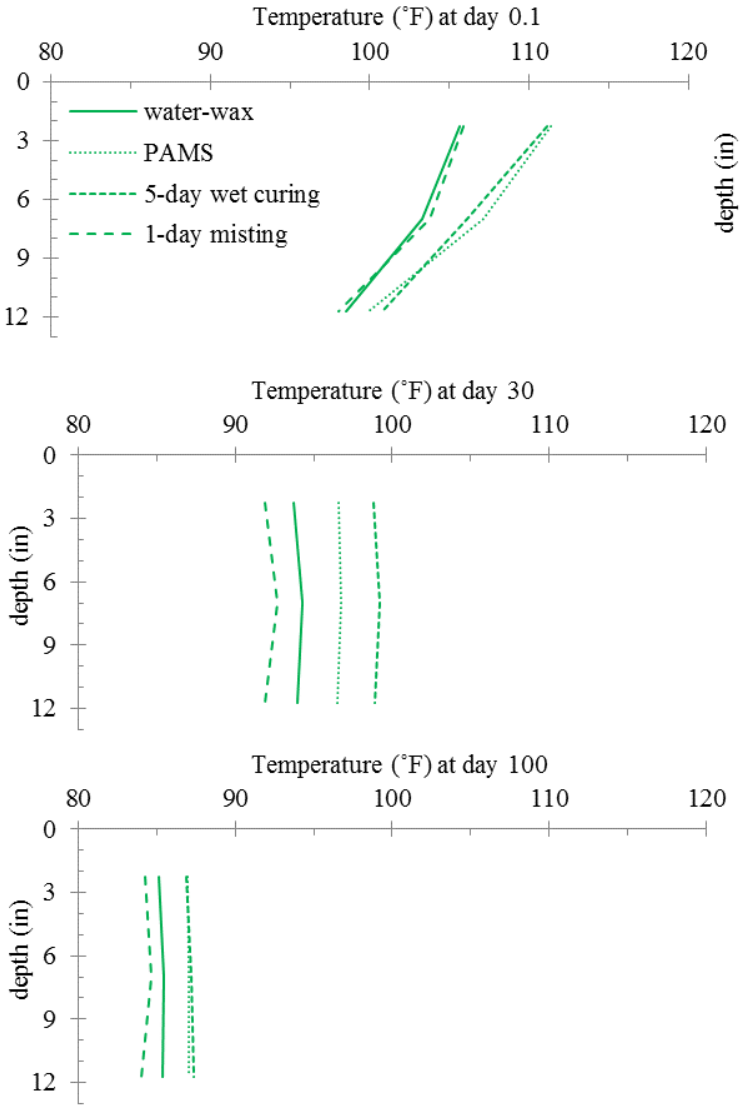

Figure VII.21 Temperature profiles for location 2 at 0.1, 30, and 100 days after paving

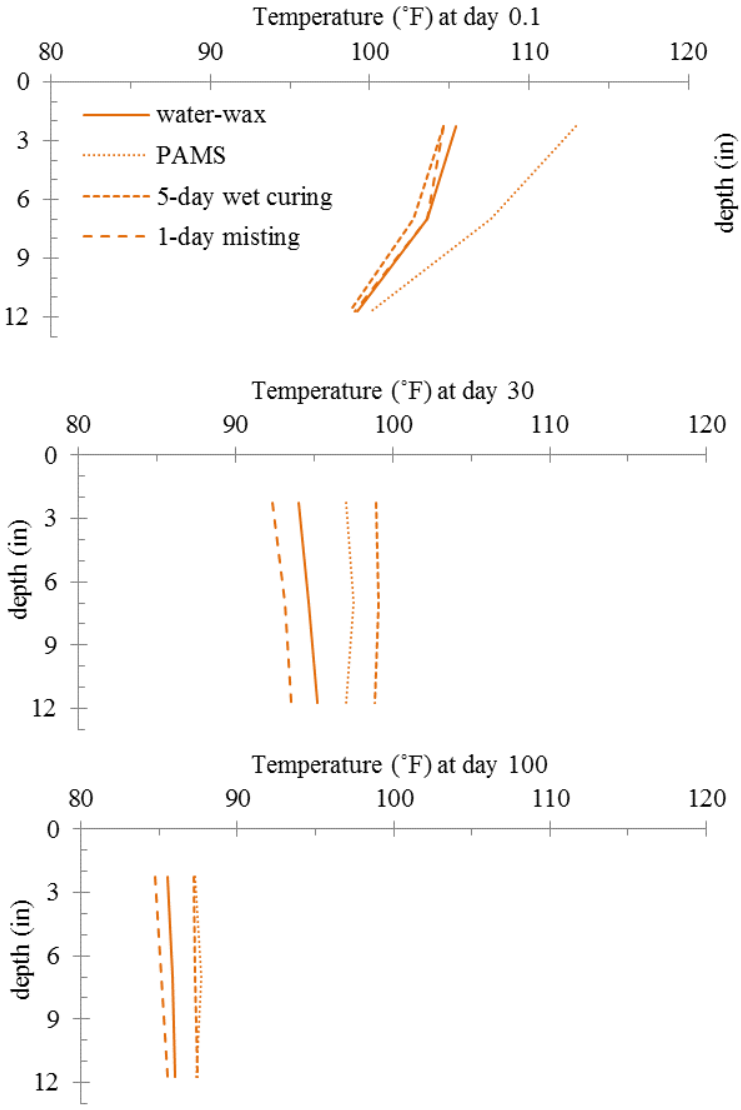

Figure VII.22 Temperature profiles for location 3 at 0.1, 30, and 100 days after paving

The temperature gradient is the most at early ages; for examples, about 0.1 day after paving the temperature gradient within the slabs cured either with the PAMS curing compound or the 5-day wet curing is noticeable. However, the gradient becomes negligible over the time for all curing techniques. This low temperature gradient leads to less warping deflections.

Moreover, the temperature is always higher in 5-day wet curing and PAMS and lower in water-wax curing compound and 1-day misting. A higher temperature may lead to expansion within the slab, which will be shown later. After 100 days this difference has become less as well.

Finally, comparing the three graphs, it should be pointed out that the temperature and its gradients are the same in all sections 28", 56", and 84" from the edge of the slab at all edges, which leads to the same thermal stresses. Also, the slab experiences a temperature gradient due to the daily temperature change and therefore a small strain gradient. But since a running average has been used, this daily temperature gradient has not been shown here.

Figures 7.23-25 show the strain profiles of the slabs cured with different techniques for the marked locations 1, 2, and 3 of Figure 7.4. These locations are at 28", 56", and 84" from the edge of the slab, respectively. A running average for every 6 hours has been used. The profiles show the strain gradients within the slab for 0.1, 30, and 100 days after paving. The positive values show the swelling and negative values are for shrinkage.

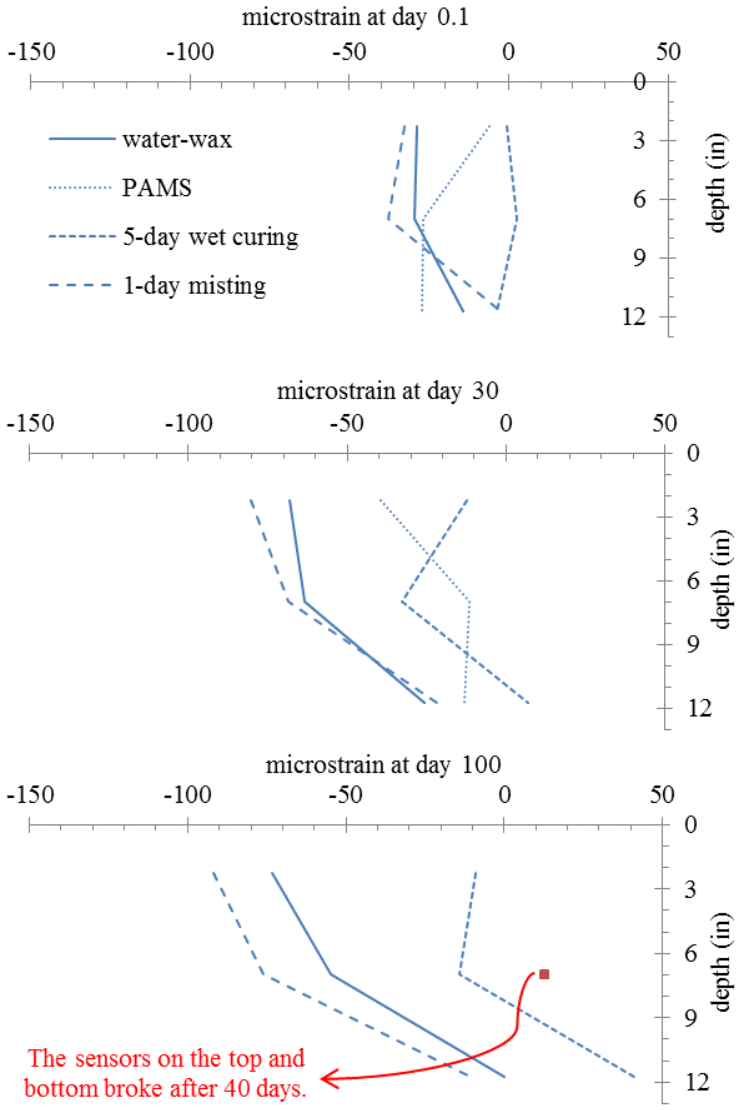

Figure VII.23 Strain profiles for location 1 at 0.1, 30, and 100 days after paving

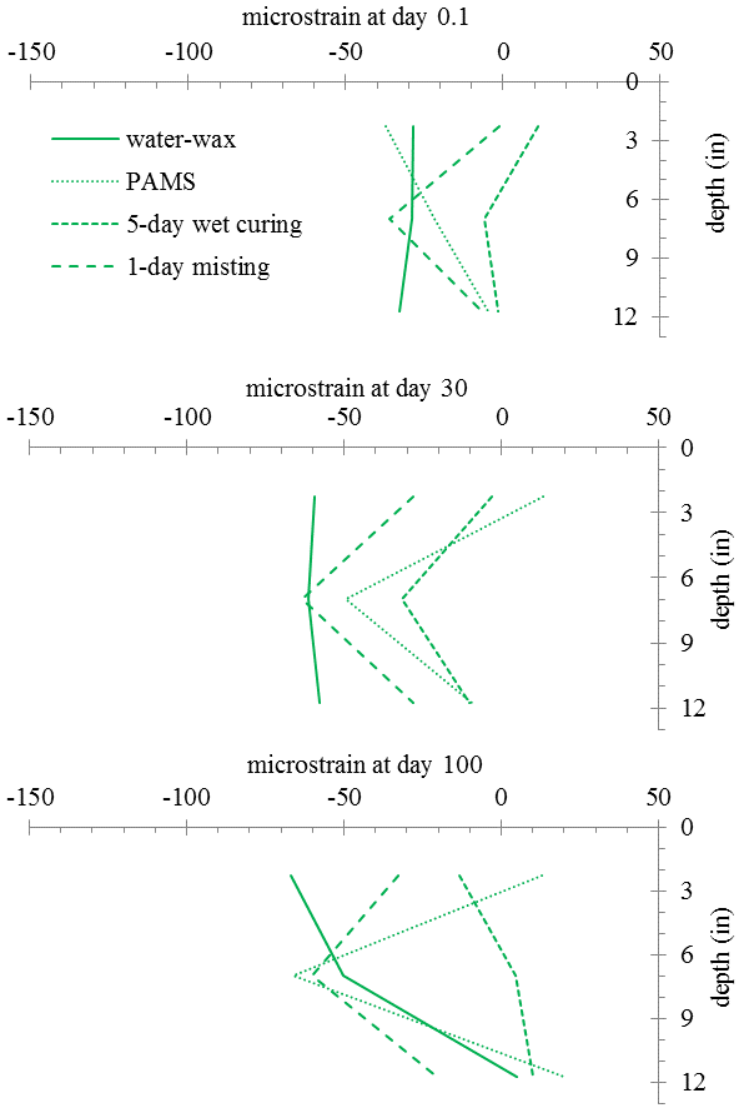

Figure VII.24 Strain profiles for location 2 at 0.1, 30, and 100 days after paving

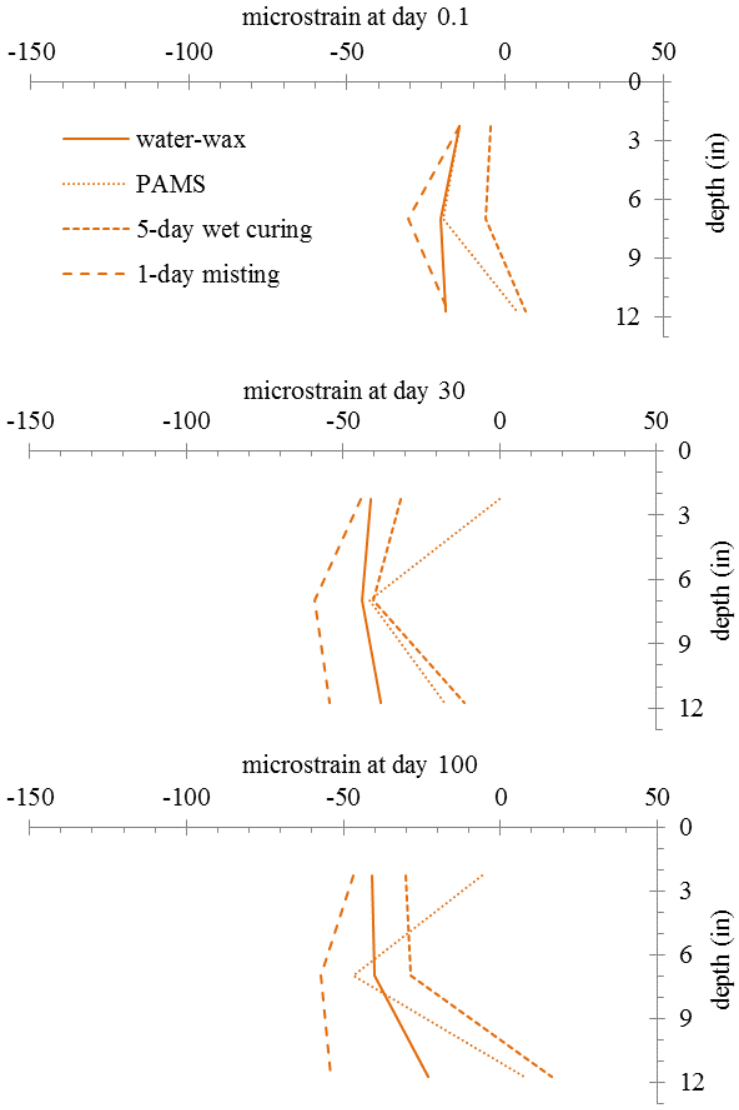

Figure VII.25 Strain profiles for location 3 at 0.1, 30, and 100 days after paving

Based on Figures 7.23-25 it appears that there is significantly more curling that is occurring at the edge of the pavement than is happening in the middle. Also, the magnitudes of shrinkage are not more than -50 microstrain on average for locations 2 and 3, which is very small. This could be caused by moisture or temperature gradients. However, based on the measured temperature profiles in the pavements this gradient is likely caused by moisture. This curling does not appear to be caused by the type of curing. Instead it appears to be caused by a large moisture gradient in

the pavement. During construction the water table was observed to be very near the surface in this pavement. This means that the bottom of the pavement is likely wet while the top dries. This creates a large gradient in the pavement and leads to the increased curling that is observed. This curling may become a problem over time and should be watched closely.

As mentioned earlier in the instrumentation section, several *RH* sensors at different depths of the slab were used at the marked locations A and B in Figure 7.4. These sensors broke due to the very high *RH* over the depth of slab after about 30 days. This might be due to either a very high water level underneath the road or the penetration of the water through the drilled holes. Therefore, the *RH* values higher than 100% or the data after 30 days are not valid. As an example, the changes in *RH* at location B are shown in Figure 7.26 for different depths.

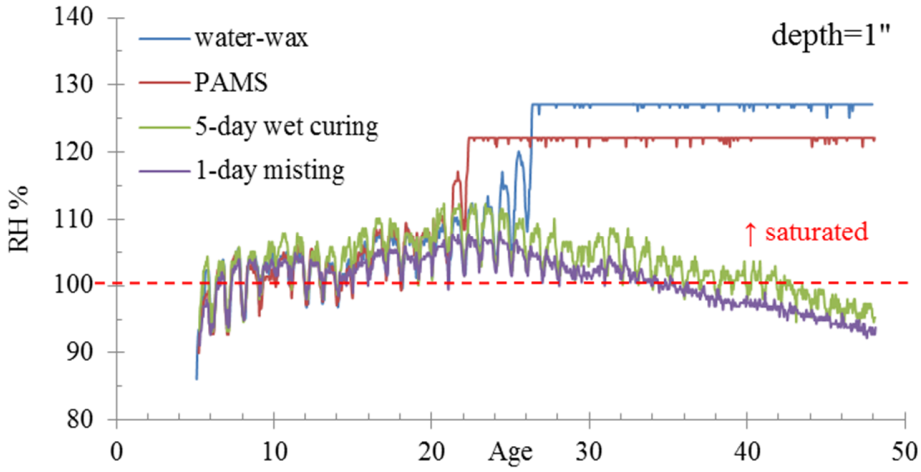

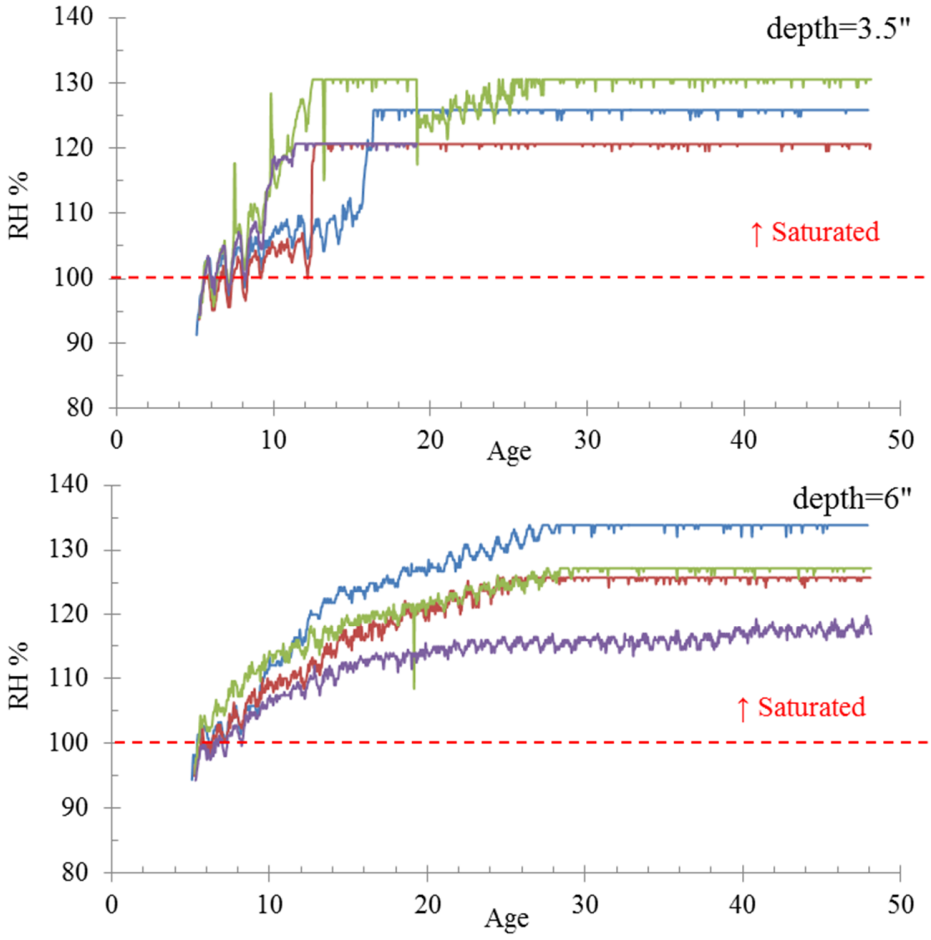

Figure VII.26 *RH* over the time for location B at different depths

The *RH* at depth 1" as shown in Fig. 32 starts to decrease around 40 days from paving for 1-day misting and 5-day wet curing. However, the sensors show saturated conditions for the other depths and curing methods. It seems that these other sensors have been destroyed. Because of this it is difficult to draw conclusions from this data. The observation that the slab has very high moisture content is confirmed because of the malfunctioning of so many gages due to moisture.

7.4 PRACTICAL IMPLICATION

The data from this study confirm that when the field *RH* of concrete is near 70% then the curling strains caused by drying are minimal because the concrete does not significantly dry. However, if

concrete is going to be used in dry conditions (~ 40% *RH*), then wet curing can lead to greater volume changes in the structure on drying. So, if the concrete is to be used in a moist environment such as present in Oklahoma (~ 65-70% *RH*), the type of curing that is used on concrete pavements will have very little impact on their curling deformations. It should be pointed out that these curing methods may have an impact on a number of other important concrete properties such as the strength, permeability, and abrasion resistance.

7.5 CONCLUSIONS

Several useful conclusive remarks need to be mentioned from the comparison investigated in this testing:

- Increasing the wet curing length increased the degree of saturation of the paste. This increased level of saturation led to increased strains on subsequent drying, which caused greater curling in wet cured paste and concrete samples in both 40% and 70% RH's.
- In a less severe environment, such as 70% RH, the magnitudes were smaller.
- The average temperature in Oklahoma City has consistent fluctuations each year with the highest peak around August of each year, while the average RH has not changed over the five years and remained on average to be about 65%.
- The wet cured samples in the field showed less mass change than the samples with curing compound and no curing.
- Surface of samples cured with PAMS based curing compound and resin based curing compound have not significantly changed after long term exposure, while surface of samples cured with water-wax based curing compound has been considerably eroded after five months of exposure.

- Drying shrinkage would not be expected as a major reason for strain changes in RH conditions that are on average 65% as is the case in Oklahoma. In this environment a gradual ambient temperature and moisture raise can make the samples swell where the high RH minimizes the intensity of the drying condition.

- Different curing compounds performed very similarly in the above mentioned condition and strain changes were statistically similar, which were caused by continuous fluctuations in temperature and RH during the test.

- The temperature gradient was almost constant in the full scale pavement. However, the strain gradient was not.

- The strain at the edge of the pavement was much higher than the middle. This is likely caused by a significant moisture gradient in the pavement that is caused by a very high water table.

- In general, the data from the pavement showed similar findings to those found in the field test, which was the curling being less affected by the curing type.

CHAPTER VIII

VIII. CONCLUSION

In this project the impacts of different curing methods on the drying shrinkage induced curling of cement and concrete elements with different sizes at different drying conditions have been studied. The samples investigated were exposed to drying on one side without rewetting and no moisture loss on the other sides. Understanding this phenomenon is becoming more important in the design of volume change sensitive structures such as pavements, slabs on grade, and concrete dams. However, care should be taken before extending the use of these findings to the mentioned structures that may have different boundary conditions, support, restraint, temperature, or drying conditions.

In severe drying conditions, wet and sealed curing can increase the potential for surface drying shrinkage and curling of slabs on grade or pavements with the wet cured samples deflecting at a faster rate. Due to the wet curing process, the surface of paste or concrete will have a finer pore-structure, which will reduce the permeability and porosity. This reduction in porosity will lead to a higher degree of saturation and smaller pore sizes, which in turn suggests greater capillary tension induced strain on drying. So, for members with high sensitivity to volume change long term prolonged wet curing is not desirable in severe drying conditions.

Moreover, samples with lower w/cm ratios has less curling deflections and a lower drying rate for the same curing periods. Sometimes it is necessary to wait until concrete floors have dried before

applying coverings in order to minimize mold or ensure adhesives will properly function. Therefore, using a low w/cm and a sealed curing method is suggested as wet curing extends the time required for drying.

Also, in severe drying conditions, curing compounds of different types and costs have statistically different performance. The poly-alphamethylstyrene (PAMS) based curing compound provides better moisture retention than the wax based and resin based compounds. This superior performance at lower application rates or the same level of cost can be a way to reduce the cost of the curing compound. Moreover, a double layer application of curing compounds increases effectiveness of water retention without increasing the amount of material used.

In addition, the use of wet curing followed by the usage of a curing compound has a slower drying rate than wet cured specimens after the curing is removed. Therefore, a combination of these two curing methods can promote hydration and create a denser pore structure and improve the durability and strength of the surface of the concrete. It should be noted that field concrete may have a rougher surface than tested paste beams, which can increase the required amount of curing compound. Therefore, more quantitative work is needed to compare the performance of concrete with different levels of surface texture and application procedures.

This study has suggested both experimentally and via a mechanistic 1-D drying shrinkage model, developed previously by Grasley et al. (Grasley, 2010; Grasley & Leung, 2011), that prolonged wet curing may cause increased magnitude of shrinkage strain gradients and therefore curling, when measured desorption isotherms and drying diffusion coefficients are used as inputs in the model. It also should be mentioned that the nonlinear simulations took approximately 60x more computational time to complete than the linearized, approximate model.

Assuming similar values of mechanical properties for both uncured and cured specimens causes underpredictions in modeling post deflections of cured samples. Also, predictions are more

accurate in lower humidity regions of concrete beams, which can be related to either a more accurate relative humidity (*RH*) measurements or surface microcracks that would tend to offset any reductions in the diffusion coefficient associated with lower internal *RH* values. Further refinement of the model shows promise to be used in more detailed prediction of the shrinkage strains caused by different curing methods, boundary conditions, material properties, and drying.

On the other hand, in less severe drying conditions the curling strains caused by drying are minimal because the paste and concrete do not significantly dry. So, if the concrete pavements are to be used in a moist environment such as present in Oklahoma (~ 65-70% *RH*), the type of curing that is used on pavements will have very little impact on their curling deformations. It should be pointed out that these curing methods may have an impact on a number of other important concrete properties such as the strength, permeability, and abrasion resistance.

REFERENCES

AASHTO-M85. (2012). Standard Specification for Portland Cement (pp. 14). Washington, DC: American Association of State Highway and Transportation Officials.

ACI-302.1R. (2004). Guide for Concrete Floor and Slab Construction. Farmington Hills, MI: American Concrete Institute.

ACI-308R. (2001). Guide to Curing Concrete. Farmington Hills, MI: American Concrete Institute.

ACI-360R. (2006). Design of Slabs-on-Ground. Farmington Hills, MI: American Concrete Institute.

ACI-C318. (2014). Building Code Requirements for Structural Concrete. Farmington Hills, MI: American Concrete Institute.

Adamson, A. W., & Gast, A. P. (1967). *Physical chemistry of surfaces*.

Aïtcin, P. C. (1999). Does concrete shrink or does it swell? *Concrete International, 21*(12), 77-80.

Anderson, T., & Roper, H. (1977). *Influence on an impervious membrane beneath concrete slabs on grade.* Paper presented at the Symposium on Concrete for Engineering; Engineering for Concrete, 1977, Brisbane, Australia.

ASTM-C39/C39M. (2016). Standard Test Method for Compressive Strength of Cylindrical Concrete Specimens. West Conshohocken, PA: ASTM International.

ASTM-C138/C138M. (2010). Standard Test Method for Density (Unit Weight), Yield, and Air Content (Gravimetric) of Concrete (pp. 4). West Conshohocken, PA: ASTM International.

ASTM-C143/C143M. (2010). Standard Test Method for Slump of Hydraulic-Cement Concrete (pp. 4). West Conshohocken, PA: ASTM International.

ASTM-C150/C150M. (2011). ASTM C150/C150M: Standard Specification for Portland Cement (pp. 9). West Conshohocken, PA: ASTM International.

ASTM-C156. (2011). Standard Test Method for Water Loss [from a Mortar Specimen] Through Liquid Membrane-Forming Curing Compounds for Concrete. West Conshohocken, PA: ASTM International.

ASTM-C231/C231M. (2010). Standard Test Method for Air Content of Freshly Mixed Concrete by the Pressure Method (pp. 10). West Conshohocken, PA: ASTM International.

ASTM-C305. (2011). Standard Practice for Mechanical Mixing of Hydraulic Cement Pastes and Mortars of Plastic Consistency (pp. 3). West Conshohocken, PA: ASTM International.

ASTM-C618. (2008). Standard Specification for Coal Fly Ash and Raw or Calcined Natural Pozzolan for Use in Concrete (pp. 3). West Conshohocken, PA: ASTM International.

ASTM-E104. (2012). Standard Practice for Maintaining Constant Relative Humidity by Means of Aqueous Solutions (pp. 5). West Conshohocken, PA: ASTM International.

Baroghel-Bouny, V. (1997). Experimental investigation of self-desiccation in high-performance materials—Comparison with drying behaviour. *Self-Desiccation and Its Importance in Concrete Technology, Lund Institute of Technology, Lund, Sweden*, 72-87.

Baroghel-Bouny, V., Mainguy, M., Lassabatere, T., & Coussy, O. (1999). Characterization and identification of equilibrium and transfer moisture properties for ordinary and high-performance cementitious materials. *Cement and Concrete Research, 29*(8), 1225-1238.

Bazant, Z. P., & Baweja, S. (2000). Creep and shrinkage prediction model for analysis and design of concrete structures: Model B3. *ACI SPECIAL PUBLICATIONS, 194*, 1-84.

Bazant, Z. P., & Najjar, L. J. (1971). Drying of concrete as a nonlinear diffusion problem. *Cement and Concrete Research, 1*(5), 461-473.

Bazant, Z. P., & Najjar, L. J. (1972). Nonlinear water diffusion in nonsaturated concrete. *Matériaux et Construction, 5*(1), 3-20.

Bentz, D. P. (2008). A review of early-age properties of cement-based materials. *Cement and Concrete Research, 38*(2), 196-204.

Bentz, D. P., Garboczi, E. J., & Quenard, D. A. (1998). Modelling drying shrinkage in reconstructed porous materials: application to porous Vycor glass. *Modelling and Simulation in Materials Science and Engineering, 6*(3), 211-236.

Bentz, D. P., Jensen, O. M., Hansen, K. K., Oleson, J. F., Stang, H., & Haecker, C. J. (2001). Influence of Cement Practice Size Distribution on Early Age Autogenous Strains and Stresses in Cement-Based Materials. *Journal of the American Ceramic Society, 84*(1), 129-135.

Berke, N. S., & Li, L. (2004). *Early Age Shrinkage and Moisture Loss of Concrete.* Paper presented at the International RILEM Symposium on Concrete Science and Engineering: A Tribute to Arnon Bentur.

Bisschop, J. (2002). *Drying Shrinkage Microcracking in Cement-Based Materials.* (PhD), Delf University, Netherland.

Bolander, J. E., & Berton, S. (2004). Simulation of shrinkage induced cracking in cement composite overlays. *Cement and concrete composites, 26*(7), 861-871.

Bramhall, G. (1995). Diffusion and the drying of wood. *Wood science and technology, 29*(3), 209-215.

Browne, R. D. (1967). *Properties of Concrete in Reactor Vessels, Group C, Paper 13*. Paper presented at the Conference on Prestressed Concrete Pressure Vessels, London.

Cather, B. (1994). Curing: the true story? *Magazine of Concrete Research, 46*(168), 157-161.

Coussy, O. (1995). *Mechanics of porous continua* (Vol. 1016): Wiley Chichester.

Coussy, O., Dangla, P., Lassabatere, T., & Baroghel-Bouny, V. (2004). The equivalent pore pressure and the swelling and shrinkage of cement-based materials. *Materials and Structures, 37*(265), 15-20.

Coussy, O., Eymard, R., & Lassabatere, T. (1998). Constitutive modeling of unsaturated drying deformable materials. *Journal of Engineering Mechanics-Asce, 124*(6), 658-667.

D'ambrosia, M. D. (2012). *Early age creep and shrinkage of emerging concrete materials.* (PhD), University of Illinois at Urbana-Champaign.

Darter, M., Khazanovich, L., Snyder, M. B., Rao, S., & Hallin, J. (2001). *Development and calibration of a mechanistic design procedure for jointed plain concrete pavements.* Paper presented at the Seventh International Conference on Concrete Pavements. The Use of Concrete in Developing Long-Lasting Pavement Solutions for the 21st Century.

Darwin, D., Browning, J., & Lindquist, W. D. (2004). Control of cracking in bridge decks: observations from the field. *Cement, Concrete and Aggregates, 26*(2), 1-7.

Dhir, R. K., Hewlett, P. C., & Chan, Y. N. (1991). Near-surface characteristics of concrete: abrasion resistance. *Materials and Structures, 24*(2), 122-128.

Dhir, R. K., Levitt, M., & Wang, J. (1989). Membrane curing of concrete: water vapour permeability of curing membranes. *Magazine of Concrete Research, 41*(149), 221-228.

Duncan, D. B. (1955). Multiple range and multiple F tests. *Biometrics, 11*(1), 1-42.

Gao, Y., Zhang, J., & Luosun, Y. (2014). Shrinkage stress in concrete under dry–wet cycles: an example with concrete column. *Mechanics of Time-Dependent Materials, 18*(1), 229-252.

Gardner, N. J. (2000). *Design provisions for shrinkage and creep of concrete.* Paper presented at the Adam Neville Symposium: Creep and Shrinkage-Structural Design Effects.

Gowriplan, N., Cabrera, J. G., Cusens, A. R., & Wainwright, P. J. (1990). Effect of Curing on Durability. *Concrete International, 12*(2), 47-54.

Grasley, Z. C. (2010). Closed-Form Solutions for Uniaxial Passive Restraint Experiments. *ACI Special Publication, 270*.

Grasley, Z. C., Lange, D. A., & D'Ambrosia, M. D. (2005). Drying stresses and internal relative humidity in concrete. *Materials Science of Concrete VII, (J. Skalny, American Ceramic Society)*.

Grasley, Z. C., & Leung, C. K. (2011). Desiccation shrinkage of cementitious materials as an aging, poroviscoelastic response. *Cement and Concrete Research, 41*(1), 77-89.

Grasley, Z. C., & Rajagopal, K. R. (2012). Revisiting total, matric, and osmotic suction in partially saturated geomaterials. *Zeitschrift fur Angewandte Mathematik und Physik, 63*(2), 373-394.

Grasley, Z. C., Rajagopal, K. R., & Leung, C. K. (2011). Equilibrium of partially dried porous media influenced by dissolved species and the development of new interfaces. *International Journal of Engineering Science, 49*(7), 711-725.

Hajibabaee, A. (2011). *Reducing Curling from Drying Shrinkage of Concrete Pavements Through the Use of Different Curing Techniques.* (MS), Oklahoma State University.

Hajibabaee, A., Grasley, Z. C., & Ley, M. T. (2016). Mechanisms of dimensional instability caused by differential drying in wet cured cement paste. *Cement and Concrete Research, 79*, 151-158.

Hajibabaee, A., Khanzadeh Moradllo, M., & Ley, M. T. (2016). Comparison of curing compounds to reduce volume change from differential drying in concrete pavement. *International Journal of Pavement Engineering*, 1-10.

Hajibabaee, A., & Ley, M. T. (2015). Impact of Wet and Sealed Curing on Curling in Cement Paste Beams from Drying Shrinkage. *ACI Materials Journal, 112*(1), 79-84.

Hajibabaee, A., & Ley, M. T. (2016). The Impact of Wet Curing On Curling in Concrete Caused By Drying Shrinkage. *Materials and Structures, 49*(5), 1629-1639.

Hansen, K. K. (1986). Sorption Isotherms: The Technical University of Denmark.

Hansen, T. C., & Mattock, A. H. (1966). *Influence of Size and Shape of Member on the Shrinkage and Creep of Concrete.* Paper presented at the ACI Journal Proceedings.

Hansen, W. (1987). Drying shrinkage mechanisms in Portland cement paste. *Journal of the American Ceramic Society, 70*(5), 323-328.

Hansen, W., Wei, Y., Bennet, A., & Smiley, D. (2007). *Warping of Jointed Plain Concrete Pavement from Inadequate Base Drainage*. Paper presented at the International Workshop on Best Practices for Concrete Pavements.

Hedenblad, G. (1997). Drying of construction water in concrete (Vol. 9). Stockholm, Sweden: Swedish Council for Building Research.

Hetnarski, R. B., & Eslami, M. R. (2009). Thermal Stresses in Beams. In R. B. Hetnarski & M. R. Eslami (Eds.), *Thermal Stresses - Advanced Theory and Applications* (Vol. 158): Springer.

Hiller, J. E., & Roesler, J. R. (2002). Transverse joint analysis for mechanistic-empirical design of rigid pavements. *Transportation Research Record: Journal of the Transportation Research Board, 1809*(1), 42-51.

Hobbs, D. W. (1974). *Influence of aggregate restraint on the shrinkage of concrete.* Paper presented at the ACI Journal Proceedings.

Holmes, N., & West, R. P. (2013). Enhanced accelerated drying of concrete floor slabs.

Holt, E. (2002). *Very early age autogenous shrinkage: governed by chemical shrinkage or self-desiccation.* Paper presented at the Proceedings of the Third International Research Seminar in Lund, Lund, Sweden.

Hunter, A. J. (1993). On movement of water through wood—The diffusion coefficient. *Wood science and technology, 27*(6), 401-408.

Hunter, W. G., Hunter, J. S., & George, E. P. (1978). *Statistics for experimenters: an introduction to design, data analysis, and model building*: Wiley New York.

Hveem, F. N. (1951). *Slab warping affects pavement joint performance.* Paper presented at the ACI Journal Proceedings.

Hveem, F. N., & Tremper, B. (1957). *Some factors influencing shrinkage of concrete pavements.* Paper presented at the ACI Journal Proceedings.

Hwang, C. L., & Young, J. F. (1984). Drying shrinkage of portland cement pastes I. Microcracking during drying. *Cement and Concrete Research, 14*(4), 585-594.

Jackson, F., & Kellermann, W. (1939). *Tests of concrete curing materials.* Paper presented at the Journal Proceedings.

Jensen, O. M., & Hansen, P. F. (1996). Autog enous Deformation and Change of the Relative Humidity in Silica Fume-Modified Cement Paste. *ACI Materials Journal, 93*(6).

Kim, J. K., & Lee, C. S. (1999). Moisture diffusion of concrete considering self-desiccation at early ages. *Cement and Concrete Research, 29*(12), 1921-1927.

Kosmatka, S. H., Kerkhoff, B., & Panarese, W. C. (2011). *Design and Control of Concrete Mixtures* (15 ed.): Portland Cement Association.

Kutner, M. H., Nachtsheim, C., & Neter, J. (2004). *Applied linear regression models*: McGraw-Hill/Irwin.

Mackenzie, J. K. (1950). The Elastic Constants of a Solid Containing Spherical Holes. *Proceedings of the Physical Society of London Section B, 63*(361), 2-11.

Mather, B. (1990). Curing Compounds. *Concrete International, 12*(2), 40-41.

McDonald, D. B., & Roper, H. (1993). *Prediction of Drying Shrinkage of Concrete from Internal Humidities and Finite Element Techniques, in Creep and Shrinkage of Concrete*, London.

Meeks, K. W., & Carino, N. J. (1999). *Curing of high-performance concrete: Report of the state-of-the-art*: Citeseer.

Montgomery, F. R., Basheer, P. A. M., & Long, A. E. (1992). Influence of Curing Conditions on the Durability Related Properties of Near Surface Concrete and Cement Mortars. *ACI Special Publication, 131*.

Mu, R., & Forth, J. P. (2009). Modelling shrinkage of concrete from moisture lost using moisture diffusion theory. *Magazine of Concrete Research, 61*(7), 491-497.

Nicholson, L. P. (1981). How to minimize cracking and increase strength of slabs on grade. *Concrete Construction, 26*(9), 739-741.

Perenchio, W. F. (1997). The drying shrinkage dilemma. *Concrete Construction*, 379-383.

Pickett, G. (1946). *Shrinkage stresses in concrete.* Paper presented at the ACI Journal Proceedings.

Pickett, G. (1956). *Effect of aggregate on shrinkage of concrete and a hypothesis concerning shrinkage.* Paper presented at the ACI Journal Proceedings.

Pihlajavaara, S. (1964). On the interrelation of the moisture content and the strength of mature concrete, and its reversibility.

Powers, T. C. (1968). The thermodynamics of volume change and creep. *Matériaux et Construction, 1*(6), 487-507.

Radlinska, A., Rajabipour, F., Bucher, B., Henkensiefken, R., Sant, G., & Weiss, J. (2008). Shrinkage mitigation strategies in cementitious systems: A closer look at differences in sealed and unsealed behavior. *Transportation Research Record: Journal of the Transportation Research Board, 2070*(1), 59-67.

Ramezanianpour, A. A., & Malhotra, V. M. (1995). Effect of curing on the compressive strength, resistance to chloride-ion penetration and porosity of concretes incorporating slag, fly ash or silica fume. *Cement and concrete composites, 17*(2), 125-133.

Rao, S., & Roesler, J. R. (2005). Characterizing effective built-in curling from concrete pavement field measurements. *Journal of Transportation Engineering, 131*(4), 320-327.

Schmitt, T. R., & Darwin, D. (1999). Effect of material properties on cracking in bridge decks. *Journal of Bridge Engineering, 4*(1), 8-13.

Scott, L., Lane, D. S., & Weyers, R. E. (1997). Relationship Between Capillary Pore Pressure and Early Shrinkage Cracking of Concrete: Virginia Transportation Research Council.

Senbetta, E. (1988). Concrete curing practices in the United States. *Concrete International, 10*(11).

Shariat, S. M. S., & Pant, P. D. (1984). Curing and Moisture Loss of Grooved Concrete Surfaces. *Transportation Research Record*(986).

Springenschmid, R., & Plannerer, M. (2001). Experimental research on the test methods for surface cracking of concrete. Germany: Technical University Munich, Institute for Building Materials.

Suprenant, B. A. (2002). Why Slabs Curl: Part 2- Factors Affecting the Amount of Curling. *Concrete International, 24*(4), 59-64.

Taylor, P. C. (2013). *Curing Concrete*: Taylor & Francis.

Tazawa, E. (1999). *Autogenous shrinkage of concrete*: CRC Press.

Tazawa, E., Miyazawa, S., & Kasai, T. (1995). Chemical shrinkage and autogenous shrinkage of hydrating cement paste. *Cement and Concrete Research, 25*(2), 288-292.

Thorpe, G. R. (1981). Moisture diffusion through bulk grain. *Journal of Stored Products Research, 17*(1), 39-42.

Turenne, R. G. (1978). The Use of Vapor Barriers Under Concrete Slabs on Ground (D. o. B. Research, Trans.) (pp. 3): National Research Council of Canada.

Vandenbossche, J. M. (1999). A review of the curing compounds and application techniques used by the Minnesota Department of Transportation for concrete pavements.

Wang, J., Dhir, R. K., & Levitt, M. (1994). Membrane curing of concrete: moisture loss. *Cement and Concrete Research, 24*(8), 1463-1474.

Wang, K., Cable, J. K., & Ge, Z. (2002). Investigation into Improved Pavement Curing Materials and Techniques: Part 1 (Phases I and II): Iowa Department of Transportation.

Wang, K., Cable, J. K., & Ge, Z. (2006). Evaluation of pavement curing effectiveness and curing effects on concrete properties. *Journal of materials in civil engineering, 18*(3), 377-389.

West, R. P., & Holmes, N. (2005). Predicting moisture movement during the drying of concrete floors using finite elements. *Construction and building materials, 19*(9), 674-681.

Whiting, N. M., & Snyder, M. B. (2003). Effectiveness of Portland cement concrete curing compounds. *Transportation Research Record: Journal of the Transportation Research Board, 1834*(1), 59-68.

Wittmann, F. H. (1973). Interaction of hardened cement paste and water. *Journal of the American Ceramic Society, 56*(8), 409-415.

Wong, H., & Buenfeld, N. (2009). Determining the water–cement ratio, cement content, water content and degree of hydration of hardened cement paste: Method development and validation on paste samples. *Cement and Concrete Research, 39*(10), 957-965.

Xi, Y., Bazant, Z. P., Molina, L., & Jennings, H. M. (1994). Moisture diffusion in cementitious materials moisture capacity and diffusivity. *Advanced Cement Based Materials, 1*(6), 258-266.

Ye, D., Mukhopadhyay, A. K., & Zollinger, D. G. (2009). Laboratory and Field Evaluation of Concrete Paving Curing Effectiveness: Texas Transportation Institute, Texas A&M University System.

Young, J. F., Mindess, S., & Darwin, D. (2002). *Concrete*: Prentice Hall.

Ytterberg, R. (1987a). Shrinkage and Curling of Slabs on Grade (Part a). *Concrete International, 9*(4), 22-31.

Ytterberg, R. (1987b). Shrinkage and Curling of Slabs on Grade (Part b). *Concrete International, 9*(5), 54-61.

Ytterberg, R. (1987c). Shrinkage and Curling of Slabs on Grade (Part c). *Concrete International, 9*(6), 72-81.

Zhang, J., Gao, Y., & Han, Y. (2011). Interior humidity of concrete under dry-wet cycles. *Journal of materials in civil engineering, 24*(3), 289-298.

Zollinger, D. G., & Barenberg, E. J. (1989). Proposed mechanistic based design procedure for jointed concrete pavements. *Illinois Cooperative Highway Research Program, 518*.

APPENDICES

In CHAPTER 3, a regression analysis for the weight loss and maximum curling of different curing compounds was used as shown in Table A1.

Table A1 Regression analysis for the weight loss and maximum curling

	Regression parameters	Weight loss[1]				Maximum curling[2]			
		$AX + B$	AX^B	$Ae^{B.X}$	$A\ln(X) + B$	$AX + B$	AX^B	$Ae^{B.X}$	$A\ln(X) + B$
C1	A	-1.02	0.06	0.44	-0.14	-1.71	1.55	2.59	-0.39
	B	0.37	-0.61	-5.03	-0.06	2.53	-0.19	-0.88	1.51
	F-statistic	5.15	51.2	47.9	6.71	0.06	21.1	20.3	0.21
	p-value	0.07	0.00	0.00	0.05	0.81	0.00	0.00	0.67
	Adjusted R^2	0.41	0.51	0.48	0.49	-0.18	-0.14	-0.18	-0.15
C2	A	0.09	0.29	0.25	0.02	-6.18	3.13	5.63	-0.89
	B	0.25	0.07	0.33	0.30	5.52	-0.19	-1.37	2.83
	F-statistic	0.17	247	237	0.39	1.87	147	148	1.89
	p-value	0.69	0.00	0.00	0.56	0.24	0.00	0.00	0.24
	Adjusted R^2	-0.16	-0.12	-0.16	-0.11	0.15	0.15	0.15	0.15
C3	A	-0.63	0.38	0.72	-0.14	-25.46	3.33	17.13	-5.64
	B	0.70	-0.26	-1.16	0.34	14.71	-0.64	-2.95	0.32
	F-statistic	8.44	1010	899	10.2	37	1120	779	54.7
	p-value	0.03	0.00	0.00	0.02	0.00	0.00	0.00	0.00
	Adjusted R^2	0.51	0.58	0.53	0.57	0.84	0.91	0.87	0.88
C3D	A	-1.89	0.11	0.91	-0.31	10.48	4.56	10.87	-2.40
	B	0.75	-0.74	-4.68	0.14	-15.43	-0.30	-1.94	3.49
	F-statistic	19.6	357	268	28.5	7.2	360	387	6.48
	p-value	0.01	0.00	0.00	0.00	0.04	0.00	0.00	0.05
	Adjusted R^2	0.76	0.85	0.81	0.82	0.51	0.46	0.50	0.48

[1] Power regression has been used for C1, C2, C3, and C3D.
[2] Power regression for C1 and C3 and exponential regression for C2 and C3D have been used.

In CHAPTER 5, the following estimations were used in the model for the input parameters:

Density of water: $\rho = 1000\ \frac{kg}{m^3}$

Universal gas constant: $R = 8.314\ \frac{J}{mol.K}$

Temperature: $T = 293\ K$

Depth of the member: $L = 1.27\ \ cm$

Width of the member: $b = 6.09\ \ cm$

Length of the member: $l = 100\ \ cm$

Concentration of dissolved species in the pore fluid: $n_l^{diss} = 1.91\ \frac{mol}{L}$

Concentration of pure water: $n_l^w = 55\ \frac{mol}{L}$

Molar volume of water: $v_l^w = \frac{1}{1000 n_l^w} = 1.82 \times 10^{-5}\ \frac{L}{mol}$

Fixed boundary $RH = 40\%$

Initial *RH* within the pore network prior to drying: $\frac{100 n_l^w}{n_l^{diss} + n_l^w} = 96.64\%$

Pore volume fraction: $\varphi = 0.3$

Bulk modulus of the solid phase: $K_s = 40\ GPa$

Instantaneous Poisson's ratio of the porous body: $\nu_p = 0.2$

Viscoelastic Young's modulus of the porous body: $E_p(t) = 0.1E_0 e^{-t/\tau} + 0.9E_0$

Time: *t* in days

Instantaneous Young's modulus of the porous body: $E_0 = 17.5\ GPa$

Viscoelastic relaxation time for the viscoelastic Young's modulus: $\tau = 10\ \ days$

VITA

AMIR HAJIBABAEE

Candidate for the Degree of

Doctor of Philosophy

Thesis: IMPACT OF DIFFERENT CURING METHODS AND DRYING CONDITIONS ON DRYING SHRINKAGE INDUCED CURLING

Major Field: Civil Engineering

Biographical: Amir Hajibabaee, born in 1985, in Karaj, Iran

Education:

- ✓ Completed the requirements for the Doctor of Philosophy in Structural Engineering at Oklahoma State University, Stillwater, Oklahoma in December, 2016.
- ✓ Completed the requirements for the Master of Science in Structural Engineering at Oklahoma State University, Stillwater, Oklahoma in December, 2011.
- ✓ Completed the requirements for the Bachelor of Science in Civil Engineering at University of Tehran, Tehran, Iran in 2008.

Experience:

- ✓ Utilize extensive analytical skills while researching various curing methods to reduce curling and drying shrinkage of paste and concrete elements.
- ✓ Proficiently instrument a major pavement in Oklahoma, and log strain, temperature, and relative humidity data.
- ✓ Employ model drying shrinkage with a poromechanical approach and numerical solutions.
- ✓ Extend this research to alternative cement systems (repair materials) to enhance research efficiency.
- ✓ Effectively import, clean, transform, validate and model data to understand and make conclusions for decision-making purposes.
- ✓ Collaborated on a project to retrofit severely corroded concrete piles of an old wharf in the Persian Gulf.
- ✓ Proficiently provided quality control of the retrofit, including checking sand-blasted piles before casting, batching, mixing, casting, curing of the fresh concrete and coating piles.
- ✓ Utilized various types of cements, pozzolans, admixtures, aggregates and curing conditions to investigate electrical resistivity of concrete.
- ✓ Employed chemical methods such as titration to test concrete cores and investigate steel corrosion in an old hotel in Kish Island, Iran.

Professional Memberships:

- ✓ American Concrete Institute (201, 209, & 308 ACI committees)
- ✓ American Ceramic Society
- ✓ American Society of Civil Engineers